

TITLE

**SYNTHESIS AND APPLICATION POTENTIAL OF GRAPHENE
AND GRAPHENE OXIDE NANO COMPOSITE FOR
TREATMENT OF DYES AND AROMATIC HYDROCARBONS**

TITLE

SYNTHESIS AND APPLICATION POTENTIAL OF GRAPHENE AND GRAPHENE OXIDE NANO COMPOSITE FOR TREATMENT OF DYES AND AROMATIC HYDROCARBONS

Submitted by: Sudipta Goswami

Doctor of Philosophy (Engineering)

Dr. Papita Das, Professor

Chemical Engineering Department

Faculty Council of Engineering and Technology

Jadavpur University

Kolkata – 700032, India

2018

**CERTIFICATE FROM THE SUPERVISOR/S AT THE TIME OF
SUBMISSION OF THESIS**

The candidate Shri Sudipta Goswami was registered on 31st December, 2014 and has fulfilled the residence and other requirements for submitting the thesis for the Ph.D degree of this University as per rules.

The thesis is a genuine piece of research carried out by the candidate under my/our supervision.

In my opinion this is a fit piece of work for submission for the Ph.D degees.

Papita Das 27/07/2018
Signature of Supervisor



Dr. Papita Das
Professor
Dept. of Chemical Engineering
Jadavpur University, Kolkata

ACKNOWLEDGEMENTS

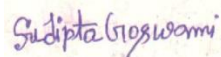
I would like to express my most sincere gratitude to my supervisors, Prof. Papita Das for her invaluable guidance, advices and constant inspiration throughout the entire research program.

I am gratefully acknowledging the financial support, given by MOES, Government of India, New Delhi. I acknowledge the help of Dr. Suvendu Manna, Dr. Subholaxmi Sengupta and Dr. Azizur Rahamn throughout this research. I also grateful to thank Ms. Priya Banerjee for her help and advice during this research work. I also personally thank to Mrs. Dolonchapa Sikdar, Mrs. Antara Ganguli for their constant support.

I am highly grateful to thank the Head of the Department (Chemical Engineering) and all the Teachers for their support. I therefore also gratefully acknowledge Department of Chemical Engineering, Jadavpur University for providing me an excellent research environment and technical facilities to carry out the research work.

I am thankful to all my collages and friends for their help and support. I would like to thank all the staffs of Chemical Engineering department for their constant help.

My acknowledge would be incomplete without mentoring about my parents and my brother who are always with me and giving their valuable support.



Date: 27.07.2018

(Sudipta Goswami)

CONTENTS

Preface	i
List of Tables	ii
List of Figures	v
List of symbols and abbreviations	xiii
CHAPTER 1: Introduction and Literature Review	
1.1 Background	1
1.1.1 Dyes and water pollution	2
1.1.2 Poly aromatic hydrocarbons and water pollution	3
1.2 Current technology for the removal of Dye and PAH	4
1.3 Adsorption Technology	6
1.4 Properties of Graphene oxide	9
1.5 Scope and Objectives	10
CHAPTER 2: Materials and methods	
2.1 Materials	12
2.2 Physico-Chemical properties of adsorbates	13
2.3 Methods	15
2.3.1 Batch experimental procedure	15
2.3.2 XRD analysis	16
2.3.3 Fourier transforms infrared spectroscopy	17
2.3.4 Atomic force microscope analysis	17

2.3.5	Scanning electron microscope analysis	18
2.3.6	Raman Spectroscopy analysis	18
2.4	Response Surface Methodology	18
2.5	Adsorption column study	19
2.6	Experimental setup for column study	19
2.7	Toxicity Analysis	20

CHAPTER 3: Preparation and Characterization of Adsorbents

3.1	Preparation of adsorbents	21
3.1.1.	Preparation of Graphene oxide from graphite powder	21
3.1.2	Preparation of Reduced-Graphene oxide from graphite powder	21
3.1.3	Preparation of GO and R-GO from rice straw bio char	22
3.1.4	Preparation of GONC	22
3.2	Characterization of Adsorbents	22
3.2.1	XRD analysis	22
3.2.2	FTIR analysis	24
3.2.3	SEM analysis	25
3.2.4	AFM analysis	27
3.3.5	Raman analysis	28

CHAPTER 4: Theoretical Consideration

4.1	Removal percentage and error analysis	30
4.2	Adsorption Isotherms	31

4.2.1	Langmuir Isotherms	32
4.2.2	Freundlich Isotherms	32
4.2.3	Temkin Isotherms	33
4.3	Adsorption Kinetics	33
4.3.1	Pseudo-first-order kinetic model	33
4.3.2	Pseudo-second-order kinetic model	34
4.3.3	Intra-particle Diffusion model	34
4.4	Adsorption Thermodynamics study	35
4.5	Activation Energy	35
4.5.1	Activation enthalpy, entropy and free energy	36
4.6	Response surface methodology	37
4.7	Column study	37
4.7.1	Column performance	37
4.7.2	Modeling of column data	38
4.7.2.1	Thomas model	38
4.7.2.2	BDST model	39
CHAPTER 5: Experimental Analysis		
5.1	Selection of adsorbents	41
5.2	Batch experimental study	43
5.2.1	Congo red adsorption study	43
5.2.1.1	Effect of adsorbent dose (CR)	43
5.2.1.2	Effect of various concentration (CR)	43

5.2.1.3. Effect of various Temperature (CR)	45
5.2.1.4 Effect of various pH (CR)	45
5.2.2 Equilibrium study by GONC (CR)	47
5.2.3 Adsorption Isotherms (CR)	48
5.2.4 Adsorption Kinetics (CR)	49
5.2.5 Adsorption Thermodynamics (CR)	51
5.2.6 RSM study by GONC (CR)	53
5.2.6.2 ANOVA analysis (CR)	56
5.2.7 Graphical Interpretation of RSM model (CR)	56
5.2.7.1 Effect of RSM analysis (Dose and pH)	57
5.2.7.2 Effect of RSM analysis (Time and pH)	57
5.2.7.3 Effect of RSM analysis (Time and Dose)	58
5.2.8 Optimization and confirmation of model (CR)	60
5.2.9 Column experimental study (CR)	60
5.2.9.1 Column performance (CR)	60
5.2.9.2 Effect of Bed height (CR)	60
5.2.9.3 Effect of Flow rate (CR)	61
5.2.9.4 Initial adsorbate concentration (CR)	62
5.2.10 Modeling of column data	63
5.2.10.1 Thomas model (CR)	63
5.2.10.2 BDST model (CR)	63
5.3 Metanil yellow (MY)	65
5.3.1 Batch adsorption experiments (MY)	65

5.3.1.1 Effect of adsorbent dose (MY)	65
5.3.1.2 Effect of various concentrations (MY)	65
5.3.1.3 Effect of various pH (MY)	67
5.3.1.4 Effect of various Temperature (MY)	67
5.3.2 Equilibrium study by GONC (MY)	69
5.3.3 Adsorption Isotherms (MY)	70
5.3.4 Adsorption kinetics (MY)	71
5.3.5 Adsorption Thermodynamics (MY)	72
5.3.6 RSM study by GONC (MY)	74
5.3.7 ANNOVA analysis (MY)	74
5.3.8 Graphical Interposition (MY)	77
5.3.8.1.Effect of RSM analysis (Time Vs pH) (MY)	79
5.3.8.2.Effect of RSM analysis (Dose Vs Time) (MY)	79
5.3.9 Column study (MY)	81
5.3.9.1 Effect of Bed height (MY)	81
5.3.9.2 Effect of Flow rate (MY)	82
5.3.9.3 Effect of Concentration (MY)	82
5.3.10. Column Study (MY)	83
5.3.10.1 Column Study Thomas model (MY)	83
5.3.10.2 Column Study BDST model (MY)	84
5.4. Crystal Violet	85
5.4.1 Batch adsorption study (CV)	85
5.4.2 Equilibrium study (CV)	89

5.4.3 Adsorption Isotherms (CV)	90
5.4.4 Adsorption Kinetics (CV)	90
5.4.5 Adsorption Thermodynamics (CV)	91
5.4.6 RSM study (CV)	92
5.4.7. Graphical Interpretation (CV)	97
5.4.8 Column Study (CV)	100
5.4.8.1 Column Study Bed height (CV)	100
5.4.8.2 Column Study Flow Rate (CV)	101
5.4.9. Modeling column Data (CV)	102
5.4.9.1. Thomas Model (CV)	102
5.4.9.2 BDST Model (CV)	103
5.5. Poly Aromatic Hydrocarbons (Phenol) (PH)	104
5.5.1 Batch Study (PH)	104
5.5.2 Equilibrium Study (PH)	108
5.5.3 Isotherms Study (PH)	108
5.5.4 Kinetics Study (PH)	109
5.5.5. Thermodynamics Study (PH)	110
5.5.6 RSM Analysis (PH)	112
5.5.7 Graphical Interpretation (PH)	115
5.5.8. Column Study (PH)	118
5.5.8.1 Column Study Bed height (PH)	118
5.5.8.2 Column Study Flow Rate (PH)	118
5.5.9 Column Study Thomas Model (PH)	119

5.5.10. Column Study BDST Model (PH)	120
5.5.2 Naphthalene (NAP)	122
5.5.2.1 Batch Study (NAP)	122
5.5.2.2 Equilibrium Study (NAP)	125
5.5.2.3 Isotherms Study (NAP)	126
5.5.2.4 Kinetics Study (NAP)	127
5.5.2.5. Thermodynamics (NAP)	128
5.5.2.6 RSM Study (NAP)	129
5.5.2.7 Graphical Interpretation (NAP)	132
5.5.2.8 Optimization Study (NAP)	135
5.5.2.9 Column Study (NAP)	135
5.5.2.9.1 Column Study Bed height (NAP)	135
5.5.2.9.2 Column Study Flow rate (NAP)	136
5.5.2.9.3 Column Study Concentration (NAP)	136
5.5.2.10 Column Study Thomas Model (NAP)	137
5.5.2.11 Column Study BDST Model (NAP)	138
5.6 Toxicological Analysis	139
5.7 Regeneration Study	141
CHAPTER 6: Reaction Mechanism, Summary and Conclusion	
6.1 Reaction Mechanism	143
6.1.1 Congo red adsorption mechanism	143
6.1.2 Metanil Yellow adsorption mechanism	144
6.1.3 Crystal Violet adsorption mechanism	145

6.1.4 Phenol adsorption mechanism	146
6.1.5 Naphthalene adsorption mechanism	146
6.2 Comparison Study of GONC	147
6.3 Summary	149
6.4 Cost analysis GO and R-GO	151
6.5 Limitations	152
6.6 Future Scope of Work	153
6.7 Conclusion	153
References	155

PREFACE

In twenty first century water became polluted in many ways with growing industrialization and urbanization. Dyes and poly aromatic hydrocarbons are contaminated effluents, discharged by the mainly textile and petrochemical industries. In this research the potential of removing dye and poly aromatic hydrocarbons by adsorption process has been explored. Among the various adsorbents graphene oxide and reduce graphene oxide were selected based on chemical structure. graphene oxide and reduced graphene oxide was prepared by modified Hummers method. Graphene oxide nano composite has been prepared and used to analyze the removal efficiency of dyes and poly aromatic hydro carbons. The adsorbents are characterized by XRD, FTIR, SEM, AFM and Raman analysis. For instance only 0.1 g of GONC removes around 90% of dye in 100 ml of solution containing 50 mg/l of dye. Among PAH's compounds naphthalene and phenol have been used, around 60 % of PAH molecules have been removed in 100 ml solution containing 10 mg/l of PAH. The removal of dye and PAH are pH dependent. Langmuir isotherms model was best fitted the adsorption data for all the cases. Reaction kinetics followed by pseudo second order kinetic model for dye and PAH. Thermodynamic study reveals that the process is spontaneous and physisorption in nature with high randomness between solid solute interface. RSM analysis shows that process better correlate the experimental data with statistical model. Column study revealed that breakthrough time increased with the increased of bed height and decreased with the increased flow rate and influent adsorbate concentration. Toxicological analysis was carried out to measure root-shoot length of *Cicer arietinum*. Thermodynamic study shows that only physical adsorption take place during this process, so mainly hydrogen bonds, van der Waals bonds, London separation force were acted between adsorbate and adsorbent (GONC) molecules.

Keywords: Reduce graphene oxide, graphene oxide, graphene oxide nano composite, adsorption.

LIST OF TABLES

Table no:	Page no:
Table no:1.1: List of low cost adsorbent efficiency for Dye removal	7
Table no:1.2: List of low cost adsorbent efficiency for PAH removal	8
Table no:2.1: List of chemicals used for adsorbents	13
Table no:2.2: Physicochemical properties of adsorbate	14
Table no:2.3: List of Batch studies variable parameters	17
Table no:2.4: Specification of Column study	21
Table no:3.1: XRD analysis of R-GO, GO, GONC	25
Table no:3.2: Surface texture of AFM analysis	29
Table no:5.1: Isotherms parameters of CR	52
Table no:5.2: Adsorption Kinetics parameters of CR	54
Table no:5.3: Thermodynamics parameters of CR	55
Table no:5.4: List of RSM experiments of CR	58
Table no:5.5: Fit summary of different models of CR	57
Table no:5.6: ANOVA table of CR	61
Table no:5.7: Column study of CR	64
Table no:5.8: Thomas model of CR	66
Table no:5.9: BDST model of CR	67
Table no:5.10: Column study of unknown concentration of CR	67
Table no:5.11: Isotherms parameters of MY	74
Table no:5.12: Kinetics parameters of MY	76
Table no:5.13: Thermodynamics parameters of MY	76

Table no:5.14: List of RSM experiments of MY	79
Table no:5.15: Fit summary model of MY	78
Table no:5.16: ANOVA model of MY	81
Table no:5.16: ANOVA model of MY	81
Table no:5.17: Column study of MY	85
Table no:5.18: Thomas model of MY	87
Table no:5.19: BDST model of MY	87
Table no:5.20: Column study of MY (unknown concentration)	88
Table no:5.21: Isotherms parameters of CV	95
Table no:5.22: Kinetics parameters of CV	96
Table no:5.23: Thermodynamics parameters of CV	97
Table no:5.24: List of RSM experiments of CV	98
Table no:5.25: Fit Summary model of CV	99
Table no:5.26: ANOVA model of CV	99
Table no:5.27: Column study of CV	104
Table no:5.28: Thomas model of CV	106
Table no:5.29: BDST model of CV	106
Table no:5.30: Column study of CV (unknown concentration)	107
Table no:5.31: Isotherms parameters of PH	112
Table no:5.32: Kinetics parameters of PH	114
Table no:5.33: Thermodynamics parameters of PH	113
Table no:5.34: Thermodynamics parameters of PH	113
Table no:5.35: List of RSM experiments of PH	117
Table no:5.36: Fit Summary model of PH	116
Table no:5.37: Column study of PH	122

Table no:5.38: Thomas model of PH	124
Table no:5.39: BDST model of PH	124
Table no:5.40: Thomas model of PH	124
Table no:5.41: Isotherms parameters of NAP	131
Table no:5.42: Kinetics parameters of NAP	131
Table no:5.43: Thermodynamics parameters of NAP	132
Table no:5.44: List of RSM experiments of NAP	134
Table no:5.45: Fit Summary model of NAP	133
Table no:5.46: ANOVA model of NAP	135
Table no:5.47: Column study of NAP (Bed height)	139
Table no:5.48: Column study Thomas model	141
Table no:5.48: Column study BDST model	141
Table no:5.48: Column study unknown concentration	142
Table no:6.1: Comparison study of efficiency of GONC with others	154
Table no:6.2: Cost analysis of prepared GO	159
Table no:6.3: Cost analysis of prepared R-GO	159

LIST OF FIGURES

Figure no:	Page no:
Figure no : 1.1: Structure of Graphene oxide	11
Figure no : 2.1: Structure of Congo red	15
Figure no : 2.2: Structure of Metanil yellow	15
Figure no : 2.3: Structure of Crystal violet	15
Figure no : 2.4: Structure of Phenol	16
Figure no : 2.5: Structure of Naphthalene	16
Figure no : 2.6a: Column setup Congo red	22
Figure no : 2.6b: Column setup Metanil yellow	22
Figure no : 2.6c: Column setup Crystal violet	22
Figure no : 3.1: XRD analysis of R-GO	25
Figure no : 3.2: XRD analysis of GO	25
Figure no : 3.3: XRD analysis of GONC	25
Figure no : 3.4: FTIR analysis of R-GO	26
Figure no : 3.5: FTIR analysis of GO	26
Figure no : 3.6: FTIR analysis of GONC	27
Figure no : 3.7: SEM image of R-GO	28
Figure no : 3.8: SEM image of GO	28
Figure no : 3.9: SEM image of GONC	28
Figure no : 3.10: SEM (Porous) image of GONC	28
Figure no : 3.11 and 3.12: SEM-EDX analysis of GONC	29
Figure no : 3.13: AFM image of R-GO	30

Figure no : 3.14: AFM image of GO	30
Figure no : 3.15: AFM image of GONC	30
Figure no : 3.16: Raman analysis of R-GO, GO, GONC	31
Figure no : 5.1: Comparative efficiency graph of CR	45
Figure no : 5.2: Comparative efficiency graph of PAH	45
Figure no : 5.3: Removal of CR by R-GO (R-GO Amount)	47
Figure no : 5.4: Removal of CR by GO (GO Amount)	47
Figure no : 5.5: Removal of CR by GONC (GONC Amount)	47
Figure no : 5.6: Removal of CR by R-GO at conc.	47
Figure no : 5.7: Removal of CR by GO at conc.	48
Figure no : 5.8: Removal of CR by GONC at conc.	48
Figure no : 5.9: Removal of CR by R-GO at temp.	49
Figure no : 5.10: Removal of CR by GO at temp	49
Figure no : 5.11: Removal of CR by GONC at temp	49
Figure no : 5.12: Removal of CR by R-GO at pH	49
Figure no : 5.13: Removal of CR by GO at pH	50
Figure no : 5.14: Removal of CR by GONC at pH	50
Figure no : 5.15: Equilibrium study of CR by GONC	50
Figure no : 5.16: Experimental image of CR by R-GO	51
Figure no : 5.17: Experimental image of CR by GO	51
Figure no : 5.18: Experimental image of CR by GONC	51
Figure no : 5.19: Normal probability vs Residual (CR)	60
Figure no : 5.21: Contour plot of CR (Dose Vs pH)	62
Figure no : 5.22: 3D plot of CR (Dose Vs pH)	62
Figure no : 5.23: Contour plot of CR (Time Vs pH)	62

Figure no : 5.24: 3D plot of CR (Time Vs pH)	62
Figure no : 5.25: Contour plot of CR (Time Vs Dose)	62
Figure no : 5.26: 3D plot of CR (Time Vs Dose)	62
Figure no : 5.27: Column study of CR (Bed height)	65
Figure no : 5.28: Column study of CR (Flow rate)	65
Figure no : 5.29: Column study of CR (Concentration)	65
Figure no : 5.30: Column study of CR (Experimental setup)	65
Figure no : 5.31: Removal of MY by R-GO (R-GO Amount)	69
Figure no : 5.32: Removal of MY by R-GO (GO Amount)	69
Figure no : 5.33: Removal of MY by R-GO (GONC Amount)	69
Figure no : 5.34: Removal of MY by R-GO (Concentration)	69
Figure no : 5.35: Removal of MY by GO (Concentration)	70
Figure no : 5.36: Removal of MY by GO (Concentration)	70
Figure no : 5.37: Removal of MY by R-GO (pH)	71
Figure no : 5.38: Removal of MY by GO (pH)	71
Figure no : 5.39: Removal of MY by R-GO (pH)	71
Figure no : 5.40: Removal of MY by R-GO (Temperature)	71
Figure no: 5.41: Removal of MY by GO (Temperature)	71
Figure no: 5.42: Removal of MY by GONC (Temperature)	71
Figure no : 5.43: Equilibrium study of MY by GONC	72
Figure no : 5.44: Experimental Image of MY by R-GO	72
Figure no : 5.45: Experimental Image of MY by GO	72
Figure no : 5.46: Experimental Image of MY by GONC	72
Figure no : 5.47: Normal % probability of MY	80
Figure no : 5.48: Predicted vs Actual of MY	80

Figure no: 5.49: Contour plot of MY (Dose Vs pH)	82
Figure no: 5.50: 3D plot of MY (Dose Vs pH)	82
Figure no: 5.51: Contour plot of MY (Time Vs pH)	83
Figure no: 5.52: 3D plot of MY (Time Vs pH)	83
Figure no: 5.51: Contour plot of MY (Time Vs Dose)	83
Figure no: 5.51: 3D plot of MY (Time Vs Dose)	83
Figure no: 5.52: Column study of MY (Bed height)	86
Figure no: 5.53: Column study of MY (Flow rate)	86
Figure no: 5.54: Column study of MY (Concentration)	86
Figure no: 5.55: Column study of MY (Experimental set up)	86
Figure no: 5.56: Removal of CV by R-GO (R-GO Amount)	89
Figure no: 5.57: Removal of CV by GO (GO Amount)	89
Figure no: 5.58: Removal of CV by GO (GONC Amount)	89
Figure no: 5.59: Removal of CV by R-GO (Concentration)	89
Figure no: 5.60: Removal of CV by GO (Concentration)	90
Figure no: 5.61: Removal of CV by GO (Concentration)	90
Figure no: 5.62: Removal of CV by R-GO (pH)	91
Figure no: 5.63: Removal of CV by GO (pH)	91
Figure no: 5.64: Removal of CV by GONC (pH)	91
Figure no: 5.65: Removal of CV by R-GO (Temperature)	91
Figure no: 5.66: Removal of CV by GO (Temperature)	91
Figure no: 5.67: Removal of CV by GONC (Temperature)	91
Figure no: 5.68: Equilibrium study of CV by GONC	92
Figure no: 5.69: Experimental Image of R-GO	92
Figure no: 5.70: Experimental Image of GO	92

Figure no: 5.71: Experimental Image of CV by GONC	92
Figure no: 5.72: Normal probability Vs Residual of CV	100
Figure no: 5.72: Predicted Vs Actual of CV	100
Figure no: 5.73: Contour plot of CV (Dose Vs pH)	101
Figure no: 5.74: 3D plot of CV (Dose Vs pH)	101
Figure no: 5.75: Contour plot of CV (Time Vs pH)	102
Figure no: 5.76: 3D plot of CV (Time Vs pH)	102
Figure no: 5.77: Contour plot of CV (Time Vs Dose)	102
Figure no: 5.78: 3D plot of CV (Time Vs Dose)	102
Figure no: 5.79: Column Study of CV (Bed height)	105
Figure no: 5.80: Column Study of CV (Flow rate)	105
Figure no: 5.81: Column Study of CV (Concentration)	105
Figure no: 5.82: Column Study (Experimental setup)	105
Figure no: 5.83: Removal of PH by R-GO (R-GO Amount)	108
Figure no: 5.84: Removal of PH by GO (GO Amount)	108
Figure no: 5.85: Removal of PH by GONC (GONC Amount)	108
Figure no: 5.86: Removal of PH by R-GO (Concentration)	108
Figure no: 5.87: Removal of PH by GO (Concentration)	109
Figure no: 5.88: Removal of PH by GONC (Concentration)	109
Figure no: 5.89: Removal of PH by R-GO (pH)	110
Figure no: 5.90: Removal of PH by GO (pH)	110
Figure no: 5.91: Removal of PH by GONC (pH)	110
Figure no: 5.92: Removal of PH by R-GO (Temperature)	110
Figure no: 5.93: Removal of PH by GO (Temperature)	110
Figure no: 5.94: Removal of PH by GONC (Temperature)	110

Figure no: 5.95: Equilibrium study of PH by GONC	111
Figure no: 5.96: Normal probability Vs Residual of PH	118
Figure no: 5.97: Actual Vs Predicted graph of PH	118
Figure no: 5.98: Contour plot of PH (Dose Vs pH)	120
Figure no: 5.99: 3D plot of PH (Dose Vs pH)	120
Figure no: 5.100: Contour plot of PH (Time Vs pH)	120
Figure no: 5.101: 3D plot of PH (Time Vs pH)	120
Figure no: 5.102: Contour plot of PH (Time Vs Dose)	120
Figure no: 5.103: 3D plot of PH (Time Vs Dose)	120
Figure no: 5.104: Column Study of PH (Bed height)	123
Figure no: 5.105: Column Study of PH (Flow rate)	123
Figure no: 5.105: Column Study of PH (Concentration)	123
Figure no: 5.106: Removal of NAP by R-GO (R-GO Amount)	126
Figure no: 5.107: Removal of NAP by GO (GO Amount)	126
Figure no: 5.108: Removal of NAP by GONC (GONC Amount)	127
Figure no: 5.109: Removal of NAP by R-GO (Concentration)	127
Figure no: 5.110: Removal of NAP by GO (Concentration)	127
Figure no: 5.111: Removal of NAP by GONC (Concentration)	127
Figure no: 5.112: Removal of NAP by R-GO (pH)	127
Figure no: 5.113: Removal of NAP by GO (pH)	127
Figure no: 5.114: Removal of NAP by GONC (pH)	128
Figure no: 5.115: Removal of NAP by R-GO (Temperature)	128
Figure no: 5.116: Removal of NAP by GO (Temperature)	128
Figure no: 5.117: Removal of NAP by GONC (Temperature)	128
Figure no: 5.118: Equilibrium study of NAP by GONC	129

Figure no: 5.119: Normal Vs Residual graph of NAP	136
Figure no: 5.120: Actual Vs Predicted graph	136
Figure no: 5.121: Contour plot of NAP (Dose Vs pH)	137
Figure no: 5.122: 3D plot of NAP (Dose Vs pH)	137
Figure no: 5.123: Contour plot of NAP (Time Vs pH)	137
Figure no: 5.124: 3D plot of NAP (Time Vs pH)	137
Figure no: 5.125: Contour plot of NAP (Dose Vs pH)	137
Figure no: 5.126: 3D plot of NAP (Dose Vs pH)	137
Figure no: 5.127: Column study of NAP (Bed height)	140
Figure no: 5.128: Column study of NAP (Flow rate)	140
Figure no: 5.129: Column study of NAP (Unknown concentration)	140
Figure no: 5.130: Toxicology analysis of CR	142
Figure no: 5.131: Toxicology graph of CR	142
Figure no: 5.132: Toxicology analysis of CR	143
Figure no: 5.133: Toxicology analysis of MY	143
Figure no: 5.134: Toxicology graph of MY	143
Figure no: 5.135: Toxicology analysis of CV	143
Figure no: 5.136: Toxicology graph of CV	143
Figure no: 5.137: Toxicology analysis of PH	143
Figure no: 5.138: Toxicology graph of PH	143
Figure no: 5.139: Toxicology analysis of NAP	144
Figure no: 5.140: Toxicology graph of NAP	144
Figure no: 5.141: Regeneration study of CR	145
Figure no: 5.142: Regeneration study of MY	145
Figure no: 5.143: Regeneration study of CV	145

Figure no: 5.144: Regeneration study of PH	145
Figure no: 5.145: Regeneration study of NAP	145
Figure no: 6.1: Schematic diagram of CR removal by GONC	150
Figure no: 6.2: Schematic diagram of MY removal by GONC	151
Figure no: 6.3: Schematic diagram of CV removal by GONC	152
Figure no: 6.4: Schematic diagram of PH removal by GONC	153

CHAPTER 1

INTRODUCTION AND LITERATURE REVIEW

1.1 Background

The progress of society, science and technology has forced the environment to tremendously suffer by the serious water crisis. Water is one of the main necessities for day to day survival of living bodies (Toor, et al., 2010). The ever-growing population, fast urbanization, rapid industrialization and improper utilization not only increase the demand in domestic and industrial level but also pollute the water affecting the environment. Statistically, nearly 1.2 billion people are affected by the shortage of safe and healthy water (Rijsberman et al., 2006). The socio-economical prosperity and aquatic systems could be endangered by the human activities on the quality and quantity of pure water (Ramachandra et al., 2002). The global water scarcity estimated that two-thirds of the world population will be affected due to the shortage of water in coming decades. India was already enlisted as a water deficit country by the statistic (Yang et al., 2003). To resolve this big problem the only way is appropriate use of fresh water as well as recycling and reuse of wastewater produced from agricultural, industrial as well as domestic activities. UNESCO reported that the production of wastewater by industrial effluents, domestic waste and agricultural waste is nearly about 1,500 km³. According to the UNESCO, 1 L of wastewater pollutes 8 L of fresh water (UNESCO, 2003). Thus, inefficiently treated industrial wastewater may create a chronic threat to the fresh groundwater resources by unremitting discharge of effluents into it, this water are considered unsafe harmful for environment and industrial purposes.

Focus on the reduction of pollution and removal of polluting constituents from the waste water. The major water pollutants which are seriously affecting the biodiversity of the eco-system are classified in mainly two categories- 1.Organic 2. Inorganic materials

When organic molecules having large molecular weight accumulate with it then separation process is very difficult (Karaka et al., 2016). Dyes and PAH are the compounds having one or more number of benzene ring in structure which makes them toxic in nature (Zhu et al., 2016) (Lamichhane et al., 2016). In this research an acidic, basic and azo type of dyes and for PAH naphthalene and phenol selected for the analysis.

1.1.1. Dyes and water pollution:

Since the dawn of civilization, humans have been fascinated by the beautiful and overwhelming vision of the colors of environment. In scientific terms color is called dyes, which consist of organic material with multiple aromatic ring used to impart the color to other substance. The two major components i.e. chromophores (-N=N, -C=C-, -C=O- etc) and auxochrome (-OH, -NH₂, -CHO, -COOH, -SO₃ etc) present in its structure is responsible for color. In primitive times, humans exploited natural resources, particularly flora and fauna, for the extraction of dyes and colorants: mainly for coloration of textile fibers and decoration of their caves and dwellings, thereby marking the beginning of a colorful life style and what followed next was the accidental discovery of synthetic dye (Mauveine) by English chemist Sir William Henry Perkin in 1856 (Gupta et al., 2009). This event triggered a marked decrease in the wide and exclusive use of natural dyes for colouration of materials. Synthetic dyes were much easier to manipulate and were judged “better” than natural dyes in any aspect of use, such as brilliance and range of colour, durability and costs. Generally some basic organic chemicals such as benzene, naphthalene etc were used and convert them into dye intermediates by adding some functional groups like chloro, bromo, nitro etc.(Senai et al., 1997).

Textile industry consumes approximately 70% of the total dye manufactured. Inefficiencies in dying process result in a large amount of (approx 10-15 % of the total dye used) dyestuff being directly lost in the wastewater (Yang et al., 2009). The textile manufacturing industry alone discharges about 146,000 tonnes of dyes per year along with its wastewater which ultimately finds its way into the environment (Onal et al., 2006).

By design, dyes are highly stable molecules; specifically resist fading upon exposure to sweat, light, water, heat and oxidizing agents. Huge amounts of non-biodegradable, toxic and inhibitory nature of spent dyes being lost directly into water channels constitutes an accumulative, persistent, carcinogenic, mutagenic and detrimental impact towards the survival of aquatic compartments, flora, fauna and environmental matrix (water and soil) (Sekhar et at 2009). In this study the investigation is done to evaluate the efficiency of adsorbents on acidic dye (Metanil yellow), basic dye (Crystal violet) and azo dye (Congo red).

In a wider sense, sporadic and excessive exposure to coloured effluents is susceptible to a broad spectrum of immune-suppression, respiratory, circulatory, central nervous and neurobehavioral disorders presage as allergy, autoimmune diseases, multiple myeloma, leukemia, vomiting, hyperventilation, insomnia, profuse diarrhea, salivation, cyanosis, jaundice, quadriplegia, tissue necrosis, eye or skin infections, irritation to even lung edema (Crini et al., 2007). Based on application dyes can be classified into three major groups

1. Acidic 2. Basic and 3. Azo (Gregory 1990).

1.1.2. Poly aromatic hydrocarbon and water pollution:

Now-a-days water becomes polluted by directly or indirectly discharged constituents in to water without adequate treatment. Water pollution affects the entire biosphere – plants and organisms living bodies of water. In most of the cases the effect is destructive not only to individual species and inhabitants, but also to the environment. Important pollutants include organic pollutants originating mainly from industrial (trade) and domestic sewage (raw or treated) farm wastes. Sewage effluents are the greatest source of organic pollutants discharged to the freshwaters. The behavior of organic compounds is dependent upon their molecular structure, size and shape and the mainly presence of functional groups which leads to toxicity parameters (Ghoshal et al 2013).

Poly aromatic hydrocarbons (PAHs) are organic compounds containing only carbon and hydrogen along with multiple aromatic rings (containing delocalized π -electrons) (Shi et al., 2014). Poly nuclear aromatic hydrocarbons (PNAs) are a subset of PAHs that have fused aromatic rings (Wenzl et al., 2006). Petroleum is one of the main source of PAHs, which occurs due to mainly leakage of oil from underground or above ground storage oil tanks, spill off during transportation of petroleum products and different industrial applications (Getha et al., 2013). Naphthalene and phenol are the components of PAH's which have adverse effect towards the environment.

In our atmosphere PAHs are generally found to be in complex form. They occur naturally in nature, but the pure form of PAH can be manufactured for research purposes. As pure chemicals, PAHs generally exists as colorless, white or pale yellow-green in color and exist in solid state with high melting and boiling point (Takagi et al., 2010). In plant they disturb the exchange between seeds, soil and atmosphere. Thus it hampers the growth of the plant. Sometimes they alter the plant tissues. Researchers have found that PAHs contact for a long

period of time can cause skin, lung, bladder, liver, and stomach cancer in laboratory animals. They also affect on their body fluid and immune system (Getha et al., 2013)(Liu et al., 2015). The National Institute for Occupational Safety and Health has set a recommended exposure limit at 10 ppm (50 mg/m³) over an eight hour time-weighted average, as well as a short-term exposure limit at 15 ppm (75 mg/m³) (Rajeshwaria et al., 2011). So PAH compounds should be removed from the wastewater before discharging into the environment. Naphthalene and phenol have been analyzed during this study as a PAH compounds.

Several low cost adsorbents are available to remove naphthalene and phenol from its aqueous solution (Table no 1.2).

1.2. Current technologies for dye and PAH removal:

With the growing awareness and environmental concerns, it is essential that reduce, reuse and degrade of dye and PAH form wastewater before discharge it into the environment. Now-a-days a number of physical, chemical and biological methods are applied to remove the dye and PAH from wastewater such as coagulation and flocculation, ion-exchange, membrane separation (ultra filtration, reverse osmosis and etc), adsorption and precipitation process (Moghaddam et al., 2010).

1.2.1. Coagulation and flocculation:

Owing to simplicity in nature and low treatment cost, coagulation has been opted for many years as a main treatment process to remove the contaminants from wastewater. It involves either the addition of some electrolytic compounds or electrical charge to the wastewater which alters the physical state of the dissolved or suspended contaminants and produce sludge by sedimentation or precipitation (Verma et. at, 2012) (Golbaz et al., 2014). A large number of literatures are available to remove synthetic dyes and PAH of various kinds by coagulation method using different electrolytic compounds such as ferric chloride (Anouzla 2009), electrode (Abdelwahab et al., 2009), magnesium chloride and alum (Gohary et al., 2009), polyaluminum chloride (Moghaddam et al., 2010), aluminum sulphate (Khayet et al., 2011), peroxi- coagulation (Junior et al., 2018).

However, the main disadvantages for this process the generation of huge number of highly toxic sludge, large chemical consumption (Saad et al., 2010) which is a big problem for the implementation for this process.

1.3.2. Ion-exchange:

Ion-exchange is a reversible chemical process where an ion of the solution is exchanged by the similar charged ion which is present in the solid phase of the adsorbent. Acidic, Basic and Azo all types of dyes were degraded by ion-exchange method. A various type of synthetic resins was used to remove contaminants from wastewater such as alumina gel and silica gel (Wasay et al., 1996), SDS (Chuang et al., 2016), amberlite IRA-958 (Greluk et al., 2009), sodium sulphate (Wawrzekiewicz et al., 2011), IRA-97, IRA- 458 (Greluk et al., 2011), carbon material (Sperczyn et al., 2016).

However, high treatment cost, low efficiency due to the presence of common salts into the wastewater was makes this process less adoptable (Verma et. at, 2012).

1.3.3. Membrane separation:

This technique consists of micro filtration, ultra filtration, reverse osmosis are integral part of wastewater treatment. In this technique a membrane is required which can separate the constituent molecules at constant temperature, pressure and microbial elements. However the recurrent congestion of elements into the membrane pores restricted their application in several times. High pressure driven force is required for this process which can damage the membrane (Gupta et al., 2009) (Gong et al., 2017). This process is an integral of several processes such as ultra filtration, reverse osmosis and etc.

The major drawback for this process it requires high set up cost, high energy, high membrane cost and residual disposal problem which makes it less adoptable.

1.3.3.1. Ultra filtration:

Ultra filtration or Nano filtration is a pressure-driven system and proficient to remove the constituents (organic and inorganic) from wastewater (Gong et at., 2017) (Smol et al., 2012), PAX-1910 and CWZ-22 dsed for PAH removal by ultra filtration (Rosinska et al., 2018). This process is used to purify the water in many countries such as France and Finland (Keskitalo et al., 2000) (Nicoll et al., 2001).

However, this process is less adoptable because high expensive to set up the process and requires high energy. A large number of biological and chemical fouling occurred during the process operation.

1.3.3.2. Reverse Osmosis:

Reverse osmosis is another part of membrane separation technique where an external pressure is required to overcome the osmotic pressure between the molecules. This technology requires a semipermeable membrane which separate the contaminants present in the water. It is an effective technology for water purification system. Dye and PAH molecules are being removed by this technique (Mulyanti et al., 2018) (Sun et al., 2018).

Though it is an efficient process but still it is less adaptable due to economical consideration and membrane fouling. A large number of separated molecules clogging the pores of the membrane reduce the removal efficiency.

1.3.4. Adsorption Technology:

Adsorption is one of the most popular, fundamental and simplest process which can remove the most of the constituents from wastewater effectively. This is basically a mass transfer process where an amount of solute is transfer from the liquid phase to the surface of solid adsorbent and bound by the physical or chemical or both forces together. Though it's high efficiency, simplicity and less time consuming features makes it more attractable by the researchers since so many years. The overall process cost is mainly depends on adsorbents cost. According to the literature there is several number of low cost adsorbent present but most of them are less treatment efficiency or high efficient adsorbent requires high cost. So nowadays the researchers have focused their attentions to find out a novel high efficient low cost adsorbent. A voluminous literature are available for low cost adsorbents which were already studied and there are endless prospect existing to develop the new one which poses high efficiency and low cost. As such a number of natural products, industrial waste and synthetically developed material which was used by the researches for the removal of dyes (Table no 1.1) and PAH (Table no 1.2) from aqueous solutions.

Table no 1.1. Adsorption efficiency of some low cost adsorbents for dye adsorption

Adsorbents	Adsorbate	Adsorption capacity(mg/g)	Reference
Cattail root	Congo red	38.79	Hu. et al 2010
Orange peel	Congo red	14.0	Annadurai et al 2002
Core pith	Congo red	6.7	Namasivayam et al 2008
Crassipes root	Congo red	15.32	Chuah et al 2014
Activated red mud	Congo red	12.4	Ali et al 2007
Ground nut shells	Congo red	56.8	Rani et al 2014
Graphene oxide	Congo red	145.6	Ansari et al 2017
Coinage nanoparticle	Congo red	36.4	Ozacar et al., 2005
Neem leaf powder	Congo red	41.20	Bhattacharyya et al 2004
Jute stick powder	Congo red	35.7	Panda et al 2009
Blast furnace sludge	Metanil Yellow	1.4	Jain et al 2003
Pine saw dust	Metanil yellow	39.8	Ozacar et al 2005
Saw dust carbon	Metanil yellow	183.8	Malik et al 2003
Rice husk carbon	Metanil yellow	86.9	Malik et al 2003
De-oiled soya	Metanil yellow	55.3	Mittal et al 2008
Granular sludge	Metanil yellow	18.9	Chutima et al 2015
PVA with TiO ₂	Metanil yellow	23.4	Hassan et al 2012
Graphene oxide	Metanil yellow	62.4	Chen et al 2008
Amino Graphene	Metanil yellow	71.62	Xiaoyao et al 2013
Succinamic acid	Metanil yellow	34.5	Aneesh et al 2016
Orange peel	Crystal Violet	14.3	Annadurai et al 2002

Rice bran	Crystal Violet	42.25	Wang et al 2008
Wheat straw	Crystal Violet	227.27	Gong et al 2009
Brazil nut shell	Crystal Violet	26.5	Brito et al 2010
Chitosan beads	Crystal Violet	76.9	Anjali et al 2013
Nano porous carbon	Crystal Violet	68.4	Fuat et al 2014
Chitin nano whisker	Crystal Violet	39.7	Sreerag et al 2016
Ramie biomass	Crystal Violet	16.4	Xiao et al 2016
Magnetic particle	Crystal Violet	0.25	Chandrakesh et al 2016
Graphene oxide chitosan	Crystal Violet	76.4	Zhou et al 2018

A large number of low-cost adsorbents are available which can remove PAH compounds from their aqueous solution.

Table no 1.2 listed various low cost highly efficient adsorbents which can separate naphthalene and phenol from aqueous solution.

Table no 1.2. Adsorption efficiency of some low cost adsorbents for NAP and PH removal:

Adsorbents	Adsorbate	Adsorption capacity(mg/g)	Reference
Activated carbon	Naphthalene	14.3	Ania et al 2006
Polymeric adsorbents	Naphthalene	6.3	Long et al., 2007
Activated carbon (Bean pods)	Naphthalene	85.5	Cabal et al., 2009
Heptanes	Naphthalene	26.4	Ania et al., 2006
Sonicated Talc	Naphthalene	267.2	Sener et al., 2010
Graphene oxide	Naphthalene	64.5	Pei et al., 2012
Magnetic graphene	Naphthalene	84.3	Yang et al., 2013
Graphene	Naphthalene	72.3	Xu et al., 2014
Walnut shell	Naphthalene	7.56	Zhu et al., 2016
Graphene nanoplates	Naphthalene	56.7	Bayajit et al., 2017
Lignite activated	Phenol	22.27	Guocheng et al.,

carbon			2011
Activated carbon	Phenol	33.5	Grabowska et al., 2013
Mill waste	Phenol	16.4	Abdelkreem 2013
Activated carbon	Phenol	20.4	Grilaldo et al., 2014
Graphene oxide	Phenol	13.4	Wang et al., 2013
Graphene oxide oxidative	Phenol	30.4	Yang et al., 2014
Graphene oxide saw dust	Phenol	135.5	Wu et al., 2014
Titania graphene oxide	Phenol	23.7	Fu et al., 2016
Graphene oxide flakes	Phenol	25.4	Catheri et al., 2018
Graphene oxide electrode	Phenol	45.8	Wang et al., 2018

1.4 Properties of Graphene oxide:

Graphene oxide and its derivatives have potential to remove dyes and PAH's molecules from aqueous solution. A voluminous amount of literature are available using graphene oxide itself or its derivatives for removal of dye and PAH. Such as- magnetite reduce graphene oxide Nano composite used to remove dye (Sun et al., 2011), methylene blue remove by graphene oxide (Yang et al., 2012), BR-12 and methyl orange remove by graphene oxide (Robati et al., 2017), graphene and graphene nano-composite used to remove organic compounds (Ivanov et al., 2018), hybridized reduced graphene oxide remove polycyclic aromatic hydrocarbons (Wang et al., 2014), naphthalene remove by graphene oxide (Chen et al., 2013).

Graphene, discovered in 2004, is a newly emerging member of carbon materials as well as the "mother of all graphitic forms" of nano-carbon, including 0D buckyballs, 1D carbon nano tube and 3D graphite (Juan et al., 2011). It has a two-dimensional structure composed of a single layer of sp^2 network of carbon atoms packed densely in a honeycomb crystal lattice. Reduce graphene oxide has attracted a great deal of scientific attention since its discovery due to its excellent mechanical, electrical, thermal, optical properties and very high specific surface area (Thakur et al., 2015). It exhibits great promise for potential applications in many technological aspects such as field-effect transistors, solar cells, sensors, super capacitors and transparent electrodes (Chen et al., 2011). As the large delocalized π -electron system of graphene can form strong π -stacking interaction with the benzene ring. Large quantities of

oxygen atoms are present on the surface of the resulting graphene oxide in the forms of epoxy, hydroxyl, and carboxyl groups (Tang et al., 2010) (Figure no 1.1) .

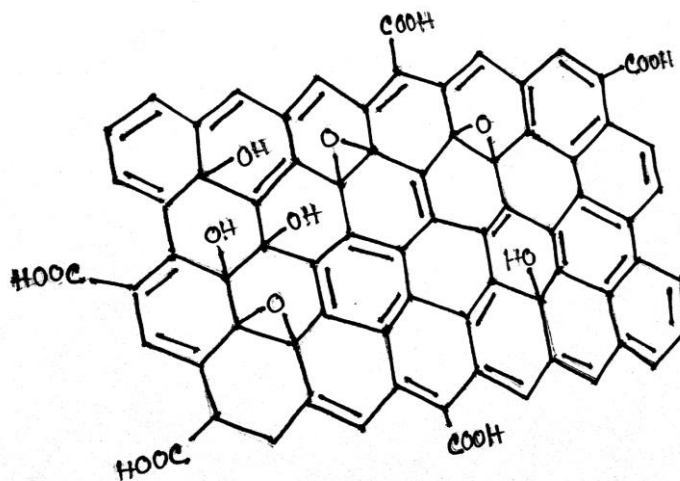


Figure no 1.1 Structure of Graphene oxide

Graphene oxide, a precursor for graphene preparation retains much of the properties of the highly valued super material pure graphene (Song et al., 2014). It is generally obtained through the strong oxidation of graphite by modified Hummer's method (Hummers et al., 1958). The presence of all these functional groups on the graphene oxide makes it extremely hydrophilic (Konios et al., 2014) and provides the capability to apply graphene oxide in the aquatic and biological environment. Due to its specific surface structure it can also be used as an adsorbent.

In this study graphene oxide (GO), reduce graphene oxide (R-GO) and graphene oxide nano composite (GONC) were used to remove dye and poly aromatic hydrocarbons from their aqueous solution as well as wastewater.

1.5. Scope and objectives:

According to the literature, those adsorbents which require less processing cost either less efficient or inactive in wider range. Activated carbon is better alternative which posses high removal efficiency but it requires high processing cost. Graphene oxide is a promising adsorbents and a good alternative of activated carbon but it requires high energy. Garphene oxide derivatives is a better substitute of graphene oxide which not only posses high

treatment efficiency in wider range but also reduce the cost of graphene oxide. The objectives of this study are—

The objectives of this study are--

1. Synthesis and characterization of reduced graphene oxide, graphene oxide and graphene-based nano-composite.
2. Investigation on dyes and aromatic hydrocarbon removal efficacy of synthesized nano-materials in batch mode of application from synthetic solution.
3. Analyze the removal efficiency of graphene oxide nano composite of dyes and aromatic hydrocarbon in column mode of application of synthetic solution.
4. Investigation the removal efficacy of graphene oxide nano composite for real wastewater through batch and column studies.
5. Equilibrium, kinetics, thermodynamics study of the adsorption process.
6. Simulation of the removal process using RSM software.
7. Toxicological analysis of adsorbate solution after treatment.

CHAPTER 2

MATERIALS AND METHODS

2.1. Materials:

Preparation of GO, R-GO and GONC several chemicals used listed in Table no 2.1.

Table no: 2.1 List of chemicals used for adsorbents preparation:

Chemical Name	Purity	Company Name
Graphite powder	99 %	Loba Chemicals
Sulphuric acid	98%	Sicco, India Mart
Potassium permanganate	96%	Sicco, India Mart
Hydrogen per-oxide	30%	Sicco, India Mart
Hydrazine hydrate	99%	Sicco, India Mart
Chitosan (medium molecular weight)	96%	Sicco, India Mart
Glacial acetic acid	35%	Sicco, India Mart
Poly vinyl alcohol	98%	SRL

All the glass wares used for this study are made by Borosil. Double distilled water has been used for this experiment.

For this study Congo red (azo dye), Metanil Yellow (acid dye) and Crystal violet (basic dye) and for PAH Phenol and Naphthalene were used listed in Table no. 2.2.

Table no. 2.2. Physicochemical properties of adsorbate

Dyes				Poly aromatic hydro carbon	
Name	Congo red	Metanil yellow	Crystal violet	Phenol	Naphthalene
Type	Azo type	Acidic type	Basic type	Organic Compound	Organic Compound
C.I. No.	22120	002146	039090	0520450	063245
Formula	$C_{32}H_{22}N_6Na_2O_6S_2$	$C_{18}H_{14}N_3NaO_3S$	$C_{25}H_{30}N_3Cl$	C_6H_6O	$C_{10}H_8$
Molecular weight (g/mol)	696.664	375.378	407.98	94.113	128.174
λ_{max}	490-495	442-448	570-590	268-270	218-220

2.2. Preparation of Adsorbate (Stock solution):

2.2.1 Congo red:

Congo red (CR) (IUPAC name- [1,1'-biphenyl] bis(4-amino naphthalene-1-sulphonic acid) is an azo dye. A stock solution of CR was prepared by dissolving the required amount (1000 mg/l) in doubled distilled water. The working solution was prepared by dissolving the stock solution with doubled distilled water. The chemical structure (Figure no 2.1) of CR as follows—

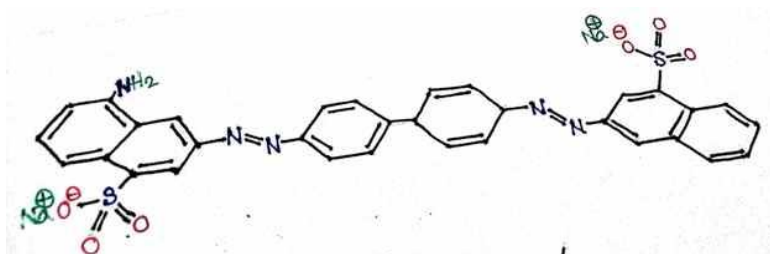


Figure no 2.1 Structure of CR

2.2.2. Metanil yellow:

Metanil yellow (MY) (IUPAC name- Sodium m-(4-anilinophenylazo) benzenesulfonate) is an acid dye. A stock solution of MY was prepared by dissolving the required amount (1000 mg/l) in doubled distilled water. The working solution was prepared by dissolving the stock solution with doubled distilled water. The chemical structure (Figure no 2.2) of MY as follows—

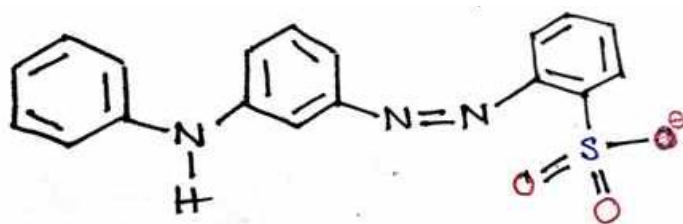


Figure no 2.2 Structure of MY

2.2.3. Crystal violet (CV):

Crystal violet (CV) [IUPAC name-Tris(4-(dimethylamino)phenyl)methylium chloride] is a basic dye. A stock solution of CV was prepared by dissolving the required amount (1000 mg/l) in doubled distilled water. The working solution was prepared by dissolving the stock solution with doubled distilled water. The chemical structure (Figure no. 2.3) of CV as follows—

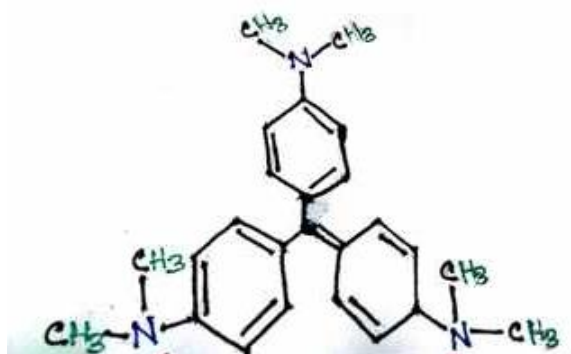


Figure no 2.3 Structure of CV

2.2.4. Phenol:

Phenol (PH) [IUPAC name-Hydroxybenzene] is an aromatic compound. A stock solution of PH was prepared by dissolving the required amount (100 mg/l) in doubled distilled water. The working solution was prepared by dissolving the stock solution with doubled distilled water. The chemical structure (Figure no 2.4) of PH as follows—

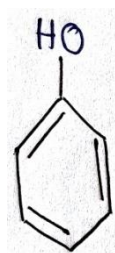


Figure no 2.4 Structure of PH

2.2.5. Naphthalene:

Phenol (NAP) [IUPAC name- Bicyclo (4.4.0)deca-1,3,5,7,9-pentaene or Bicyclo (4.4.0)deca-2,4,6,8,10-pentaene] is an aromatic compound. A stock solution of NAP was prepared by dissolving the required amount (100 mg/l) in doubled distilled water. The working solution was prepared by dissolving the stock solution with doubled distilled water. The chemical structure (Figure no. 2.5) of NAP as follows—

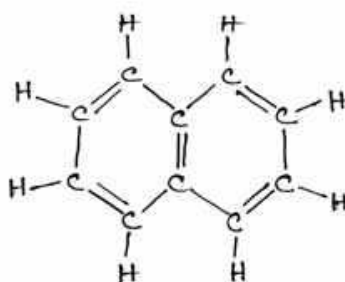


Figure no 2.5 Structure of NAP

2.3. Methods:

2.3.1. Batch Experimental Procedure:

Batch adsorption experiment was performed to understand the influence of each operational parameter on adsorbent functionalities synthesized earlier. A predetermined amount of adsorbents were added to 100 ml of adsorbate solution in 250 ml conical flask. It was placed

in incubator shaker with 120 rpm. The influence of various operational parameters like pH of the solution, adsorbent dose, temperature of the solution and initial dye concentration were examined during the present study. The pH of the solutions was adjusted with 1N HNO₃ and/or 1N NaOH solution. Samples were collected from the flasks at predetermined time intervals for analyzing the residual concentration of adsorbate present in the solution, which was measured at their respective λ_{\max} by UV/VIS spectrophotometer (Shimadzu model no.UV-1800). All experiments were repeated thrice to minimize the experimental error. The average errors were all within range $\pm 5\%$ of the mean value. Control parameters and variable parameters are listed in Table no 2.3.

Table no. 2.3. List of batch studies variable parameters:

Set no.	Control parameters	Variable parameters
1.	Initial adsorbate concentration (for dye) – 50 mg/l and (for PAH's) – 10 mg/l, pH of the solution: 7.2, Temperature – 30 °C, Agitation speed- 120 rpm.	Adsorbent dose – 0.05, 0.075, 0.1, 0.150 g/l.
2.	Adsorbent dose – optimum point, Initial adsorbate concentration (for dye) – 50 mg/l and (for PAH's) – 10 mg/l, Temperature - 30 °C, Agitation speed- 120 rpm.	pH of the solution- 2,4,6,8,10.
3.	Adsorbent dose – optimum point, pH of the solution- optimum point, Temperature - 30 °C, Agitation speed- 120 rpm.	Initial dye concentration- 10,20,50,75,100 mg/l and for PAH's – 5,10,20,25,50,100 mg/l.
4.	Adsorbent dose – optimum point, pH of the solution- optimum point, Initial adsorbate concentration- optimum point, Agitation speed- 120 rpm.	Temperature of the system- 20, 25,30,35,40 °C.

2.3.2. X-ray diffraction analysis (XRD):

The positive interference between monochromatic x-ray and a crystalline sample was analyzed during XRD analysis. It is a speedy analytical technique is mainly used for phase identification of a material and can provide the information of unit cell dimensions. X- ray diffractometer (Agilent model no: 0652) which was operated at 40 kV and 40 mA with Cu K α with scanning speed 2⁰ min⁻¹. The operating range of 2 θ (10⁰-50⁰) is used for XRD analysis. The crystallinity index, a measure of order orientation was calculated by the following equation-

$$Cryst I (\%) = \frac{I_{002} - I_{am}}{I_{002}} \times 100 \quad (1)$$

Crystallite size of the material can be calculated by the Scherrer formula-

$$Crystallite\ size = \frac{0.9 \lambda}{\beta \cos \theta} \quad (2)$$

Where λ is wavelength of x-ray beam (1.54 \AA), β is full width half maxima (FWHM) and θ angle of diffraction.

2.3.3. Fourier transforms infrared (FTIR) spectroscopy:

FTIR spectroscopy study, is a useful tool to identify the functional groups present into the material, was performed for GO, R-GO and GONC. The analysis was carried out in dried atmosphere by Perkin elmer (Spectrum two) with a scanning range from 4000 cm^{-1} to 400 cm^{-1} with a scanning speed 4 cm sec^{-1} the samples were mixed with KBr in 1:50 ratio and the samples were pelletized by pelletizer with 1mm pellet thickness. Mathematical techniques Fourier Transform then transform the raw data into the spectrum of the sample. The optical signal was generated by the functional groups presents into the samples as a function of infra-red wavelength was analyzed. The data generated by the instrument was plotted by origin software (version 8.0) and analyzed. Experimental data were processed by BIO-RAD software (version 5.3).

2.3.4. Atomic force microscope (AFM) analysis:

Scanning probe microscopy (SPM) or Atomic force microscopy (AFM) measures the surface topography of the material. AFM was performed using scanning probe microscope (SPM, multiview 1000 TM). All AFM analysis was made in tapping mode at ambient condition. Multiple images were collected for each sample and a better representative image was given in this study. AFM has ability to measure three dimensional structural image of the sample. The structural parameters (viz., average height, average roughness and average root mean square roughness) were determined by the SPM image processing software. For AFM measurements the samples were kept on clean mica surfaces. Prior to this, the powdered

samples were suspended in water and a drop was placed on top of the freshly cleaved mica surface. The water was allowed to evaporate gently overnight under ambient conditions (Bastidas et al., 2005).

2.3.5. Scanning electron microscope (SEM) analysis:

SEM provides detailed high resolution images of the sample by restirring a focused electron beam across the surface and detecting the secondary and backscattered electron signal. The morphological structure of the samples (GO, R-GO and GONC) were analyzed. The samples were coated with a thin layer of gold and scanning electron micrographs of samples were taken using SEM (ZEISS).

2.3.6. Raman Spectroscopy analysis:

Raman spectroscopy analysis is used to observe the vibrational, rotational and other low-frequency modes present into the materials. Raman spectroscopy is a vibrational spectroscopy like infrared (IR) spectroscopy whereas IR arises due to the change in dipole moment of the materials and Raman spectrum arises due to the specific molecular vibration. Samples (GO, R-GO and GONC) were prepared by drying at hot air oven and placed in Si substrate to get the spectrum. Raman analysis can be done by (Model no. T64000, M. Horiba, France).

2.4. Response surface methodology approach for optimization of the process: experimental and statistical analysis:

Statistical designing of the experiments are essential and reasonable for evaluating important information with minimum number of experiments reducing time and saving experimental as well as material cost while using. It is a tool which established the relation between mathematical and statistical model. This approach depicts the combined effect of all process parameter. Conversely for scale up studies, this approach is time consuming and also requires the number of experiments to find the optimum level and thereby mounting the overall cost of the process. These limitations can be eliminated by optimize the process using statistical experimental design by Response Surface Methodology (RSM) (Anupam et al., 2011). In this

study three level, three independent factor of CCD method (Central Composite Design) of RSM was applied to evaluate optimum process parameters condition and the individual and combined effects of the independent process variables on the response (Removal percentage). Three important individual process parameters, viz., initial pH of solution, adsorbent dose (mg) and reaction time (min) that predominantly affected the extent of adsorption by adsorbents (G,GO AND GONC) were identified as independent test variables. Twenty experiments suggested by the model and removal percentage was taken as a response. The experimental results were analyzed using Design-Expert software version 7.0 (Stat-Ease, USA).

2.5. Adsorbent column study:

The behavior of adsorbate removal from its aqueous solution as well as wastewater by adsorbent (which shows better efficiency during the batch study) in fixed-bed column mode was studied by conducting a series of column experiments with varying operational parameters viz., influent concentration, flow rate and bed depth. The detailed specifications of the column are listed in following Table no 2.4.

Table no 2.4: Specification of Adsorption Column study:

Parameters	Value
Column bed height (cm)	2,3 and 5
Internal diameter of column (cm)	2.6
Amount of adsorbent (dry) (g)	4,6 and 8
Initial dye concentration (mg/l)	100, 150
Flow rate (ml/min)	5,10,15

2.6 Experimental setup for column study:

Adsorbate solution was feed in borosilicate glass column placed vertically with stand (internal diameter 2.6 cm height 50 cm) having a glass sieve stand of 0.2 cm thickness at the bottom to provide the support to the bed a filter paper of thickness 0.03 cm was placed to the glass sieve stand which prevent washing out of adsorbent. The column was freely poured with 4 g of adsorbent to obtain the desired bed height (2 cm). Prior to experiment the dry adsorbent was soaked in distilled water for 3 hr. Attention was given to ensure the absence of air bubbles (which reduce the performance of column) within the packed bed column. The

adsorbent was packed tightly to absence of air bubbles. The top of the bed was covered by the filter paper and glass beads to avoid the floating up of the adsorbent during the experiment. Adsorbent solution of known concentration was fed through the peristaltic pump at a fixed flow rate at regular time intervals the samples was collected from the bottom of the column and concentration was measured by the UV/VIS spectrophotometer (Simdtzu UV 1800) at their respective wavelength (λ_{\max}) . The experiments were continued until the adsorbate concentration in the effluents was exceeding 98-99 % of its initial influent concentration. All the column experiments were performed at 30 ± 5 °C and pH 6.8-7.2 range. Figure 2.6 a, 2.6 b, 2.6 c represent of experimental column set-up for CR, MY and CV respectively.



Figure no 2.6a column setup (CR) Figure no 2.6b column setup (MY) Figure no 2.6c column setup (CV)

2.7 Toxicity analysis:

Toxicity analysis of untreated and treated adsorbate solution is determined by root-shoot length of *Cicer arietinum* seeds comparative analysis. Total three experiments were done consisting of control (sterile distilled water) one untreated and one treated (Goswami et al., 2013). The rate of germination growth for *Cicer arietinum* is measured for all untreated, treated as well as distilled water.

CHAPTER 3

PREPARATION AND CHARACTERIZATION OF ADSORBENTS

3.1. Preparation of Adsorbents:

The GO and R-GO were prepared from rice straw (carbonized agro-waste bio-char) and graphite powder using modified Hummer's methods (Hummers et al., 1958).

3.1.1. Graphene oxide preparation from graphite powder (GO):

GO were synthesized by strong oxidation of graphite powder by modified Hummers method (Hummers et al., 1958). Briefly, pure graphite powder was placed in a conical flask (500 ml) with flatted neck, then concentrated H_2SO_4 (98% pure) of 100 ml was added slowly with continuous stirring. The reaction was exothermic in nature the whole mixture was kept in ice bucket to reduce the system temperature. After 30 min 8 g of potassium permanganate was slowly added into the mixture with constant stirring. After 20 min 100 ml distilled water was added to it to reduce the heat of the mixture. Then the total mixture was placed in a BOD incubator shaker for 3 hr at 45°C . The reaction was terminated by adding 70 ml H_2O_2 (35% pure) into it. The brown yellow slurry was obtained. For uniform particle size the slurry was placed in a digital ultrasonic cleaner for 15 min. Finally it was filtered through filter paper and was washed repeatedly with distilled water for neutralizing the pH of the solution mixture. After that the product (GO) was dried in hot-air oven at 60°C for 6 hr.

3.1.2. Preparation of Reduce graphene oxide from graphite powder (R-GO):

Graphene oxide was reduced by some reducing agents to form R-GO (Konios et al., 2014). Hydrazine hydrate was used for this study to get R-GO. Experimentally 3 g of GO was taken in 250 ml conical flask add 100 ml of distilled water into it. After 3 ml of hydrazine hydrate was added to the mixture. The mixture was put into the magnetic starrer (Remi, model no. 14652104) for uniform distribution. Finally the product was filtered through filter paper and dried in hot-air oven at 50°C for 2 hr.

3.1.3. Preparation of GO and R-GO from rice-Straw agro waste Bio-Char:

Rice straw was collected from local rice mill located at north twenty four parganas. The collected straw was thoroughly washed with distilled water to remove dust, dirt and other impurities after that sundried for seven days. The sample was further dried in hot-air oven at 80 °C for 24 hr to remove moisture completely. The oven dried straw was placed in muffle furnace at 450 °C for 45 min in N₂ atmosphere for carbonization to bio-char (Parshetti et al., 2014). The obtained bio-char was crushed completely and sieved to get homogeneous particle size (<50 μm). The Rice straw bio-char was used as a substitute of graphite in graphine oxide synthesis. The GO and R-GO was prepared by previous method.

3.1.4. Graphene oxide Nano-composite preparation (GONC):

3 g of dispersed GO solution was added to the chitosan-acetic acid mixture. The chitosan-acetic acid mixture was prepared by dissolving 3 g of medium molecular size chitosan powder into 20 ml 5% acetic acid. The whole arrangement was put in magnetic starrer to get homogenize mixture. After 1 g of poly vinyl alcohol (PVA) solution was added to the mixture to get gel like structure. The product (GONC) was dried in hot-air oven at 50 °C for 5 hr. Finally the product was crushed, sieved and stored.

3.2. Characterization of Adsorbents:

The adsorbents GO, R-GO and GONC were characterized by XRD, FTIR, SEM, AFM and Raman analysis.

3.2.1. X-ray diffraction analysis (XRD):

X-ray diffraction patterns of R-GO, GO and GONC are shown in figure no 3.1, 3.2, 3.3 respectively. The crystallite size and crystallinity index were calculated from the diffractogram. The strong pick was observed at 26.38° for R-GO, 10.32° for GO which are similar to the R-GO and GO respectively (Wojtoniszak et al., 2012). For graphene oxide nano-composite (GONC) several picks observed which indicates the existence of GO, chitosan, PVA and other functional groups. The crystallite size, crystallinity index was decreased and amorphous component increasing for GONC compared with G and GO. The crystallite size, cryatallinity index and 2θ position were listed in the Table no 3.1.

Table no 3.1. XRD analysis of R-GO, GO, GONC:

Adsorbent	Peak position (2θ)	Crystallite size(nm)	CrI (%)
Graphene	26.38	13.89	56.42
Graphene oxide	10.56	9.26	44.26
Graphene oxide nano-composite	10.48,20.56, 25.05	5.61	26.54

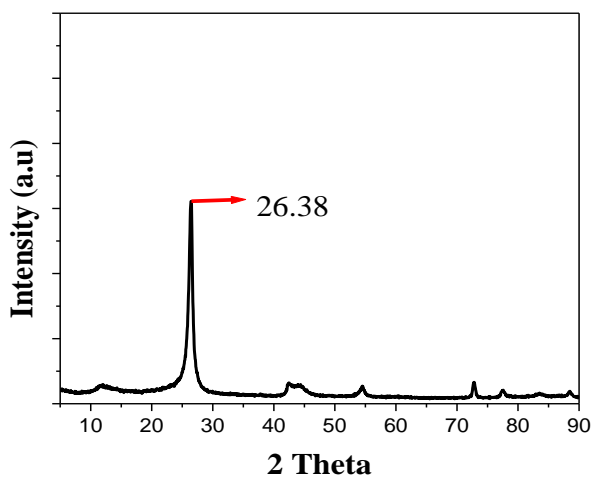


Figure no 3.1 XRD analysis of R-GO

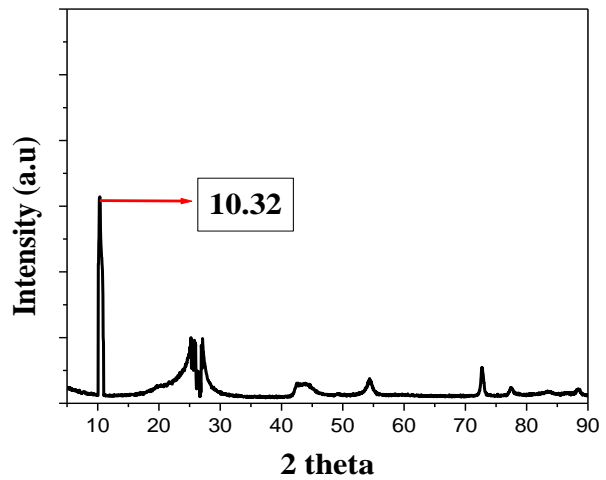


Figure no 3.2 XRD analysis of GO

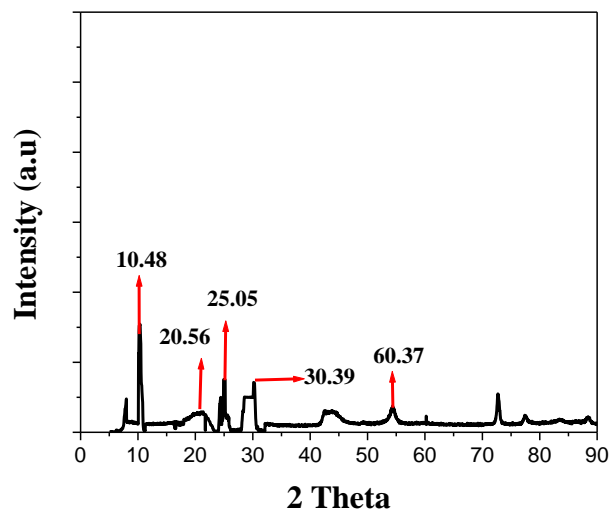


Figure no 3.3 XRD analysis of GONC

3.3.2. Fourier Transforms Infrared (FTIR) Spectroscopy:

The FTIR analysis is important to analyzed functional groups presents in the materials. The FTIR spectra of R-GO, GO and GONC were recorded and represented in the figure no. 2.4, 2.5, 2.6 respectively. For R-GO a strong peak was observed at 931 cm^{-1} is characteristic of asymmetric stretching of -NH due to hydrazine group present in the materials. The small peak at 1637 cm^{-1} represents the -CH stretching of alkenes groups presents in the materials. The stretching vibration of -OH group absorbe the light intensity and give a peak in 3418 cm^{-1} region which reflects the existence of -OH groups presents due to the un complete reduction of graphene oxide by hydrazine hydrate (Liu et.al 2012). For GO, a strong peak was observed at 3470 cm^{-1} indicates the stretching vibration of -OH group present in the material. The bands at 1630 and 1410 cm^{-1} can be attributed to the existence of asymmetric and symmetric stretching vibration of C=O. The signal at 1100 cm^{-1} is associated with symmetric vibration of -CN and a small peak at 793 cm^{-1} represents the existence of -CH groups in the materials which are similar to the graphene oxide (J.Hu et al, 2014). Figure c depict the spectra of GONC to identify the surface functionalized groups present in the material. The band at 3552 cm^{-1} represents the presence of amide group -RONH₂(-CONH₂) in the composite. The broaden band in the region of 3405 cm^{-1} reflects the stretching vibration of -OH group. The signal at 2915 cm^{-1} represents the methylene group (-CH₂) presents in the material. The bands at 1568 and 1410 cm^{-1} associated with the existence of -NH and symmetric stretching of -C=O groups in the GONC composite. The existance of C-O-C groups in the material at 1124 cm^{-1} (Karaka et al., 2017).

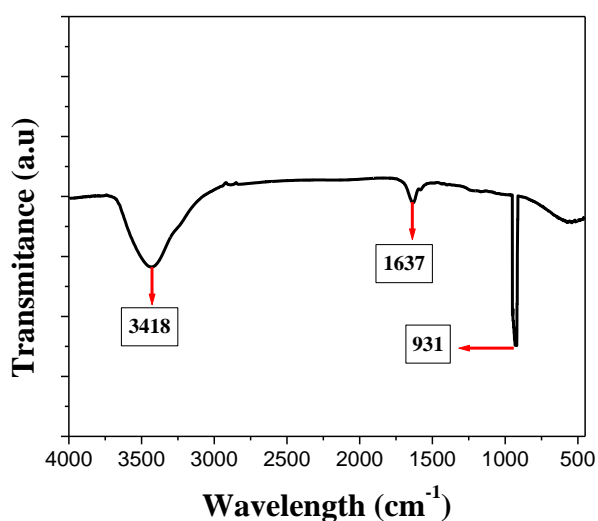


Figure no 3.4 FTIR of R-GO

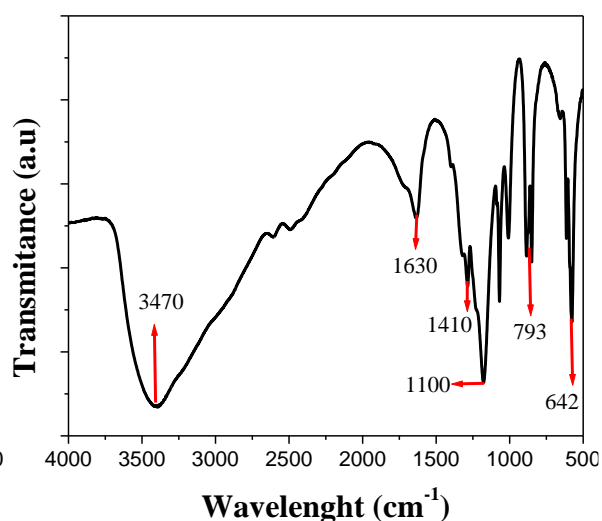


Figure no 3.5 FTIR of GO

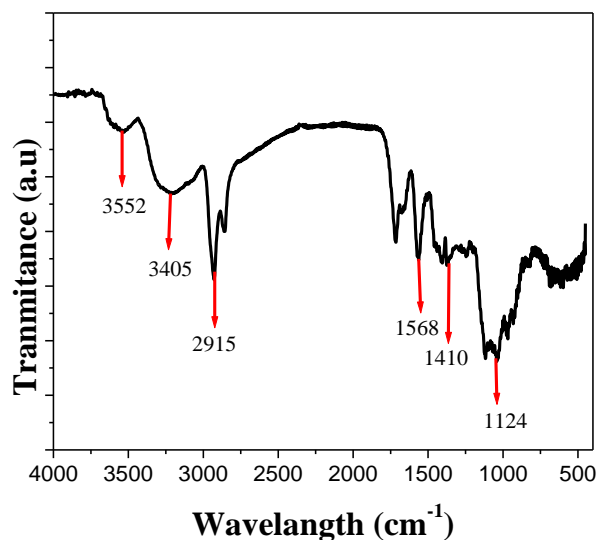


Figure no 3.6 FTIR of GONC

3.3.3. Scanning electron microscope (SEM) analysis:

SEM micrographs indicate the topographical image of R-GO, GO and GONC. From the figure no. 2.7, it was observed that R-GO has a scrambled sheet-like structure which contains a limited number of folded layered sheets but in GO has more layered structure figure no 3.8, which affords ultrathin and homogeneous films. Such films are folded in many times (B.Huang et al., 2015). Figure 3.9 shows the SEM image of GONC has continuously folded many layered sheets than GO and R-GO. Figure 3.10 shows the porous structure of GONC and figure no 3.11 and 3.12 the SEM EDX image and graph of GONC shows homogeneously distributed C and O atoms in its structure (red color dots represent the oxygen and green color dots represent the carbon atoms).

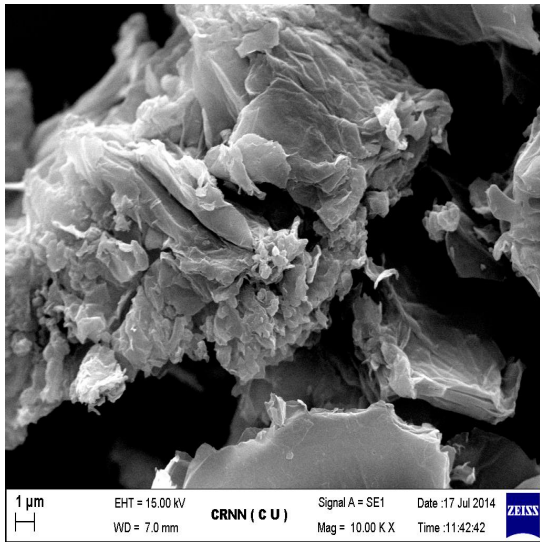


Figure no 3.7 SEM image of R-GO

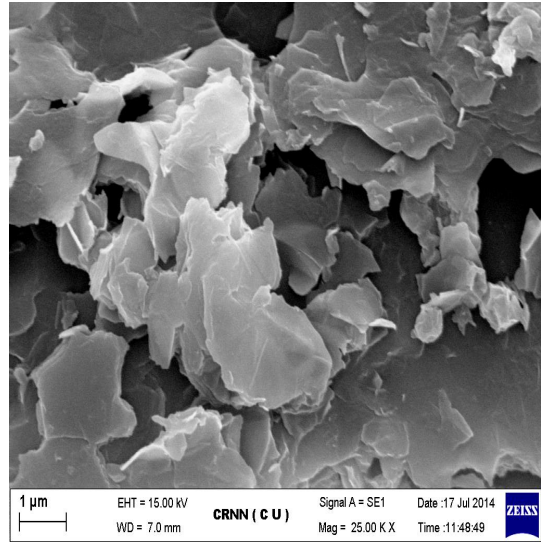


Figure no 3.8 SEM image of GO

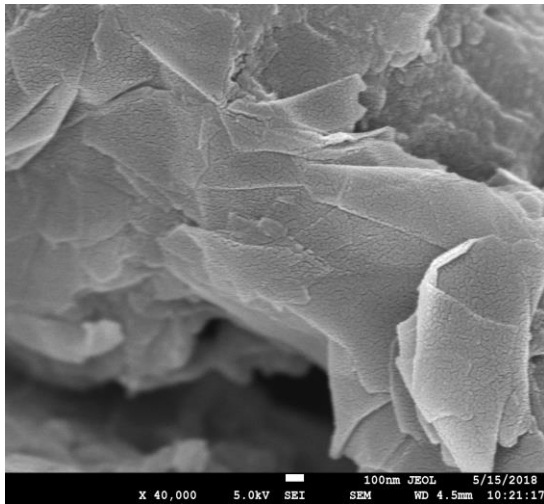


Figure no 3.9 SEM image of GONC

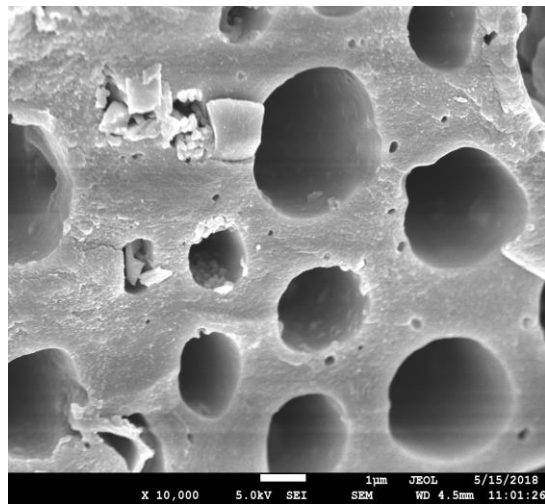


Figure no 3.10 SEM (Porous) image of GONC

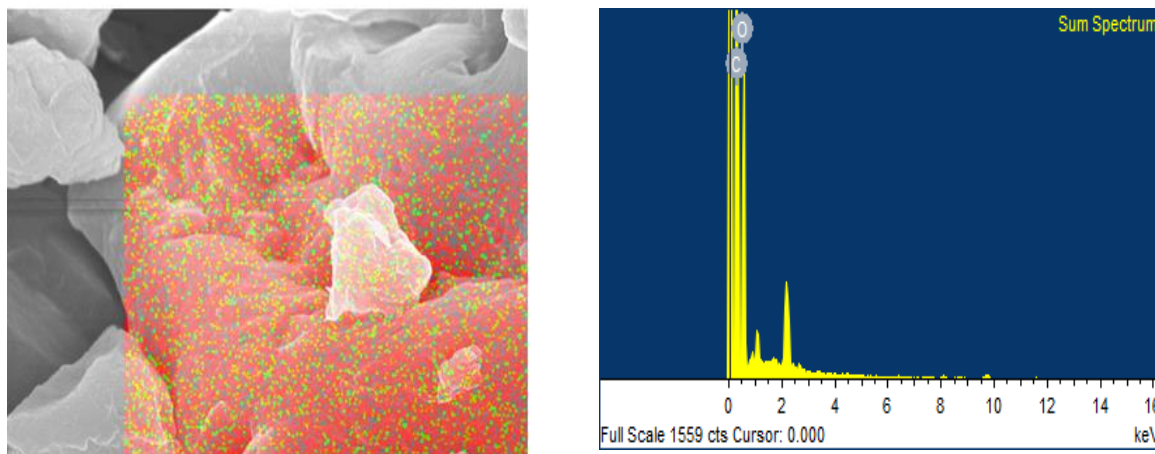


Figure no 3.11 and 3.12 SEM EDX (CO distribution) image and graph of GONC

3.3.4 Atomic force microscope (AFM) analysis:

AFM analysis was carried out to evaluate the surface topographical image of the adsorbents which indicate the surface roughness which leads to the increase adsorption process (Banerjee et al., 2015). Figure no 3.12 shows the surface roughness was moderate for R-GO. The roughness of the surface was increasing for GO, figure no 3.13 which leads to the increase in adsorption process. For GONC, figure no 3.14 show that the roughness (listed in table no 3.2) was more than R-GO and GO which leads to the better removal efficiency.

Table no 3.2 Surface texture parameters from AFM analysis:

Adsorbents	Average Roughness (Ra, nm)	Average Height (Ha, nm)
R-GO	14.8	2.25
GO	22.6	3
GONC	64.8	23.6

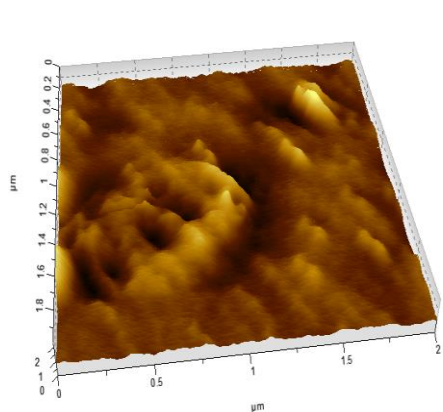


Figure no 3.13 AFM image of R-GO

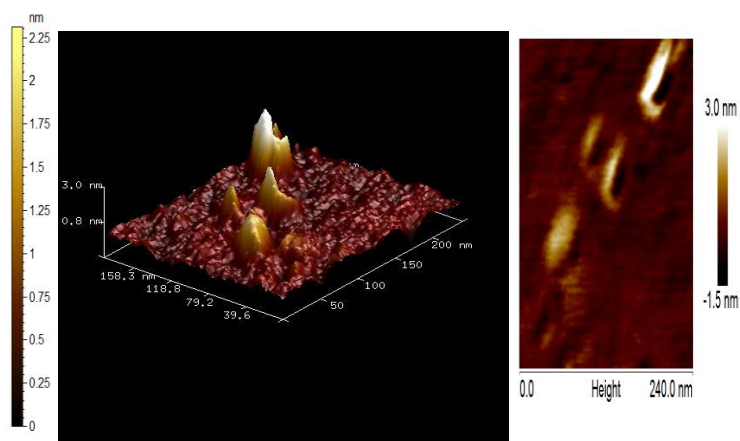


Figure no 3.14 AFM image of GO

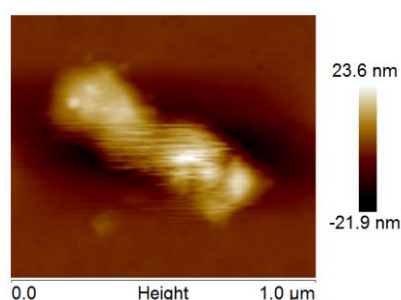
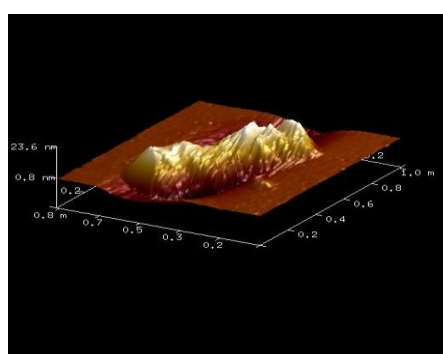


Figure no 3.15 AFM image of GONC

3.3.5. Raman Spectroscopy analysis:

A monochromatic light rays strikes the adsorbent surface and gets scattered in all direction this intensity of scattering represents the molecular vibration presents in the adsorbents. Raman spectra of R-GO, GO and GONC has been shown in figure 2.15. All the spectral response showed characteristic diamondoid (D) and graphitic (G) bands. These bands are useful for studying disorder and defects in crystal structure. The G-band formed due to the first order scattering of the E_{2g} phonon of the sp^2 C–C bonds. On the other hand, the D-band is resulting from scale defects on the graphitic plane (Kim et al., 2013), (Park et al., 2012). Disorder in the R-GO plane is determined from the intensity ratio between the D band and G band (I_D/I_G). Figure 1 indicated that the G band is seen at 1572 cm^{-1} , 1592 cm^{-1} , and 1595 cm^{-1} , and the D band at 1346 cm^{-1} , 1348 cm^{-1} , and 1359 cm^{-1} for R-GO, GO, and GONC, respectively. Analysis of all the spectra indicated that the G band is shifted to a higher wave number after introduction of oxygenated functional groups to GO and GONC. This results from the conversion of sp^2 types of carbons into sp^3 carbon atoms. The analysis

also indicated the broadening of the D band in GO and GONC after oxygenation of R-GO. This attributed to the reduction of sp^2 domains due to creation of defects, vacancies, and distortions during oxidation. The I_D/I_G ratio was found to increase from 0.26 (R-GO) to 1.13 (GO). This confirms that oxygen containing functional groups were granted to the graphitic planes. In the case of GONC the I_D/I_G ratio is further increased from 1.13 to 1.27 after the modification of GO. This result clearly indicating that the oxygen-containing functional groups on the GONC surface which generates further sp^3 C–C bonds (Kim et al., 2013b).

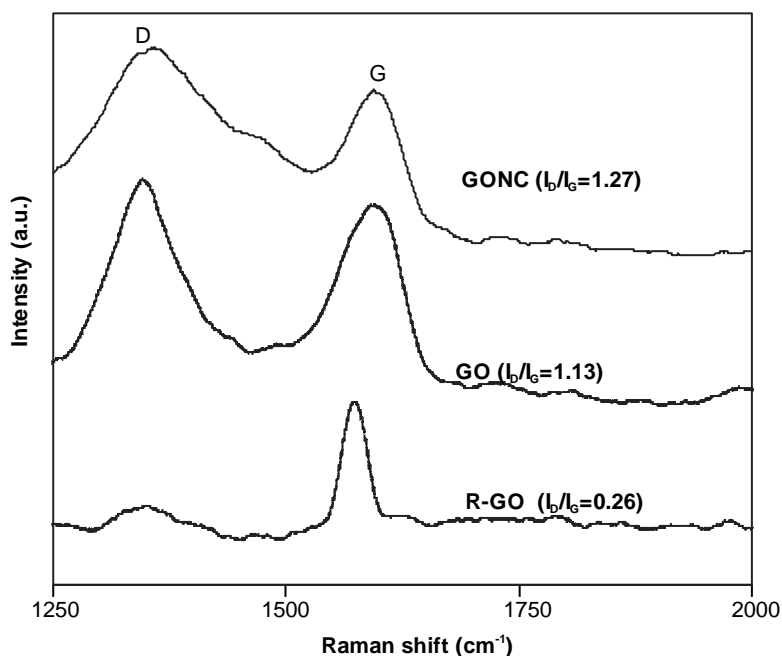


Figure no 3.16 Raman Analysis of R-GO, GO and GONC

CHAPTER 4

THEORITICAL CONSIDERATION

This chapter consists of various theories based on which the experimental data were analyzed.

4.1 Adsorbate Removal percentage and Error analysis:

The removal percentage of adsorbate concentration were calculated by following equation:

$$Removal (\%) = \left(\frac{C_0 - C_t}{C_0} \right) * 100 \quad (3)$$

Here C_0 is the initial adsorbate concentration (mg/l), C_t adsorbate concentration at time interval (mg/l).

The error analysis is important to calculate to evaluate the fitting of a model to the experimental data ad as well as measure of how well the predicted value of model constant parameters mach with the experimental value. In this study the non-linear chi-square (χ^2) test was calculated for the models as a degree of error between experimental and models predicted values. The chi-square was calculated by following equation (Chatterjee et.,al, 2009) —

$$\chi^2 = \sum \frac{(q_e - q_{e,m})^2}{q_{e,m}} \quad (4)$$

Where $q_{e,m}$ is the equilibrium adsorption capacity of adsorbent calculated from experimental data (mg/g) and chi-square (χ^2) is the non-linear error. The small value of chi-square (χ^2) indicates the better represented the model data with experimental value and large value of chi-square (χ^2) indicate the dissimilarity between them. The regrational coefficient (R^2) value indicate the model stability if R^2 value of a model is near to one so this model was better represent the experimental data.

4.2 Adsorption Isotherms:

An adsorption isotherm represents the equilibrium relationship between the adsorbate concentration in the liquid phase and that on the adsorbent surface at a solid phase at a given condition (Foo and Hameed, 2010). In equilibrium, a certain relationship prevails between solute concentration and adsorbate surface in solid phase. Typically isotherms which constitute an important role towards the modeling analysis. Data obtained experimentally were analysed using Langmuir, Freundlich and Tempkin models of adsorption isotherm.

4.2.1 Langmuir Isotherm:

The Langmuir Isotherm is possibly the best known of the entire adsorption model. This adsorption isotherm model was developed in 1916 by Irving Langmuir to describe the gas–solid phase adsorption on activated carbon (Langmuir, 1916). Its use was later developed to describe bulk liquid-solid interaction of the systems in which binding to the surface was mostly by physical forces, i.e. electrostatic or vander Waals forces. Langmuir adsorption isotherm model is based on the assumption that the adsorption of adsorbate molecules occurs only at specific sites of a homogeneous adsorbent surface consist of fixed number of active sites present into the system and saturation of these active sites ends the adsorption process. The Langmuir signify the monolayer adsorption process. The Langmuir constant describe the energy or net enthalpy of the system and q_m signifies the adsorption capacity when the surface is fully saturated with adsorbate molecules. The general form of Langmuir model equation (Gurgel and Gil, 2009):

$$q_m = \frac{q_m b C_e}{1 + b C_e} \quad (5)$$

q_m is the amount of adsorbed solute per unit mass of adsorbent (m/g), b is the Langmuir constnt describe the energy or net enthalpy of the process, q_m represent the theoretical monolayer adsorption capacity of adsorbent molecules when fully surrounded by the adsorbate molecules. The linear and rearranged form of the Langmuir equation is as follows (Ahmad, 2009)-

$$\frac{C_e}{q_e} = \frac{1}{Q_0} * \frac{1}{b} + \frac{C_e}{Q_0} \quad (6)$$

Where q_e = equilibrium amount of adsorbate adsorbed (mg/l) and C_e = equilibrium concentration of adsorbate in aqueous phase (mg/l), Q_0 and b being the Langmuir constants for adsorption capacity and energy of adsorption, respectively.

4.2.2 Freundlich Isotherm:

Freundlich model developed by German physicist Herbert Max Finley Freundlich in 1906 is the first describing relationship between the adsorbate molecules and adsorbent surface, illustrate that heterogeneity of adsorbate surface (Freundlich., 1906). The model implies that, amount of solute adsorbed in the summation of adsorption on all the active sites present in the adsorbent and bounded by the bond energy. Where stronger binding sites occupied first until the process energy was exponentially decrease upon the completion of adsorption process. The model signifies the multilayer adsorption process. The original form of Freundlich isotherm-

$$q_e = K_F C_e^{1/n} \quad (7)$$

Where q_e denotes amount of adsorbate adsorbed at equilibrium (mg/l), K_F is a Freundlich constant related to adsorption capacity (l/g), C_e denotes that adsorbate concentration at equilibrium (mg/l). the linear and rearranged form of the Freundlich equation –

$$\ln q_e = \ln K_F + \frac{1}{n} \ln C_e \quad (8)$$

$1/n$ is an empirical parameter related to adsorption intensity or surface heterogeneity. The process became more heterogeneous as its value is closer to zero (F.Haghsersht et., al 1998), q_e denotes adsorption capacity (mg/g), C_e denotes the concentration of adsorbate at equilibrium, K_F is Freundlich constant.

4.2.3 Temkin Isotherm:

The Temkin-Pyzhev isotherm model was first proposed by American scientist G. Temkin and M. Pyzhev in 1940. They considered the effect of indirect adsorbate/adsorbent interaction occurs at the adsorption isotherms. The isotherms model assumes that the heat of adsorption process decrease with the increase of coverage of the adsorbent used. The process is considered by uniform binding energy. The linear form of Temkin model equation-

$$q_e = B_T \ln K_T + B_T \ln C_e \quad (9)$$

Where K_T and B_T are temkin constant, q_e denotes amount of dye adsorbed at equilibrium (mg/l), C_e equilibrium concentration of adsorbate in aqueous phase (mg/l).

4.3. Adsorption Kinetics:

The prediction of adsorption mechanism of the system is important and vital for evaluating the affinity of adsorbent towards the adsorbate. It is also important to determine the efficacy of the process and simultaneously find out the adsorption capacity of the adsorbent. It is important to determine how the reaction rates depends on the adsorbate concentration and therefore effecting the adsorption capacity of adsorbent (Febrianto., 2009). Therefore in order to investigate the reaction mechanism and potential rate-controlling steps which include mass transfer and adsorption rate constant kinetics is desirable. For this study Pseudo first order, Pseudo second order and intra-particle diffusion models were analyzed.

4.3.1 Pseudo-first-order kinetic model:

Pseudo-first-order kinetic model was proposed by Lagergren in 1898, it was the first kinetic equation for the adsorption kinetics model (Lagregren, 1898). It demonstrate the interaction between adsorbate present in the liquid phase that on the adsorbent surface solid phase. The empirical form of the equation is-

$$\frac{dq_t}{dt} = K_1(q_e - q_t) \quad (10)$$

Where q_e and q_t are amount of adsorbate adsorbed at time t and equilibrium, K_1 is the pseudo first-order rate constant. The linearised form of Pseudo-first-order equation-

$$\ln(q_e - q_t) = \ln q_e - K_1 t \quad (11)$$

where, q_e amount of dye adsorbed at equilibrium per unit weight of adsorbent (mg/g), q_t is the amount of adsorbate adsorbed at any instant (mg/g) and K_1 is the rate constant (min^{-1}).

4.3.2 Pseudo-second-order kinetic model:

The Pseudo-second-order kinetic model was first proposed by Blanchard in 1984. The model was employed the adsorption experimental data using different adsorbate and adsorbents (Blanchard et al., 1984). The adsorption capacity of the adsorbent and the nature of reaction rate constant were evaluated from the experimental data. The empirical form of the equation-

$$\frac{d(ACS)_t}{dt} = k_2 [(ACS)_0 - (ACS)_t]^2 \quad (12)$$

Where $(ACS)_t$ represents the number of active sites occupied on the adsorbent solid surface, $(ACS)_0$ represents the number of active sites available on adsorbent surface.

The second order rate constant equation (Ho., 2006) can be written as-

$$\frac{t}{q_t} = \frac{1}{k_2 q_e^2} + \frac{t}{q_e} \quad (13)$$

Where K_2 denotes the pseudo-second-order rate constant of adsorption ($\text{g/mg}^2/\text{min}$) and q_e and q_t are the amounts of adsorbate adsorbed (mg/g) at equilibrium and at time t (min^{-1}).

4.3.3 Intra-particle Diffusion model:

For well agitated batch adsorption system there is a possibility of intra-particle pore diffusion of adsorbate ions, which may be accelerate or decelerate the adsorption process. So the process experience either surface adsorption or intra-particle diffusion or combination of

both. This phenomenon was expressed by the the Weber-Morris (Weber and Morris., 1963). The original form of Weber-Morris equation-

$$q_t = K_i t^{0.5} + I \quad (14)$$

Where q_t the amount of adsorbate adsorbed per unit of adsorbent (mg/g), K_i intra-particle rate constant and I is intercept. The general form of Intra-particle diffusion model equation is-

$$q_t = K_{diff} t^{1/2} + C \quad (15)$$

Where q_t is the amounts of dye adsorbed (mg/g) at time t (min), K_{diff} and C are constant.

4.4. Adsorption Thermodynamics study:

Temperature is the most significant and important parameters which govern the adsorption process by revise the adsorption capacity of the adsorbent for a specific adsorbate. The variation of adsorption efficiency with the variation of temperature was better expressed by the adsorption thermodynamics. Therefore an estimation of thermodynamic parameters for adsorption process is extremely necessary to better understanding the effect of temperature on adsorption. During this study the activation parameters (activation energy, enthalpy and entropy) and thermodynamics variable parameters (Gibb's free energy, standard enthalpy and entropy) were calculated for the experimental data and analyzed their nature leads to the adsorption separation process.

4.5. Activation energy:

Activation energy (E_a) is the amount of energy is required to start the exam. In practical sense the energy, which is needed to overcome the inter-molecular force of attraction by the adsorbate ions/molecules and get react or interact with the active functional groups presents in the adsorbent molecules. The activation energy of adsorption process can be calculated by the Arrhenius equation (Anirudhan and Radhakrishnan, 2008) —

$$\ln K = \ln A - \frac{E_a}{RT} \quad (16)$$

Where K is the adsorption rate constant, A is a frequency factor, E_a is the activation energy (kJ/mol), R is the universal gas constant (8.314 J/mol/K) and T is the temperature (K).

The value of activation energy may give an idea about the type of adsorption process. The adsorption mainly classified in two types Physisorption and Chemisorption. Physisorption is basically reversible in nature due to small amount of activation energy (< 40 kJ/mol) is required to start the reaction. Chemisorption is irreversible process, large amount of activation energy (> 40 kJ/mol) is required to start the reaction (Anirudhan and Radhakrishnan, 2008).

4.5.1. Activation enthalpy, entropy and free energy:

To know the insight weather of adsorption process, the process activation enthalpy (ΔH^0 , kJ/mol), activation entropy (ΔS^0 , kJ/mol) and free energy of activation (ΔG^0 , kJ/mol) were evaluated for the adsorption process. The entropy (ΔS^0), enthalpy (ΔH^0) and energy of activation (ΔG^0) were calculated by the Eyring equation (Anirudhan and Radhakrishnan, 2008)-

$$\frac{\ln K}{T} = \ln \frac{K_B}{h} + \frac{\Delta S^0}{R} - \frac{\Delta H^0}{RT} \quad (17)$$

Where K is the adsorption rate constant, K_B is the Boltzman constant (1.3807×10^{-23} J/K), h is the Plank constant (6.6261×10^{-34} Js), R is he universal gas constant (8.314 J/mol/K) and T is the temperature (K). The enthalpy (ΔH^0) and entropy (ΔS^0) can be calculated from slope and intercept of the plot $\ln K/T$ versus of $1/T$. These values was used to calculated the free energy (ΔG^0) from the equation-

$$\Delta G^0 = \Delta H^0 - T\Delta S^0 \quad (18)$$

In general the negative value of ΔG^0 indicates the feasibility and spontaneous nature of the process. A positive value of ΔH^0 suggest that the process is endothermic in nature. The magnitude and sign of ΔS^0 indicates the amount of randomness present between solid/liquid interface of the system (Dogan et al., 2009).

4.6. Response Surface Methodology:

Adsorption process was affected by numerous numbers of independent parameters. After batch study it is necessary to find out combined effects of parameters on adsorption efficiency and optimum process conditions were evaluated by applying a factorial Central composite design (CCD) of Response Surface Methodology (RSM). The response model may be expressed as an empirical form-

$$Y = f(X_1, X_2, X_3, \dots, X_n) \pm e \quad (19)$$

Where Y is the response, f is a response function and X_i is the process independent variables. Response function (f) was calculated by second-degree polynomial equation and evaluating the effect of independent process variable on response function. The linear form of quadratic polynomial equation (Tan et al., 2011) as follows-

$$Y = \beta_0 + \sum_{i=1}^n \beta_i X_i + \sum_{i=1}^n \beta_{ii} X_i^2 + \sum_{i=1}^{n-1} \sum_{j=i+1}^n \beta_{ij} X_i X_j + e \quad (20)$$

where Y is the response, X_i and X_j are independent process variable, β_0 is the constant coefficient, β_i i th linear coefficient, β_{ii} is the quadratic coefficient, β_{ij} ij th interaction coefficient, n is the number of independent process variables.

4.7. Column study:

This study is very important to evaluate the efficiency of the adsorbent in large scale application. The effect of various operational parameters viz., flow rate of the influent solution, bed height of adsorbent and concentration of the adsorbate on adsorbent capacity were analyzed.

4.7.1 Column performance:

The performance of a fixed bed column was analyzed by the concept of break through curve. The breakthrough curve is the ratio of relative concentration of adsorbate (ratio of influent concentration and effluent concentration at specific time) versus time of the experiment. The nature of the reaction and response characteristic were determined by the shape of the breakthrough curve. The break through point is defined at the point where the effluent was reached 10-15 % of the influent concentration (Uddin et al., 2009). The break through time

(t_b) and exhaustion time (t_e) was consider when effluent concentration was reached 15 mg/l and 98-99% of the influent concentration respectively.

The amount of adsorbate was removed in fixed bed column by the adsorbent at exhaustion i.e the optimum capacity of column (m_{ad} mg) for a definite influent adsorbate concentration (C_0 mg/l) and fixed flow rate (Q ml/min) can be calculated by area under the curve of the concentration of adsorbate (mg/l) versus time of the effluent (t min) (Han et al., 2009).

$$C_{ad} = C_0 - C_t \quad (21)$$

Where C_0 and C_t are the influent and effluent concentration of adsorbate (mg/l) respectively

m_{ad} can be computed from the equation—

$$m_{ad} = \frac{Q}{1000} \int_{t=t^0}^{t=t^{total}} C_{ad} dt \quad (22)$$

The amount of adsorbate molecules adsorbed per unit gram of adsorbent used for the experiment i.e. the adsorption capacity by the following equation—

$$q_{exp} = \frac{m_{ad}}{\text{Total mass of dry adsorbent in column (g)}} \quad (23)$$

4.7.2 Modeling of column data:

Several mathematical models have been developed to analyzed the column data. In this study the Thomas model and BDST (Bed Depth Service Time) model were used to analyze the column data.

4.7.2.1 Thomas model:

Thomas model is one of the most vital and widely used models for column study. Thomas model is based on the assumption that the adsorption process follows Langmuir model and

reaction rate follows pseudo-second-order kinetic model. The general equation for Thomas model is as follows—

$$\frac{C_t}{C_0} = \frac{1}{1 + \exp\left(\frac{K_{TH}q_{eTH}M}{Q} - K_{TH}C_0t\right)} \quad (24)$$

Where q_{eTH} the adsorption capacity of adsorbent (mg/g), K_{TH} constant of Thomas model (ml/min/mg), M is the dry weight of the adsorbent (g), C_t and C_0 is the effluent and influent concentration of adsorbate (mg/l) and t (min) time. The linear form of Thomas model-

$$\ln\left(\frac{C_0}{C_t} - 1\right) = \left(\frac{K_{TH}q_{eTH}M}{Q} - K_{TH}C_0t\right) \quad (25)$$

C_0 , C_t are influent and effluent concentration of dye (mg/l), K_{TH} is the kinetic rate constant of Thomas model (ml/min/mg), q_{eTH} adsorption capacity (mg/g), M is mass of adsorbent (g), Q flow rate (ml/min).

4.7.2.2. BDST model:

The BDST model was determined the relationship between bed depth and service time. The BDST model ignores the inter-particle diffusion and external film resistance during the adsorption process. The general form of BDST model equation by Bohart-Adams (Zambrano et al., 2011) —

$$\ln\left(\frac{C_0}{C_b} - 1\right) = \ln\left(\exp\left(\frac{K_a N_0 Z}{v}\right) - 1\right) - K_a C_0 t_s \quad (26)$$

C_0 and C_b influent and breakthrough dye concentration (mg/l), t_s service time at breakthrough point (min), N_0 adsorption capacity per unit volume (mg/l), Z bed depth (cm), v linear velocity (cm/min).

Later Hutchins modified Bohart- Adams equation and established the relationship between bed depth and service time-

$$t = \frac{N_0}{C_0 v} Z - \frac{1}{K_a C_0} \ln\left(\frac{C_0}{C_b} - 1\right) \quad (27)$$

where t is the service time at breakthrough point (min) of column experiment, N_o is the adsorption capacity of bed per unit bed volume (mg/l) of adsorbent used, Z is the column bed depth (cm), v is the linear velocity (cm/min) defined as the ratio of the volumetric flow rate Q (ml/min) to the cross-sectional area of bed A (cm²), C_o and C_b are influent and the breakthrough concentrations of the adsorbate (mg/l) respectively, and K_a is the rate constant (l/mg/min) of BDST model which characterizes the rate of solute transfer from liquid phase to solid phase. Assuming C_o and v , as constant throughout the column operation, N_o and K_a , can be evaluated from the slope and intercept of the plot yielded by plotting t_s versus Z (Zambrano et al., 2011).

CHAPTER 5

EXPERIMENTAL ANALYSIS

To investigate the feasibility of highly efficient, renewable, low-cost and easy to application, graphene oxide, reduced graphene oxide and graphene oxide nano-composite for effective removal of dyes (azo, acidic and basic) from their aqueous solutions was reported in this chapter in details. The removal efficiency of Congo red (azo dye), Metanil yellow (acid dye) and crystal violet (basic dye) by R-GO, GO and GONC were investigated in this chapter. The effect of amount of adsorbent, initial pH of the solution, initial dye concentration and temperature on dye uptake capacity of adsorbents was investigated over a wide range of experimental operating conditions by batch equilibrium, isotherms and kinetics study. Further the process was optimized by using RSM (Response Surface Methodology). The efficacy of the adsorbent on fixed bed column model in continuous mode was investigated by break through studies. The possible dye-adsorbent interaction was demonstrated during this single mode adsorption experimental system.

Azo dyes (consisting of major azo groups) as a consequence of π -delocalization electron and aryl azo compounds which leads to brilliant colour especially red have extreme effect towards environment as well as human being eye, skin, irritating in nature and have well known impact on human carcinogen and mutagen effect (Vimonses, 2009). Now –a-days the azo dyes are most widely used in the industry like., Textile, leather and paper (Gupta and Suhas, 2009). Due to adverse effect (Purkait et al., 2007) towards the environment congo red should be removed from the waste water before discharging to the environment.

5.1. Selection of Adsorbents:

The comparison study of removal efficiency between RG-RSB (reduce graphene oxide- rice straw bio char), RG-GP (reduce graphene oxide- graphite powder), GO-RSB (graphene oxide- rice straw bio char) and GO-GP (graphene oxide – graphite powder) for the selection of adsorbent. The study was performed by removal efficiency (dye and aromatic hydro carbon) and was investigated the removal capacity of each adsorbents, for dye CR and for PAH (NAP) have been used. Batch experiment was performed; 100 ml of 25 mg/l concentration of adsorbate (dye and aromatic hydro carbon) solution was taken in

250 ml conical flasks. 100 mg of each adsorbent was added at 30 °C to each flask, and placed in BOD incubator shaker at 120 rpm. The samples was collected from the flask after pre determined time and analyzed the concentration of adsorbate present in the samples by UV/VIS spectrophotometer at their respective wavelength. The removal efficiency of dye and aromatic hydrocarbons was shown in the following Figure no 5.1 and 5.2 respectively.

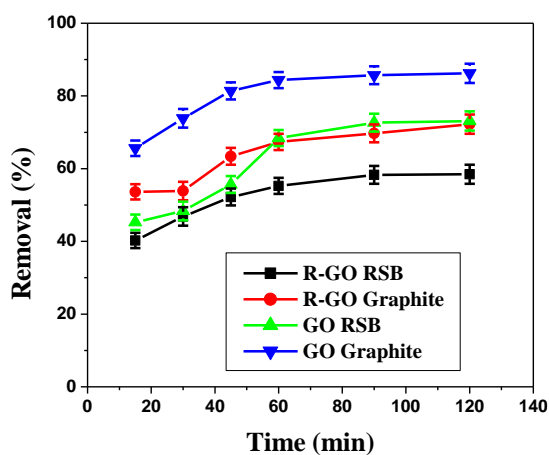


Figure no 5.1 Removal of dye (CR)

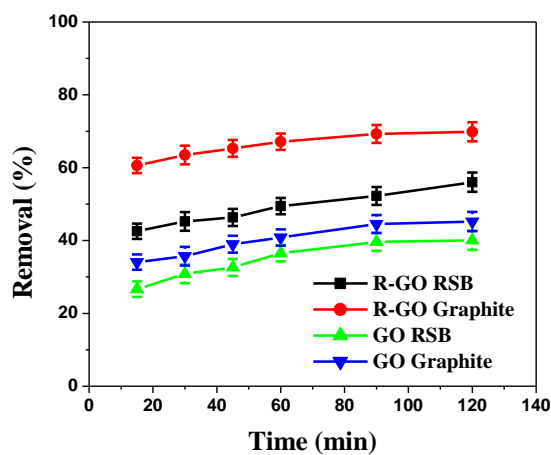


Figure no 5.2 Removal of PAH (NAP)

From the figure no 5.1, it was observed that GO-Graphite shows better efficiency than RGO-RSB, RGO-Graphite and GO-RSB for CR removal from its aqueous solution due to large amount of potential active site present in the structure.

Naphthalene is taken as a PAH to compare RGO-RSB, RGO-GP, GO-RSB and GO-Graphite. It was evident from the figure no 5.2 that RGO-Graphite shows the better efficiency than other adsorbents. A large number of delocalized π electrons present in RGO-GP structure which makes it more efficient than other adsorbents.

Form the above experiments it was seen that GO-Graphite and RGO-Graphite shows the better removal efficiency for dye and aromatic hydrocarbons so GO-Graphite (graphene oxide prepared from graphite powder) and RGO-Graphite (reduce graphene oxide prepared from graphite powder) were selected for further experiments.

5.2 Batch experimental study:

5.2.1 Congo red (CR) adsorption study:

Stock solution of CR was prepared discussed in chapter no 2 section no 2.2.1, working solutions were prepared by dissolving the stock solution with doubled distilled water.

5.2.1.1 Effect of adsorbent dose:

The necessity to investigate the effect of adsorbent dose comes from the economical point of view that required minimum amount of adsorbent was required for effective removal of dye molecules from its aqueous solution. The dye removal efficiency of adsorbent was increase with the amount of adsorbent increase up to 0.10 g/l after that for higher dose no drastic change in removal efficiency was observed. The increase in amount of adsorbent increase the surface area which may leads to the increase the active sites present in the adsorbent thus also boost the interaction between adsorbents and adsorbate (Ahmed et al., 2009). Form the figure no 5.3, 5.4, 5.5, it was clearly observed that GONC shows better removal efficiency than GR-GO and GO due to the more number of potential active sites presents in its structure.

5.2.1.2 Effect of initial Congo red concentration on adsorption:

Initial adsorbate concentration has pronounced effect on adsorption capacity of adsorbents (GO, R-GO and GONC). It is evident from the figure no 5.6, 5.7, 5.8, that the adsorbent capacity of GO, R-GO and GONC were increasing with the increasing initial dye concentration form 10-100 mg/l. Conversely, the removal percent of dye shows the opposite trend and found to be decreased with increased initial dye concentration. The optimum point is reached at 50 mg/l for all the adsorbents due to the saturation of active sites of adsorbents presents in the solution. Beyond this no drastic change is observed with the increase of dye concentration. The GONC shows the better removal efficiency comparing with R-GO and GO. During adsorption process of the initial dye concentration, the active sites of the available adsorbent surface offer the main driving force which is need to overcome the mass transfer resistance of dye molecules between the aqueous and the solid phase. Accordingly, for constant adsorbent dosage, the availability of adsorption sites is constant, at higher initial dye concentration the adsorption sites are easily saturated by the dye molecules. The maximum amount of unsaturated dye molecules present into the solution

leads to the lower removal percent and the dye adsorption becomes solely dependent on the initial concentration (Ahmad et al., 2009). At lower concentration the initial dye uptake was very rapid and reaches equilibrium easily whereas it requires more time to attain equilibrium when the initial dye concentration increased beyond 50 mg/l.

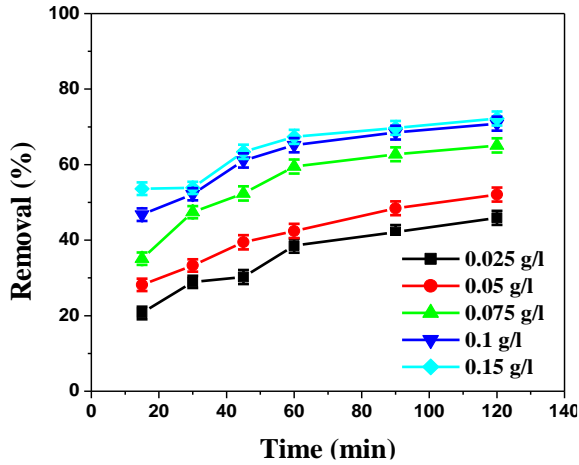


Figure no 5.3 Removal of CR by R-GO

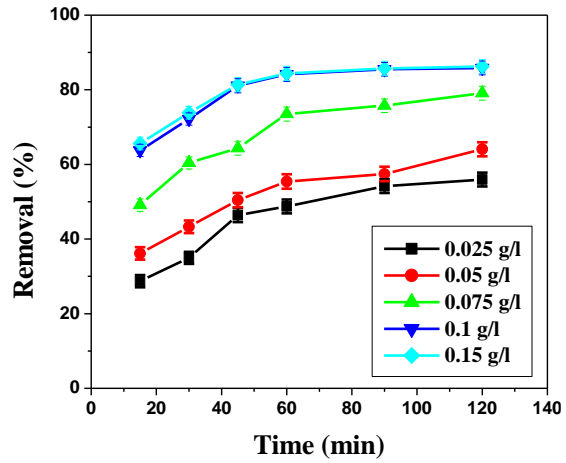


Figure no 5.4 Removal of CR by GO

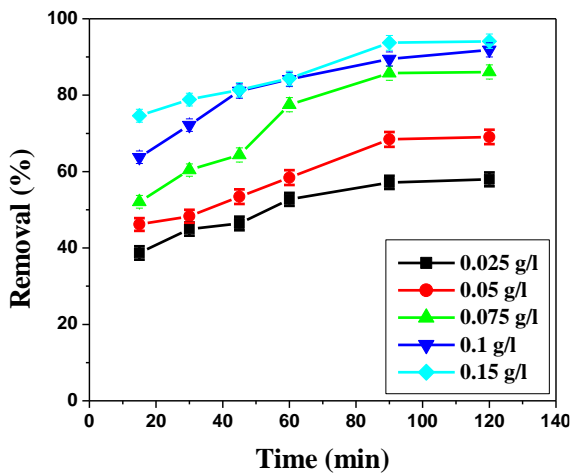


Figure no 5.5 Removal of CR by GONC

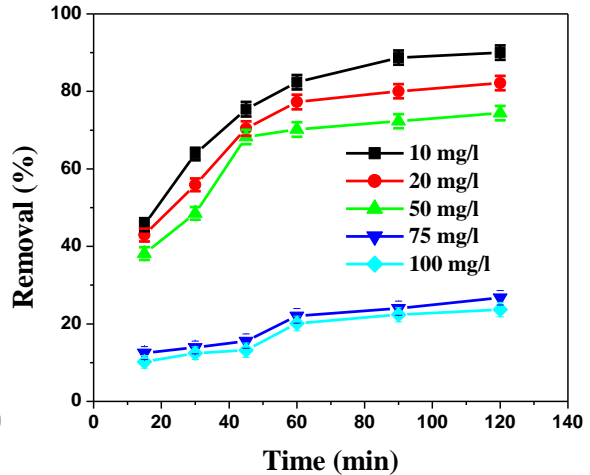


Figure no 5.6 Removal of CR (Conc.) by R-GO

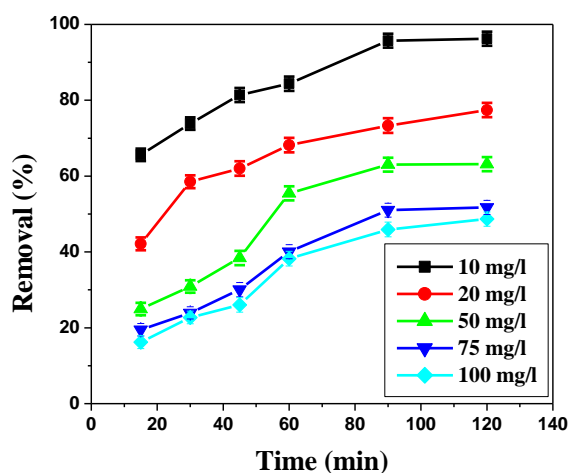


Figure no 5.7 Removal of CR (Conc.) by GO

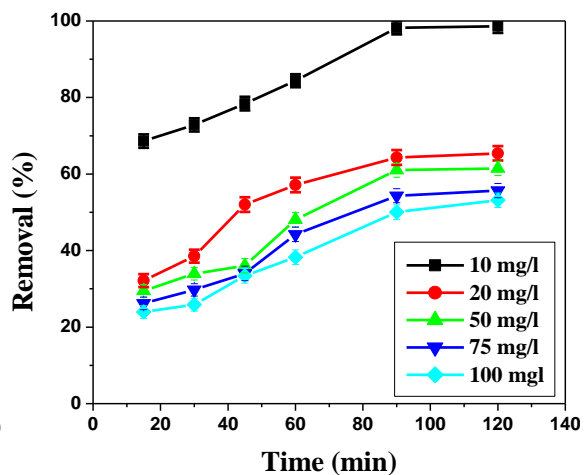


Figure no 5.8 Removal of CR (Conc.) by GONC

5.2.1.3. Effect of temperature on dye adsorption:

The influence of temperature on adsorption process is depicted in figure no 5.9, 5.10, 5.11. The removal percentage and efficiency are increased with the increasing the temperature from 20 °C to 40 °C for all adsorbent. As mentioned by Senthil kumar et al.2006, if the percentage removal of dye molecules increases with increasing temperature then the adsorption is endothermic in nature. The GONC shows the better removal than R-GO and GO, because at higher temperature the mobility between the dye molecules increases which leads to the better interaction between active sites of adsorbents and dye molecules. The increasing trend is observed up to 40 °C and after that the percentage removal is decreased. The reason behind this phenomenon as suggested by Chatterjee et al., 2007 is that at high temperature the physical bonds between the adsorbate molecules and adsorbent surface get weakened which may led to the decrease in adsorption efficiency.

5.2.1.4. Effect of pH on dye adsorption:

The pH has an important effect on dye adsorption since the pH of the medium will control the magnitude of the electro-static charges that are imparted by ionized dye molecules. As a result the rate of adsorption will increase with the increase of pH of dye solution (Khan et al., 2013). In the figure no 5.12, 5.13, 5.14 shows the percentage removal of CR at different pH with respect to time for R-GO, GO and GONC were observed. The removal

percentage of CR was increased with the increase of pH of the solution up to 6 for all adsorbents. At pH 6 dye molecules are slightly acidic in nature which imparts the positive charge into the solution and negatively charged oxygen molecules presents in to the adsorbents gets attracted by positively charged dye molecules which imparts better percentage removal. At higher pH the dye molecules discharge negative ions into the solution which gets repelled by the active oxygen atoms presents into the adsorbents. The removal efficiency was better for GONC compare with R-GO and GO due to the large number of active oxygen atoms presents into GONC structure.

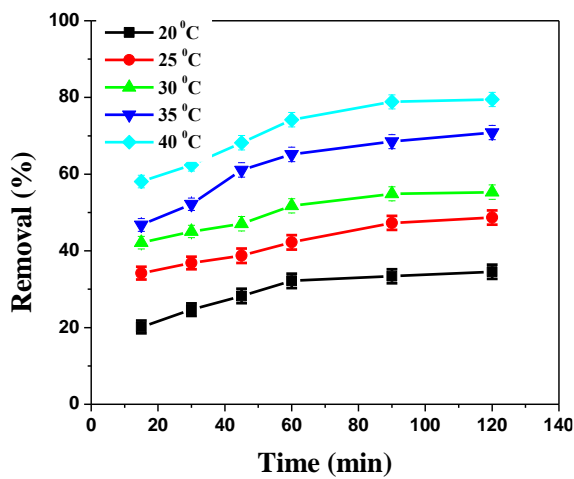


Figure no 5.9 Removal of CR (Temp) by R-GO

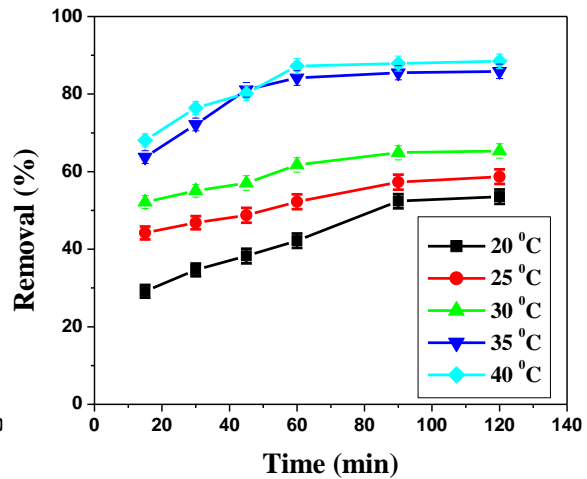


Figure no 5.10 Removal of CR (Temp) by GO

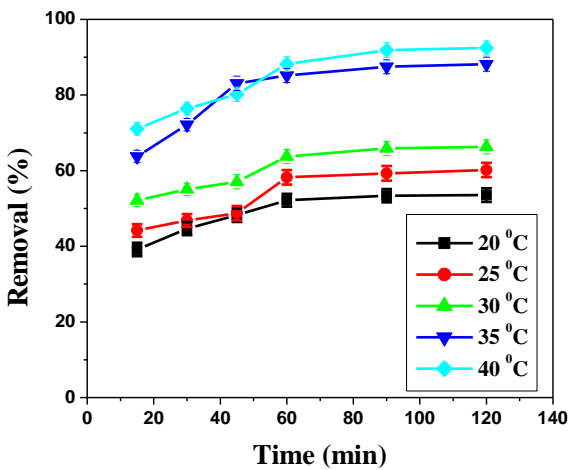


Figure no 5.11 Removal of CR (Temp) by GONC.

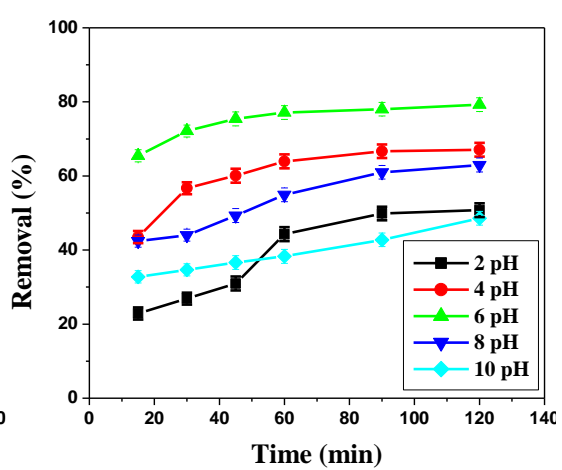


Figure no 5.12 Removal of CR (pH) by R-GO

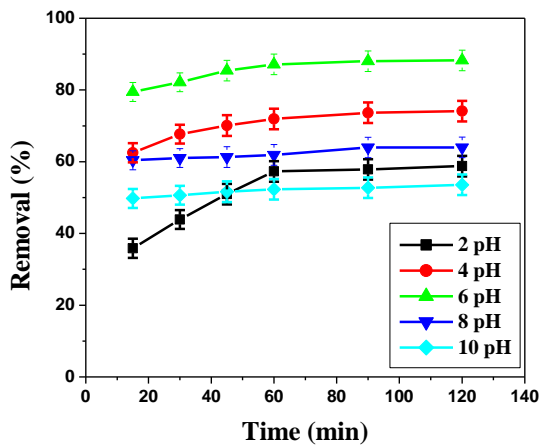


Figure no 5.13 Removal of CR (pH) by GO.

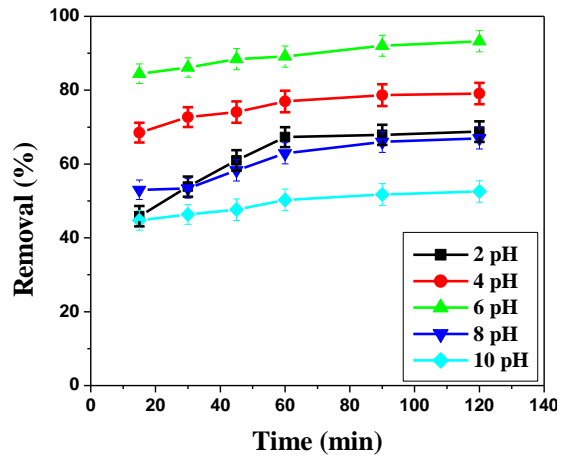


Figure no 5.14 Removal of CR (pH) by GONC

5.2.2. Equilibrium study of CR by GONC:

To evaluate the effect of all operational parameters on GONC was investigated during this experiment. All the operational parameters i.e., pH of the solution, adsorbent dose, initial dye concentration and temperature kept at its optimum point (adsorbent dose – 0.1 g/l, solution pH- 6, temperature- 40 °C and initial dye concentration-50 mg/l). Figure no 5.15 shows that up to 60 min the increasing trend was observed beyond that the removal was constant. Figure no 5.16, 5.17 and 5.18 shows experimental analysis images of CR by R-GO, GO and GONC respectively.

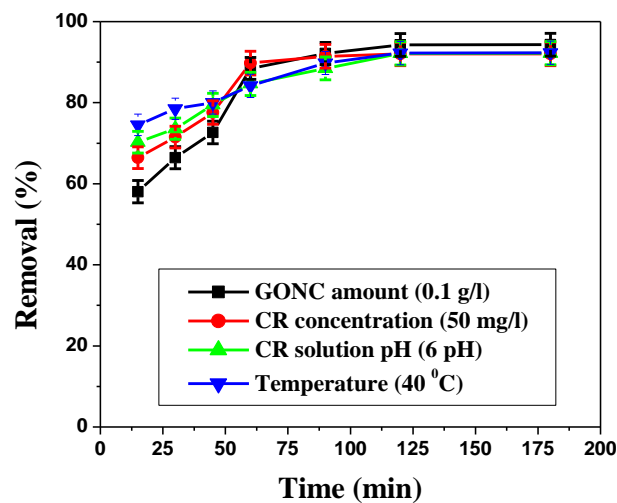


Figure no 5.15 Equilibrium study of CR by GONC



Figure 5.16 CR remove by R-GO Figure 5.17 CR remove by GO Figure 5.18 CR remove by GONC

5.2.3 Adsorption Isotherms:

An adsorption isotherm established the equilibrium connection between the adsorbate concentration in the liquid phase and that on the adsorbent surface in solid phase at a given condition (Dawood and Sen et al., 2012). Data was obtained from the experiments were analyzed by the Langmuir, Freundlich and Temkin isotherms models. An idea of adsorption capacity of adsorbents R-GO, GO and GONC for removal of CR from its aqueous solution was calculated from the models equations. The details of Langmuir, Freundlich and Temkin models were already discussed in chapter no 2. The ability of isotherms models is correlate the experimental data was assessed by the regression coefficient (R^2) and Chi-square (χ^2) analysis. The models parameters were calculated from slop and intercept of the linear equations.

Langmuir isotherms model describe the monolayer adsorption process with homogeneous distribution of dye molecules onto the adsorbent surface (Sajab et al., 2011). The Langmuir parameters q_0 and b was calculated from slop and intercept of linearized plot of C_e/q_e vs C_e . Furthermore the high R^2 value and small c indicate the applicability of the model. The R^2 of GONC is higher compare with R-GO and GO along with small χ^2 value which reflects the Langmuir model was better represent the experimental data.

Unlike Langmuir isotherms, Freundlich isotherms assume the multilayer adsorption process of adsorbate on heterogeneous adsorbent surface. The Freundlich models constant parameters K_F and n was calculated from the slop and intercept of the linear plots $\ln q_e$ vs $\ln C_e$ for R-GO, GO and GONC. The slope of $1/n$ was ranging between 0 to 1 is a measure of adsorption intensity or better called surface heterogeneity. The surface of

adsorbents is more heterogeneous when its value is close to zero (Haghseresh et al., 2005). The value of R^2 and χ^2 indicates the applicability of the model.

Temkin isotherms model assumes that the heat of adsorption process decreases linearly with the increase in coverage area of adsorbent surface. The process is characterized by uniformly distributed binding energies between the adsorbate molecules and adsorbent active sites (Limousin et al., 2007). The model constant parameters B_T and K_T was calculated from slope and intercept of the linearized plot q_e vs $\ln C_e$. The highest value of regrotational coefficient and smallest value of chi-square assure that co-relation between experimental data with the model. GONC posses the highest value of R^2 comparing with R-GO and GO. Among the three models Langmuir model was better represent the experimental data with highest R^2 value and smallest χ^2 value. The value of all constant for all the models were listed in table no 5.1.

Table no 5.1 Isotherms Parameters of CR:

Isotherms models	Parameters	Adsorbents		
		GO	R-GO	GONC
Langmuir model	q_0 (mg/g)	100	85.47	100
	B (l/mg)	0.101	0.970	0.103
	R^2	0.9919	0.8784	0.9996
	χ^2	0.263	0.426	0.157
Freundlich model	K_F (mg/g (l/mg) ^{1/n})	31.19	13.170	30.87
	$1/n$	0.548	0.615	0.499
	R^2	0.7912	0.7726	0.9654
	χ^2	18.64	22.52	12.63
Temkin model	B_T (l/g)	21.105	2.935	22.83
	K_T	4.397	9.702	2.542
	R^2	0.8414	0.8335	0.9276
	χ^2	13.62	17.85	14.33

5.2.4. Adsorption kinetics:

The prediction of adsorption reaction rate and mechanism of process is an important step to be considered. To execute this purpose, the adsorption dynamics of CR on R-GO, GO and GONC were investigated using various kinetics model viz., Pseudo-first-order, Pseudo-second-order and Inter particle diffusion model. Generally, four following steps are take place during the adsorption process: (1) migration of dye molecules take place

from its aqueous phase through liquid film to the exterior surface of adsorbent, (2) diffusion of dye molecules across the boundary liquid film surrounded by the adsorbent surface, (3) intra molecular diffusion into the interior surface of the adsorbent, and (4) adsorption occurs on the active sites of the adsorbent. The process of adsorption can be considered as a quasi-instantaneous system. Since the boundary layer diffusion does not exist, the first and second steps may play a very vital role in determining the rate constant of the adsorption process (Oladoja and Akinlabi, 2009).

In adsorption kinetics the pseudo-first-order model has limited applicability. Pseudo-first-order kinetics model does not govern by the diffusion process, the rate is directly proportional to the unit power of the concentration of the reactant (Oladoja and Akinlabi, 2009). The details of pseudo-first-order kinetics reaction were already discussed in the chapter no 2. The linear plot of $\ln(q_e - q_t)$ vs t provides poor R^2 value and large χ^2 value and shows high disparity between experimental adsorption capacity and calculated one for R-GO, GO and GONC were listed in tabulated form (Table no 5.2).

Pseudo-second-order kinetics model is the most stable and acceptable kinetics model which correlates the diffusion of liquid film on to the adsorbent surface. The linear plot of t/q_t vs t (Fig.) provides greater R^2 value and small χ^2 value depicts the better correlation between experimental data with the model (Saeed et al., 2010). The reaction rate constant K_2 and q_e (adsorption capacity) were calculated from the intercept and slope of the equation and shows the less disparity between experimental and calculated one. The chi-square (χ^2) value was small for GONC compared with R-GO and GO predicted that GONC better represents the second-order kinetics model.

Adsorption process is not only governed by the surface phenomenon but also intramolecular diffusion or combination of both. The linear plot qt vs $t^{1/2}$ provides the complexity nature of adsorption process (Mall et al., 2005). The rate constant K_{diff} was calculated from the slope of the graph. The intra-particle diffusion would be the controlling step if the line passes through the origin, if the plots do not pass through the origin it indicates that some boundary layer diffusion process takes place during adsorption experiment (Oladoja and Akinlabi, 2009). The value of R^2 and χ^2 depicts the feasibility of adsorption process were listed in table no 5.2. From the table no 5.2 it was observed that GONC possesses high R^2 value than R-GO and GO but comparing less with its pseudo-second-order kinetics model value.

Table no. 5.2 Adsorption kinetics parameters of CR:

Kinetics models	Parameters	Adsorbents					
		GO		R-GO		GONC	
		q _e exp	q _e cal	q _e exp	q _e cal	q _e exp	q _e cal
Pseudo-first-order	q _e (mg/g)	42.52	45.31	35.85	34.56	54.56	58.61
	K ₁ (h)	0.013		0.073		3.93	
	R ²	0.7210		0.5789		0.9452	
	χ ²	20.56		24.25		19.63	
Pseudo-second-order	q _e (mg/g)	44.54	47.52	33.11	33.05	71.81	73.23
	K ₂ (g g/h)	0.0057		0.0067		0.0008	
	R ²	0.9613		0.9441		0.9997	
	χ ²	17.32		21.56		15.56	
Intraparticle Diffusion	q _e (mg/g)	35.56	36.44	41.85	43.63	70.89	74.58
	K _p (mg/g h ^{1/2})	0.425		2.075		6.241	
	R ²	0.6461		0.9028		0.9847	
	χ ²	23.54		26.11		23.23	

5.2.5 Adsorption Thermodynamics:

The activation energy (E_a kJ/mol) is defined as the amount of energy that must be overcome by the adsorbate molecules and get attached or react with active sites on the surface of the adsorbent. The value of E_a (GO-41.06, RGO-31.21, GONC- 54.45 kJ/mol) obtained from the linear plot of lnK versus 1/T indicating that the adsorption process is physisorption in nature (Anirudhan and Radhakrishnan, 2008). The Eyring equation was used to calculate the standard enthalpy (ΔH⁰) and standard entropy (ΔS⁰). The value of ΔH⁰ and ΔS⁰ were computed using the following equation:

$$\ln K_d = \frac{\Delta S^0}{R} - \frac{\Delta H^0}{RT} \quad (28)$$

where R (8.314 J/mol K) is the universal gas constant, T(K) is the temperature of the solution and K_d is the distribution coefficient which can be calculated as:

$$K_d = \frac{C_{Ae}}{C_e} \quad (29)$$

where C_{Ae} is the amount of dye adsorbed on adsorbent at equilibrium and C_e is the equilibrium concentration.

The values of ΔH^0 and ΔS^0 were calculated from slope and intercept of the linear plot $\ln K_d$ versus $1/T$ and listed in table no 5.3. The positive value of ΔH^0 (GO-64.03, R-GO-11.29 and GONC- 67.30 kJ/mol) indicates the process is endothermic in nature and positive value of ΔS^0 (GO-2.17, R-GO-1.99 and GONC- 3.97 kJ/mol) demonstrate the increased randomness between solid-solute interface. The value of ΔH^0 and ΔS^0 for GONC is higher than GO and R-GO. The value of gibbs free energy (ΔG^0) determines the nature of process whether it is physisorption or chemisorption in nature. In general sense the values of ΔG^0 in between 0 to -20 kJ/mol indicates the process in physisorption in nature, while the value in between -80 to -200 kJ/mol indicates chemisorptions (Weng et al., 2009) (Nasuha et al., 2011). The negative value of ΔG^0 for various temperatures corresponds to the spontaneous nature of adsorption (Liu et al., 2012). The values of ΔG^0 , ΔH^0 , ΔS^0 for GO, R-GO, GONC were listed in table no 5.3.

Table no 5.3: Thermodynamics parameters of CR.

Temperature	Parameters	Adsorbents		
		GO	RGO	GONC
303 K	ΔG^0 (kJ/mol)	-2.568	-2.001	-5.632
	ΔH^0 (kJ/mol)	64.03	11.59	67.30
	ΔS^0 (J/mol K)	2.170	1.99	3.97
308 K	ΔG^0 (kJ/mol)	-3.213	-2.896	-6.524
	ΔH^0 (kJ/mol)	64.03	11.59	67.30
	ΔS^0 (J/mol K)	2.170	1.99	3.97
313 K	ΔG^0 (kJ/mol)	-4.460	-3.200	-9.152
	ΔH^0 (kJ/mol)	64.03	11.59	67.30
	ΔS^0 (J/mol K)	2.170	1.99	3.97

5.2.6. Response surface methodology used for optimization of CR adsorption by GONC:

5.2.6.1 Model verification and develop regression model equation:

Response surface methodology is a technique used for establish a relationship between mathematical and statistical model. It is used to refine the model and compute the relationship between the independent process factors and impact on the process response. The response surface methodology is based on two different techniques such as- 1. Central Composite Design (CCD), 2. Box-Behnken Design (BBD).

CCD is the most commonly used design have factorial or fractional factorial model with centre point along with the groups of axial points which helps to estimates the curvature or locus of the present experiments. It can fit a full quadric model with up to five levels of independent process factors.

BBD usually has fewer design points than CCD and less useful to estimate the relationship between statistical and mathematical one. BBD better represent up to three independent factors also unlike CCD, BBD can includes the runs where all the factors are at extreme settings. In this study CCD has been used to compute the relationship.

From the batch experiment and different process model it was observed that GONC posses better remove efficiency of CR from its aqueous mode with better represent process models than GO and RGO. RSM study of CR was analyzed for GONC with three independent process factors viz., adsorbent dose (mg), pH of the CR solution, reaction time (min) and their impact on the response (removal percentage) were investigated. The model was suggested twenty experiments listed in table no 5.4.

The best fitted polynomial quadratic equation for describing response (removal percentage) was obtained performing regression modeling between response and three process variable pH, dose and time. Amongst linear, two-factor interaction (2FI), quadratic and cubic polynomials models the quadratic model was considered to be most appropriate for this process by Design Expert software as it exhibit lower value of process standard deviation along with higher R^2 values and insignificant lack of fit. All the parameters value was listed in table no 5.5 (Anderson and Whitcomb, 2005). The best fitted polynomial quadratic equation for describing the response (removal percentage) was obtained performing regression modeling between response and coded values of three independent process variables using the experimental data can be written in terms of actual parameters as follows,

$$\begin{aligned} \text{Response} = & 5.823 + 15.29 * \text{pH} + 0.99 * \text{Dose} + 0.54 * \text{Time} + 0.018 * \text{pH} * \text{Dose} \\ & - 0.02 * \text{pH} * \text{Time} - 3.92 * \text{Dose} * \text{Time} - 1.32 * \text{pH}^2 - 3.37 * \text{Dose}^2 \\ & - 2.19 * \text{Time}^2 \end{aligned}$$

Both magnitude and sign are very crucial for the regression coefficients, as the earlier signify the importance of the variables on the response factor and the later decides its effect on direction. The constant 5.823 was independent for any factor and interaction of factors. A positive sign of the coefficients correspond to synergistic effect on response, while a negative sign signifies an antagonistic effect on response (Singh et al., 2011). The interaction terms (except pH*Dose), (pH* Time), (Dose*Time) and second-order terms pH², Dose² and Time² had a negative effect on response. Hence the response will decrease as the value of these terms increase. Whereas, the linear terms pH, Time, Dose, interaction term (pH *Dose) had a positive influence which indicate that with an increase of these factors there will be an increase in response i.e removal percentage of CR.

Table no: 5.5 Fit summery of different model

Source	Linear	2FI	Quadratic	Cubic
Sum of squares	76.15	72.59	15.74	8.47
Mean square	6.92	9.07	0.315	0.847
F-value	258.634	45.528	321.587	78.355
Lack of fit P-value	<0.005	0.0542	<0.0001	0.0310
Std. Dev.	2.18	2.36	0.125	1.19
R ²	0.3606	0.3905	0.9286	0.8678
Adjusted R ²	0.2407	0.1093	0.8748	0.6542
Predicted R ²	0.1154	0.0652	0.8488	0.5135
PRESS	119.13	124.75	284.18	65.34
Remarks			Suggested	Aliased

Table no: 5.4 Model experimental analysis:

Run	Factor 1 A: pH	Factor 2B: Adsorbent dose (mg)	Factor 3 C: Time (min)	Response (Removal percentage)
1	6.00	125.00	155.79	90.25
2	6.00	125.00	67.50	87.56
3	1.00	125.00	67.50	40.25
4	2.00	50.00	120.00	27.88
5	6.00	125.00	67.50	87.56
6	6.00	125.00	67.50	87.56
7	10.00	50.00	120.00	24.75
8	2.00	50.00	15.00	16.85
9	6.00	125.00	67.50	87.56
10	6.00	125.00	67.50	87.56
11	2.00	200.00	15.00	21.54
12	10.00	200.00	15.00	57.85
13	12.73	125.00	67.50	43.56
14	6.00	1.13	67.50	5.12
15	10.00	200.00	120.00	50.65
16	6.00	125.00	67.50	87.56
17	6.00	125.00	20.79	78.86
18	10.00	50.00	15.00	4.01
19	2.00	200.00	120.00	59.26
20	6.00	251.13	67.50	91.02

5.2.6.2. Analysis of variance (ANOVA)

ANOVA was performed to verify the satisfactoriness of the developed quadratic model. The model and model terms are regarded as significant only when the values of Prob>F are less than 0.003. The terms with higher F-value and lower p-value have greater importance to produce an impact on response (removal percentage). The P-value and F-value of model were found to be <0.0002 and 105.308, respectively, which implies that the model is highly significant and better, co-relate the experimental data with statistical model. Among all the parameters the linear terms (A, B, C), interaction term (A×B), and square terms, B² and C², showed most significant effect on response, having P-value <0.002 table no 5.6 represent ANOVA (significant and not significant terms). The model shows a reasonable conformity between model R² (0.9589) and predicted R² (0.9188), adjusted R² value (0.9256) was obtained by ANOVA study. Thus, the developed quadratic model was found to be suitable for representing the experimental data of adsorption of CR by GONC. The analysis of statistical properties of the model was also performed by normal percentage probability plot of the residuals, a system for assessing the better relationship between the set of observed values with the theoretical distribution (Bingol et al., 2010). Approximately linear data points indicated the process was followed normal distribution (Figure 5.17). Furthermore, a high value of R² (0.9286) and a realistic agreement of predicted R² (0.8488) with adjusted R² value (0.8748) verified the capability of the fitted quadratic model for predicting percentage removal of CR for adsorption process. The predicted Verses actual graph represents in figure no 5.18. Thus all of these statistical tests showed that the developed quadratic model was suitable for representing the data and reasonably able to interpret the relationship between the process variables and response.

5.2.7. Graphical interpretation of models by 3D response surface and contour plots: Interaction effects of process variables on response

The graphical representation of the individual parameter and their interactive effects of process variables on response (removal percentage) within the experimental range were obtained through three dimensional responses surface and contour plots. The three-dimensional response surface and contour plots were generated using Design expert software (version 7.2.0) by varying two variables within the experimental range and keeping the other parameter constant at zero level.

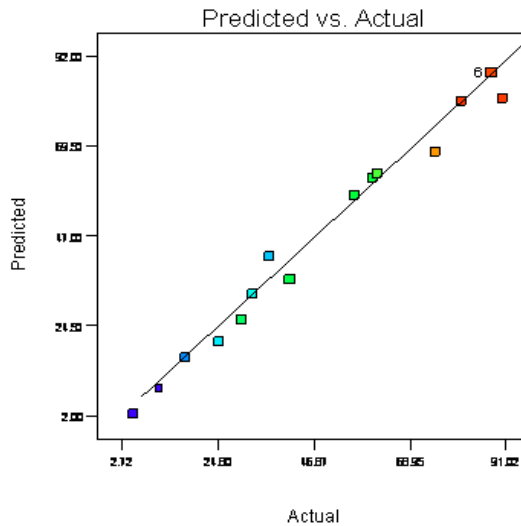
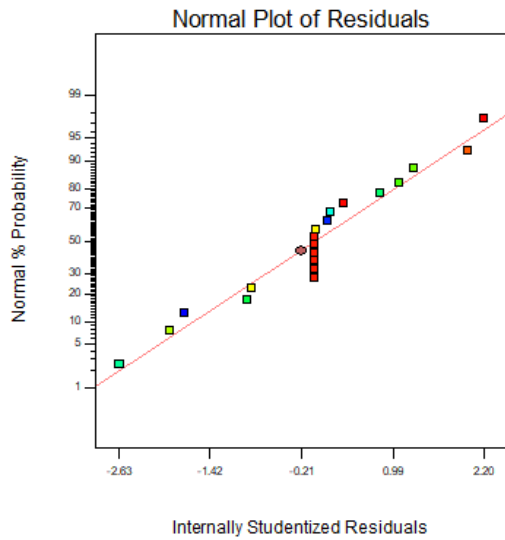


Figure no 5.19 Normal probability vs Residual Figure no 5.20 Predicted vs Actual graph

5.2.7.1. Effect of adsorbent dose (GONC) and pH of the solution:

The pH of the solution and adsorbent dose were considered to be, one of the most influencing parameter of adsorption process figure no 5.19 and 5.20. From the figure it was observed that the mutual effect of pH of the solution and adsorbent dose on process response at constant time (67.50 min). An increase in pH of the solution correspond to the increase in response function up to certain limit after that the response function shows reverse trend. The reason may be due to the fact that the accessibility of surface function enhances with the increase the pH up to certain limit beyond that the negative trend was observed. These observations were consistence with the batch study experiment.

5.2.7.2. Effect of pH of the solution and reaction time (min):

The pH of the solution and reaction time (min) were analyzed for the process figure no 5.21 and 5.22. From the figure it was observed that the effect of pH of the solution was directly related with the reaction time for the process response at constant adsorbent dose (125.00 mg). An increase in pH of the solution corresponds to the increase in response function with time increase. The reason may be due to the fact that the accessibility of surface function enhances with the increase the pH of the solution with time. These observations were better consistence with the batch study experimental data.

5.6 ANOVA table (significant and not significant terms):

Source	Sum-of Square	DF	Mean Square	F value	P-value prob> F	Remarks
Model	110.36	9	11.48	105.3	< 0.0002	Significant
A-pH	3.1218	1	4.21	65.24	< 0.0002	Significant
B-Dose	2.5641	1	8.75	32.54	< 0.0001	Significant
C-Time	1.5421	1	5.21	30.46	< 0.0002	Significant
AB	0.2478	1	0.654	5.21	< 0.0002	Significant
AC	0.2258	1	0.241	2.51	0.2425	
BC	0.2142	1	0.471	4.23	0.3145	
A²	0.2143	1	0.2143	0.452	0.2541	
B²	25.32	1	25.324	322.14	< 0.0002	Significant
C²	32.62	1	32.621	401.52	< 0.0002	Significant
Residual	0.0549	10	0.07824			
Lack of Fit	0.3842	5	0.0365	3.2145	0.5421	
Pure error	0.0322	5	0.113			Not Significant

5.2.7.3. Effect of adsorbent dose (mg) and reaction time (min):

The mutual effect of adsorbent dose and reaction time was analyzed in the figure no 5.23 and 5.24. The response function i.e, percentage removal was increased with the increase of adsorbent dose with time. The accessibility of active site of the adsorbent was enhanced with the reaction time at constant pH (6.00) of the solution. The adsorbent

molecules get more attached with the functional group of the adsorbent and hence increase the response for the process. The experimental data was better match with the model result.

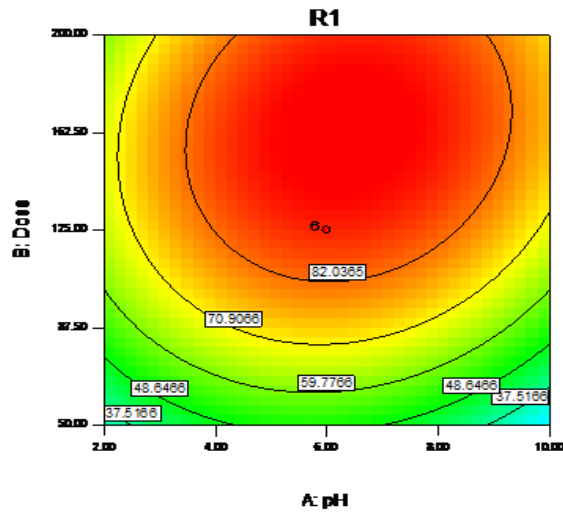


Figure no 5.21 Dose vs pH (contour plot)

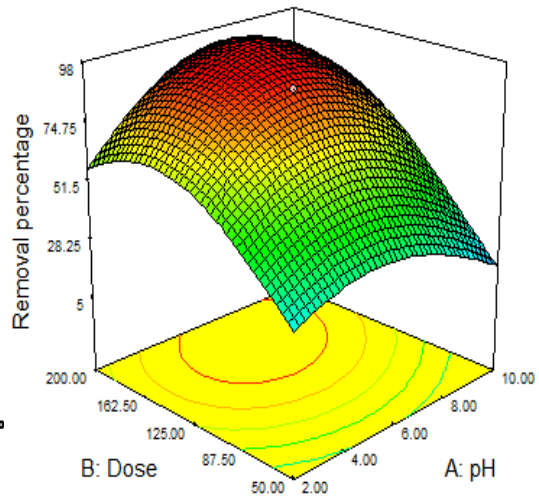


Figure no 5.22 Dose vs pH (3D plot)

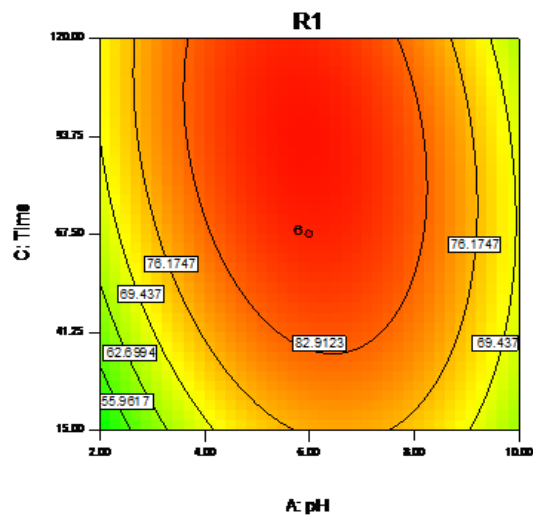


Figure no 5.23 Time Vs pH (contour plot)

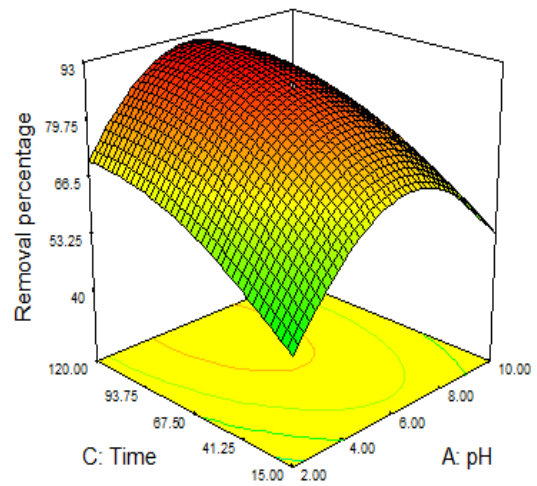


Figure no 5.24 Time Vs pH (3D plot)

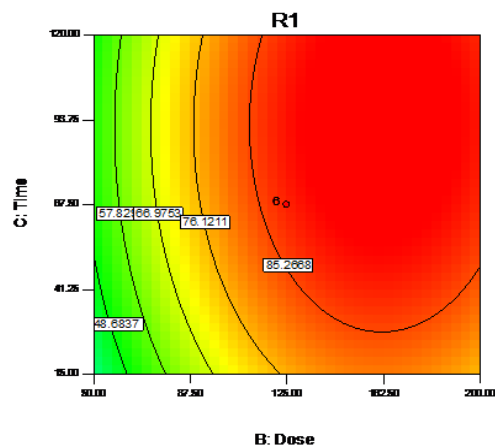


Figure no 5.25 Time Vs Dose (contour plot)

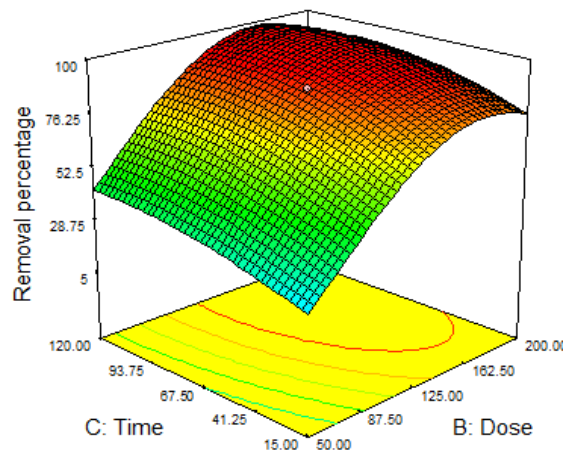


Figure no 5.26 Time Vs Dose (3D plot)

5.2.8 Optimization and confirmation of reaction condition:

Design Expert software generated a set of results to predict optimum reaction conditions using the quadratic model. To achieve maximum removal percentage (90.25), from process optimization modeling the optimum initial pH, adsorbent dose and reaction time were found to be 6.00, 125.00 mg, 67.50 min respectively. A good agreement was observed between the predicted R^2 (0.9712) by model and the corresponding R^2 (0.9885) value obtained from the experimental data, which indicates the suitability of the model for predicting the response as well as to optimize the process conditions.

5.2.9. Column experimental study:

5.2.9.1. Effect of various parameters on column performance:

The effects of various parameters like bed height, flow rate and influent dye concentration were analyzed for the adsorption of CR by GONC in column mode. The breakthrough curves of dye adsorption at column mode of different conditions were expressed by plotting C_t/C_o versus t . A breakthrough curve generated from an ideal column mode adsorption system has a typical 'S' type shape. However, the breakthrough curves obtained during this study did not match with the theoretical 'S' shaped. The reason behind the deviation of the experimental breakthrough curves from their distinctive theoretic appearance can be endorsed by the two factors. Firstly, the slow adsorption rate kinetics of dyes molecules and secondly, the use of small lab-scale column equipments makes the breakthrough faster which leads to an incomplete 'S' shape of the plot (Al-Degs et al., 2009).

5.2.9.2. Effect of bed depth

The effect of various bed heights (2, 3 and 5 cm) on column performance were evaluated during this experiment which were obtained when the column was packed with 4, 6 and 8 g of GONC respectively. Adsorption breakthrough curves (Figure no 5.27) for different bed depths at 5 ml/min of input flow rate with input concentration 100 ml/min were considered by plotting C_t/C_o versus t . the data obtained from the experiment were

presented in tabulated form and it was observed that as the bed height in column was directly proportional with the amount of total mass of dye adsorbed (m_{ad}) at exhaustion time. Maximum bed capacity was obtained at highest bed height. This is due to the fact that as the column bed height increases, the surface area of adsorbent also increases. As a result the contact time of adsorbate with active sites of adsorbent increases which give rise in the removal percentage of CR on GONC. Thus, when the column bed depth was increased from 2 to 5 cm, t_b and t_e are increased from 160 to 290 min and 230 to 380 min, respectively listed in table no 5.7.

Table no 5.7 Effect of different bed height, concentration and flow rate on column adsorption

Z (cm)	F (ml/min)	C ₀ (mg/l)	t _b (min)	t _e (min)	m _{ad} (mg)	q _{e,exp} (mg/g)
2	5	100	160	230	23.46	2.005
3	5	100	250	340	29.67	2.42
5	5	100	290	380	35.91	2.53
3	10	100	210	350	21.52	2.002
3	15	100	190	285	18.34	1.92
3	5	150	165	270	22.23	2.23

5.2.9.3. Effect of flow rate:

The effect of performance of the column at fixed bed height and concentration (3 cm, 100 mg/l) by the different flow rate were analyzed during this column study. Figure no 5.28 represent the relationship between C_t/C_0 with time at different flow rate (5, 10, 15 ml/min). The break through time and the exhaustion time decreased from 275 to 170 min and 415 to 210 min respectively when flow rate was increased from 5 to 15 ml/min respectively. The reason behind this phenomenon is that the residence time of the dye molecules was decreased when the flow rate was increased. This leads to decreased the

removal efficiency and break through time along with exhaustion time (Uddin et al., 2009).

5.2.9.4. Effect of initial dye concentration:

The influent dye concentrations have detrimental effect to the column performance. The various influent dye concentration i.e., 100 and 150 mg/l (figure no 5.29) were analyzed during this study. From the figure no 5.30 (experimental set up), it was clearly observed that the break through time and exhaustion time was decreased from 242 to 205 min and 365 to 260 min when concentration of dye increased from 100 to 150 mg/l respectively. At higher concentration the concentration gradient increased the diffusion coefficient and fast saturation of active sites of the adsorbents which may leads to the decrease of break through time and exhaustion time respectively (Han et al., 2009).

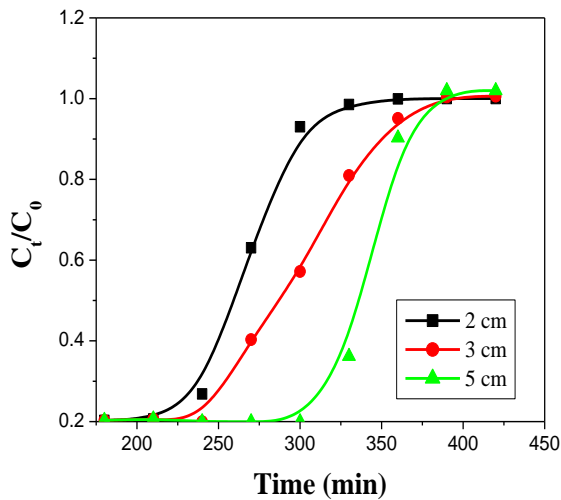


Figure 5.27 Column study (bed height)

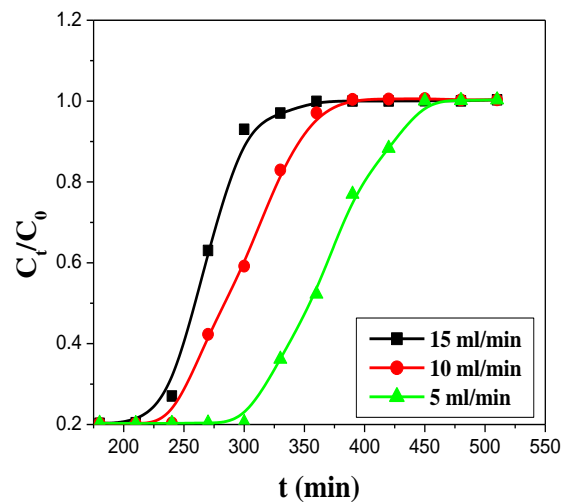


Figure 5.28 Column study (flow rate)

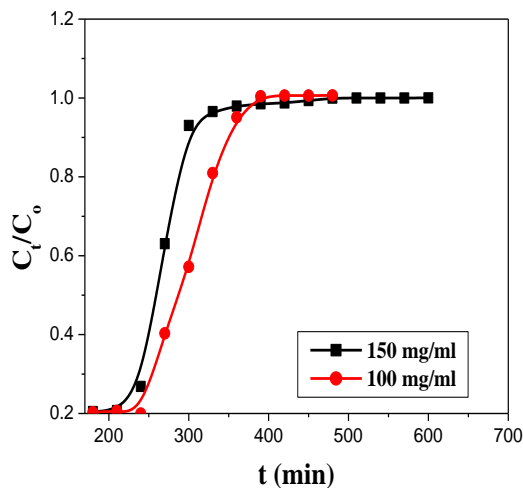


Figure no 5.29 Column study (concentration)



Figure no 5.30 Column study (experimental set-up)

5.2.10. Modeling of column data:

5.2.10.1. Thomas model:

The experimental data obtained from the column experiment for CR adsorption by GONC subjected to analyze Thomas model and BDST model. The data at C_t/C_o values was taken higher than 0.05 and lower than 0.98 were considered for modeling. Thomas rate constant (K_{Th}) and adsorption capacity (q_e) were obtained from the slope and intercepts, obtained using linear regression (Uddin et al., 2009). Thomas model parameters are presented in table. The R^2 values ranging from 0.87 to 0.92 are evaluated from regression coefficient analysis. As the flow rate of the operating column increased the bed capacity, q_e , decreased, k_{Th} , decreased. Conversely, with the increase in the initial dye concentration at constant bed height (3cm) the value of q_e decreased along with the value of k_{Th} decreased. Thus, better column performance can be achieved with lower flow rate, lower concentration at constant bed height. It is evident from Table 5.8 that the experimental and calculated adsorption capacities are close at all the operating conditions studied it evident the experimental data satisfy the column model.

Table no. 5.8 Thomas model constant value:

C_o (mg/l)	Q (ml/min)	K_{Th} (ml. min./mg)	q_e exp (mg/g)	q_e cal (mg/g)	R^2
100	5	0.0354	9.81	9.36	0.9225
150	10	0.0265	6.54	6.02	0.8754

5.2.9.2. BDST model:

The ability of BDST model to predict column performance was investigated utilizing experimental data obtained from column experiment. The constants, N_o and K_a , were calculated from t_s vs. Z plots for different column bed depth of 2, 3 and 5 cm. The high R^2 values ranging from 0.96 to 0.98 demonstrates the validity of BDST model and better represent the experimental data compare to Thomas model. The value of N_o , K_a , a , b were calculated from the equation and listed in table no 5.9 and 5.10 (unknown flow rate and unknown concentration). The lower adsorption capacity at low breakthrough point

than that at exhausted condition of column bed is due to the un-saturation of several adsorbent active sites by the dye molecules.

Table no 5.9 BDST model constant values:

Bed depth Z (cm)	a (min/cm)	b (min)	K_a (l/mg/min)	N_0 (mg/l)	R^2
2	8.47	-0.458	0.0008	152.38	0.9652
3	19.143	29.28	0.00153	286.56	0.9867
5	19.162	29.34	0.00126	288.23	0.9832

Table no 5.10 Breakthrough time calculated using BDST constant for new flow rate or new concentration of CR (Z=bed height= 3 cm):

C_t/C_0	a (min/cm)	b (min)	t_{cal} (min)	t_{exp} (min)
F= 3 ml/min C ₀ = 75 mg/l	F= 3ml/min C ₀ = 75 mg/l	F= 3ml/min C ₀ = 75 mg/l	F= 3ml/min C ₀ = 75 mg/l	F= 3ml/min C ₀ = 75 mg/l
0.2	6.423	0.415	57	65
0.9	38.98	2.65	255	240
F= 20ml/min C ₀ = 200 mg/l	F= 20ml/min C ₀ = 200 mg/l	F= 20ml/min C ₀ = 200 mg/l	F= 20ml/min C ₀ = 200 mg/l	F= 20ml/min C ₀ = 200 mg/l
0.2	1.564	0.643	45	35
0.9	7.782	0.024	150	165

5.3. Metanil yellow:

5.3.1. Batch adsorption study (MY):

The removal efficiency of MY by GO, R-GO and GONC at various operational parameters were evaluated during this experimental study. The aqueous metanil yellow solution of 100 ml was taken in 250 ml conical flask varying operational parameters and keeping other parameters constant.

5.3.1.1. Effect of adsorbent dose:

The primary importance to investigate the effect of adsorbent dose comes from the economical point of view that required minimum amount of adsorbent was required for effective removal of dye molecules from its aqueous phase. The dye removal efficiency of adsorbents were increased with the amount of adsorbent increase up to 0.10 g/l after that for higher dose no drastic change in removal percentage was observed. The increase in amount of adsorbents leads to the increase the surface area which may leads to the increase the active sites present in the adsorbent thus also boost up the interaction between adsorbents and dyes molecules presents in aqueous phase (Ahmed et al., 2009). Form the figure no 5.31, 5.32, 5.33, it was clearly observed that GONC shows better removal efficiency than R-GO and GO due to the more number of potential active sites presents in its structure.

5.3.1.2. Effect of initial dye concentration:

Initial adsorbate concentration has adverse effect on adsorption capacity of adsorbents (GO, R-GO, GONC). It is evident from the figure no 5.34, 5.35, 5.36 that the removal percentage of MY by R-GO, GO and GONC were decreasing with the increasing initial dye concentration form 10-100 mg/l, at lower concentration the molecules being attached by the active sites of the adsorbents. Further increase the concentration, the more number of molecules of dye gets un-reacted and hence decreases the removal percentage because the constant adsorbents dose (Ahmad et al., 2009). The GONC shows the better removal efficiency comparing with R-GO and GO because large number of active sites presents in its structure. Accordingly, for constant adsorbent dosage, the availability of adsorption sites is constant, at higher initial dye concentration the adsorption sites are easily saturated by the

dye molecules. The maximum amount of unsaturated dye molecules presents into the solution which leads to the lower removal percent and the dye adsorption becomes solely depended on the initial concentration.

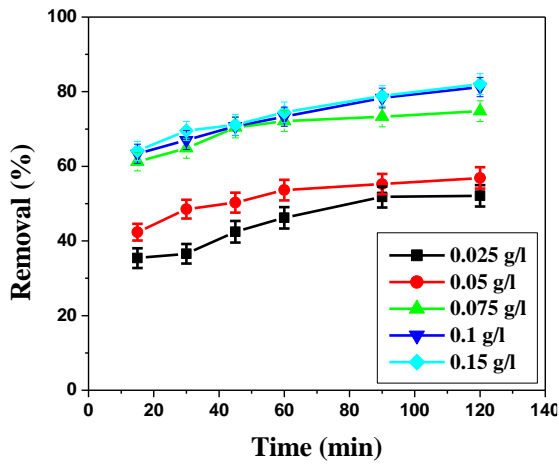


Figure no 5.31 MY removal by R-GO

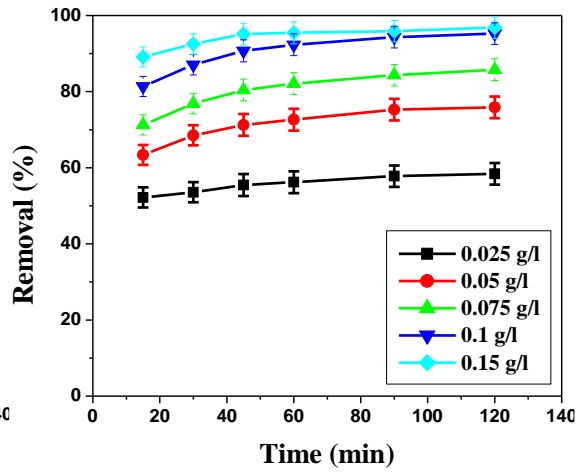


Figure no 5.32 MY removal by GO

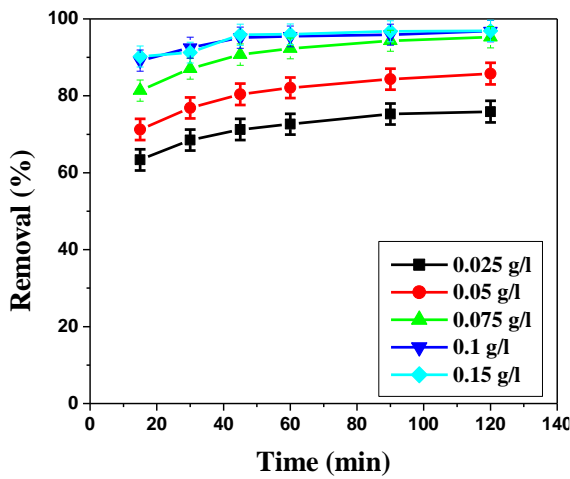


Figure no 5.33 MY removal by GONC

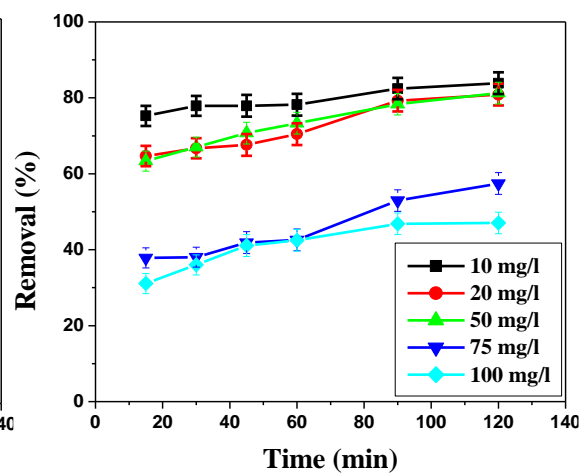


Figure no 5.34 MY removal by R-GO (Concentration)

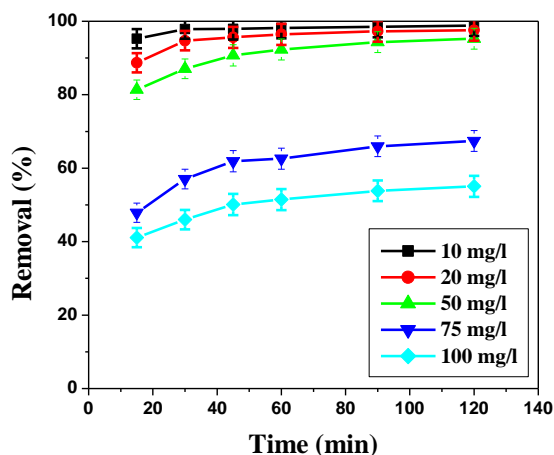


Figure no 5.35 MY removal by GO at conc.

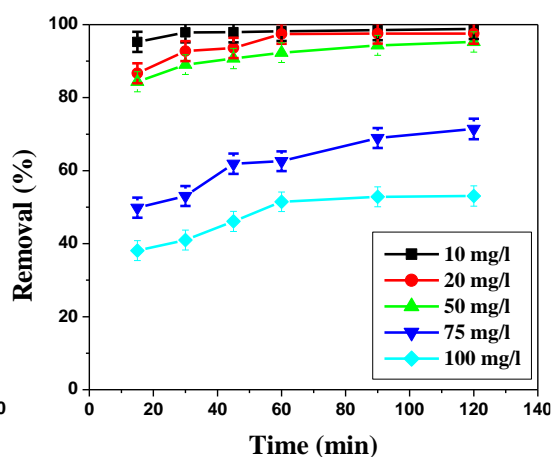


Figure no 5.36 MY removal by GONC at conc.

5.3.1.3. Effect of pH of the solution:

The pH has an important effect on dye adsorption experiment; the pH of the medium will control the magnitude of the electro-static charges that are produced by the ionized dye molecules (Khan et al., 2013). In the figure no 5.37, 5.38, 5.39 shows the percentage removal of MY at different pH with respect to time for R-GO, GO and GONC were evaluated during this study. The removal percentage of MY was decreased with the increase of pH of the solution for all adsorbents, the better result was observed at pH 2. Though MY is an acidic in nature, at dissociation its colour containing groups (chromophoric groups) are negatively charged which attract positively charged active sites of the adsorbent. The removal efficiency was better for GONC compare with R-GO and GO due to the large number of active sites presents into GONC structure which attract more number of ionized dye molecules present into the solution.

5.3.1.4. Effect of temperature on dye adsorption:

The influence of temperature on adsorption process is very important for dye adsorption as shown on figure no 5.40, 5.41, 5.42. The removal percentage and efficiency were increased with the increasing the temperature from 20 °C to 40 °C for all adsorbent. If the percentage removal of dye molecules increases with increasing temperature then the adsorption is an endothermic in nature (Senthil kumar et al.2006). The GONC shows the better removal than R-GO and GO, because at higher temperature the mobility between the dye molecules increased which leads to the better interaction between active sites of adsorbents and dye molecules. The increasing trend was observed up to 40 °C beyond that the percentage removal decreased. The reason behind this phenomenon as suggested by (Chatterjee et al., 2007) (Chiou et. al., 2009) at high temperature weakening the physical

bonds between the adsorbate molecules and active sites which may leads to the decrease in adsorption efficiency.

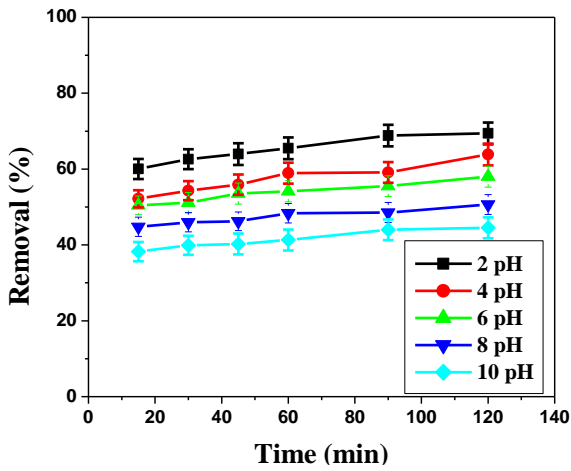


Figure no 5.37 MY removal by R-GO at pH

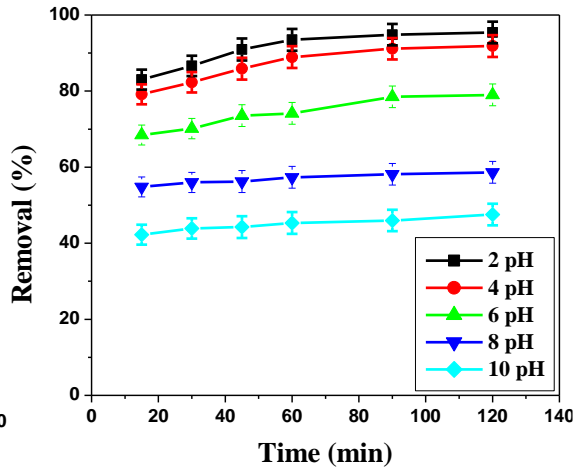


Figure no 5.38 MY removal by GO at pH

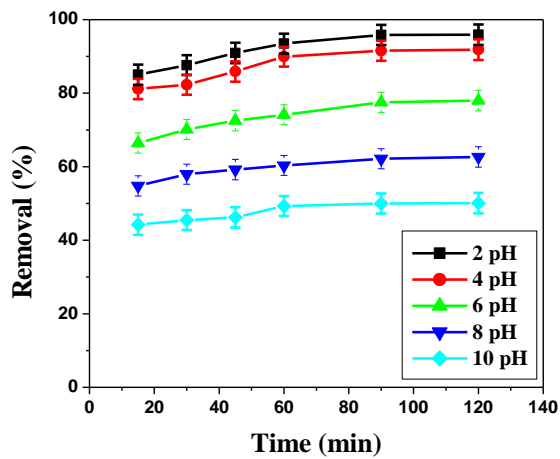


Figure no 5.39 MY removal by GONC at pH

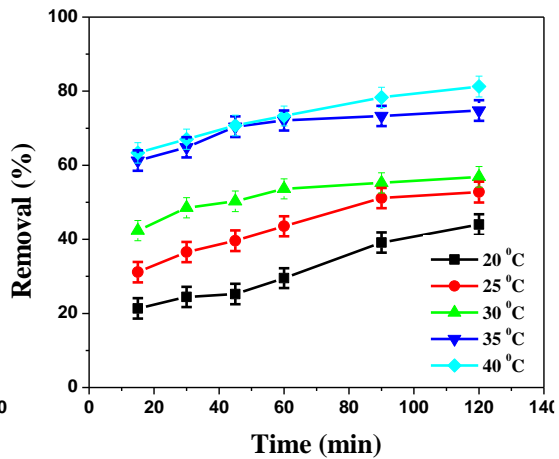


Figure no 5.38 MY removal by R-GO at Temp (°C)

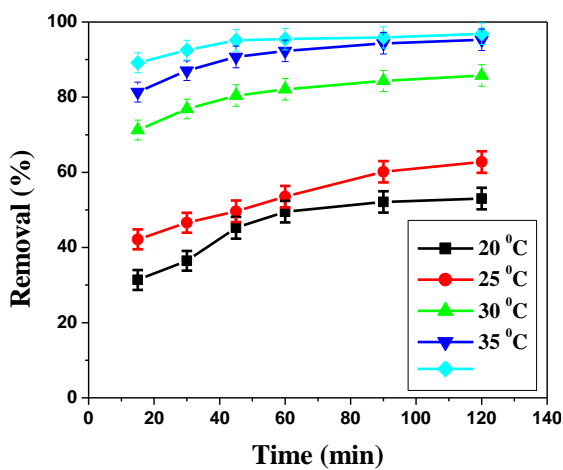


Figure no 5.39 MY removal by GO at Temp.

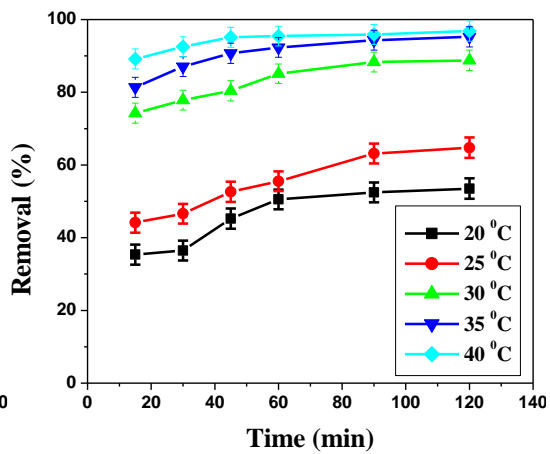


Figure no 5.40 MY removal by GONC at Temp

5.3.2. Equilibrium study of MY by GONC:

To evaluate the effect of all operational parameters on MY removal by GONC was investigated during this experiment. All the operational parameters i.e., pH of the solution, adsorbent dose, initial dye concentration and temperature kept at its optimum point (adsorbent dose – 0.1 g/l, solution pH- 2, temperature- 40 °C and initial dye concentration-50 mg/l). Figure no 5.43 (equilibrium graph) 5.44, 5.45, 5.46 (experimental study) shows that up to 40 min the increasing trend was observed beyond that the removal was constant. It was evident that more than ninety percent of MY molecules were removed from its aqueous phase by GONC effectively at approximately 60 min.

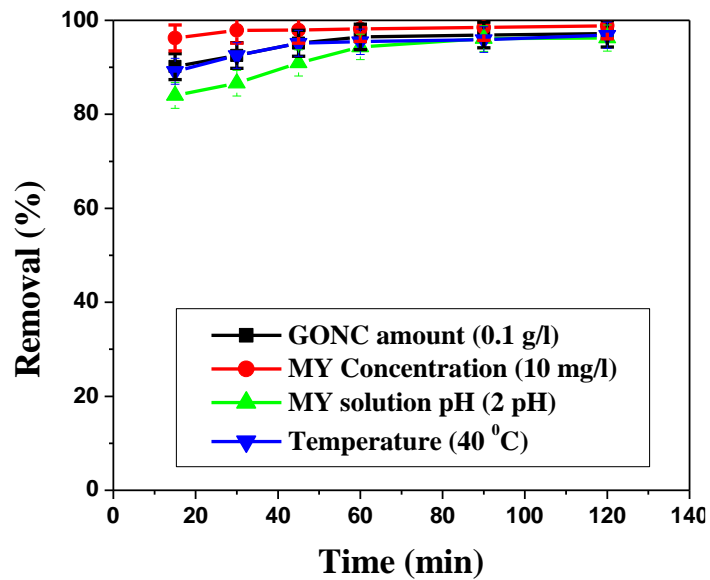


Figure no 5.43 Equilibrium study of MY by GONC



Figure no 5.44 MY remove by R-GO



Figure no 5.45 MY remove by GO



Figure no 5.46 MY remove by GONC

5.3.3. Adsorption Isotherms:

Experimental data were analyzed by the Langmuir, Freundlich and Temkin isotherms models. The adsorption capacity of adsorbents (GR-GO, GO and GONC) for removal of MY from its aqueous phase was calculated from the models equations. The details of Langmuir, Freundlich and Temkin models were already discussed in chapter no 4.

Langmuir isotherms model describe the monolayer adsorption process with homogeneous distribution of dye molecules onto the adsorbent surface (Sajab et al., 2011). The Langmuir parameters q_0 and b was calculated from slope and intercept of linearized plot of C_e/q_e vs C_e . Furthermore the high R^2 value and small χ^2 indicate the applicability of the model. The R^2 of GONC is higher compare with GR-GO and GO along with small χ^2 value which reflects the Langmuir model was better represent the experimental data.

Freundlich isotherm assumes the multilayer adsorption process of adsorbate on heterogeneous adsorbent surface. The Freundlich models constant parameters K_F and n was calculated from the slop and intercept of the linear plots $\ln q_e$ vs $\ln C_e$, for R-GO, GO and GONC. The surface of adsorbents is more heterogeneous when the value of n is close to zero (Haghseresh et al., 2005). The value of R^2 and χ^2 indicates the applicability of the model.

Temkin isotherms model assumes that the heat of adsorption process decreases linearly with the increase in coverage area of adsorbent surface (Limousin et al., 2007). The model constant parameter B_T and K_T was calculated from slope and intercept of the linearized plot q_e vs $\ln C_e$. GONC posses the highest value of R^2 comparing with GR-GO and GO. Among the three models Langmuir model was better represent the experimental data with highest R^2 value and smallest χ^2 value for GONC comparing with the GR-GO and GO. The values of all constant for all the models were listed in table no 5.11.

Table no 5.11 Isotherms parameters of MY:

Isotherms models	Parameters	Adsorbents		
		R-GO	GO	GONC
Langmuir model	q_0 (mg/g)	273.9	278.858	526.32
	B (l/mg)	0.002	0.003	0.385
	R^2	0.9789	0.9926	0.9992
	χ^2	25.63	22.34	20.42
Freundlich model	K_F (mg/g (l/mg) ^{1/n})	185.4	245.6	268.4
	$1/n$	0.618	0.305	0.297
	R^2	0.953	0.982	0.985
	χ^2	24.36	20.11	18.52
Temkin model	B_T (l/g)	12.17	13.72	14.75
	K_T	6.184	1.505	1.206
	R^2	0.9435	0.9647	0.9830
	χ^2	28.92	25.31	21.52

5.3.4. Adsorption kinetics:

The prediction of adsorption reaction rate and mechanism of process is an important step to be considered. To find out the reaction rate constant is a useful way to execute this purpose. The four kinetics model viz., Pseudo-first-order, Pseudo-second-order and Inter particle diffusion model were analyzed to find out the experimental adsorption rate constant. The process of adsorption can be considered as a quasi-instantaneous diffusion system (Oladoja and Akinlabi, 2009). The details of all the kinetics process were discussed in previous chapter no , for the pseudo-first order. linear plot of $\ln(q_e - q_t)$ vs t provides poor R^2 value and large χ^2 value and shows high disparity between experimental adsorption capacity and calculated one for R-GO, GO and GONC were listed in tabulated form (Table no 5.12).

Pseudo-second-order kinetics model is the most stable and acceptable kinetics model which correlate the diffusion of liquid film on to the adsorbent surface. The linear plot of t/q_t vs t provides greater R^2 value and small χ^2 value depict the better correlation between experimental data with the model (Saeed et al., 2010). The reaction rate constant K_2 and

q_e (adsorption capacity) were calculated from the intercept and slope of the equation and shows the less disparity between experimental and calculated one. The chi-square (χ^2) value was small for GONC compare with R-GO and GO predicted that GONC better represent the second-order kinetics model.

Adsorption process is not only governed by the surface phenomenon but also intramolecular diffusion or combination of both. The linear plot q_t vs $t^{1/2}$ provides the complexity nature of adsorption process (Mall et al., 2005). The rate constant K_{diff} was calculated from the slope of the graph. The value of R^2 and χ^2 depict the feasibility of adsorption process were listed in table 5.12. From the table it was observed that GONC posses high R^2 value than R-GO and GO but comparing less with its pseudo-second-order kinetics model value.

5.3.5. Adsorption Thermodynamics:

The activation energy (E_a kJ/mol) is playing a very vital role for adsorption process the value of E_a (GO-52.06, RGO-44.12, GONC- 66.54 kJ/mol) obtained from the linear plot of $\ln K$ versus $1/T$ indicating that the adsorption process is physisorption in nature (Anirudhan and Radhakrishnan, 2008). The values of ΔH^0 and ΔS^0 were calculated from slope and intercept of the linear plot $\ln K_d$ versus $1/T$. The positive value of ΔH^0 (R-GO-52.17, GO-65.37 and GONC- 73.80 kJ/mol) indicates the process is endothermic in nature and positive value of ΔS^0 suggested that (R-GO-2.08, GO-2.19 and GONC- 3.14 kJ/mol) the increased randomness between solid-solute interface. The value of ΔH^0 and ΔS^0 for GONC is higher than GO and R-GO. The value of gibbs free energy (ΔG^0) determines the nature of process whether it is physisorption or chemisorption in nature. The negative value of ΔG^0 for various temperatures corresponds to the spontaneous nature of adsorption (Liu et al., 2012). The values of ΔG^0 , ΔH^0 , ΔS^0 for GO, R-GO, GONC were listed in table no 5.13.

Table no 5.12 Kinetics model of MY:

Kinetics models	Parameters	Adsorbents					
		R-GO		GO		GONC	
		q_e exp	q_e cal	q_e exp	q_e cal	q_e exp	q_e cal
Pseudo-first-order	q_e (mg/g)	23.45	25.03	25.79	28.64	36.23	39.56
	K_1 (h)	0.263		0.276		0.376	
	R^2	0.9411		0.9445		0.9769	
	χ^2	32.52		26.66		24.61	
Pseudo-second-order	q_e (mg/g)	133.1	134	254.3	258	358.24	361.5
	K_2 (g g/h)	0.185		0.069		0.025	
	R^2	0.9728		0.989		0.9983	
	χ^2	27.54		23.36		22.14	
Intraparticle Diffusion	C	2.47		3.216		3.73	
	K_{diff} (mg/g h ^{1/2})	11.24		14.02		14.81	
	R^2	0.9234		0.9492		0.9888	
	χ^2	36.42		31.25		27.64	

Table no. 5.13 Thermodynamics parameters for removal of MY by R-GO, GO and GONC.

Temperature	Parameters	Adsorbents		
		R-GO	GO	GONC
303 K	ΔG^0 (kJ/mol)	-1.85	-2.86	-2.26
	ΔH^0 (kJ/mol)	52.17	65.37	73.80
	ΔS^0 (J/mol K)	2.08	2.19	3.14
308 K	ΔG^0 (kJ/mol)	-2.14	-3.04	-3.84
	ΔH^0 (kJ/mol)	52.17	65.37	73.80
	ΔS^0 (J/mol K)	2.08	2.19	3.14
313 K	ΔG^0 (kJ/mol)	-2.93	-3.17	-4.21
	ΔH^0 (kJ/mol)	52.17	65.37	73.80
	ΔS^0 (J/mol K)	2.08	2.19	3.14

5.3.6. Response surface methodology used for optimization of MY adsorption by GONC:

5.3.6.1. Model verification and develop regression model equation:

Response surface methodology is a technique used for establish a relationship between mathematical and statistical model. It is used to refine the model and compute the relationship between the independent process factors and impact on the process response (Anderson and Whitcomb, 2005).

From the batch experiment and different process model it was established that GONC posses better remove efficiency of MY from its aqueous mode than GO and R-GO. RSM study of MY was analyzed for GONC with three independent process factors viz., adsorbent dose (mg), pH of the MY solution, reaction time (min) and their impact on the response (removal percentage) were investigated. The model was suggested twenty experiments listed in table no 5.14 and 5.15 (different model fitting).

The best fitted polynomial quadratic equation for describing response (removal percentage) was obtained performing regression modeling between response and three process variable pH, dose and time. All the parameters value was listed in table no . The polynomial quadratic equation with their actual variables were expressed as –

$$\begin{aligned} \text{Response (Removal Percentage)} = & 7.082 + 4.03 * \text{pH} + 0.74 * \text{Dose} + 0.531 * \text{Time} \\ & - 0.014 * \text{pH} * \text{Dose} - 7.5 * \text{pH} * \text{Time} - 1.33 * \text{Dose} * \text{Time} \\ & - 0.48 * \text{pH}^2 - 1.64 * \text{Dose}^2 - 1.29 * \text{Time}^2 \end{aligned}$$

The constant 7.082 was independent for all factor and interaction between them. The interaction terms (pH*Dose), (pH* Time), (Dose*Time) and second-order terms pH², Dose² and Time² should posses antagonistic effect on response i.e the response will decrease as the value of these terms increase. Whereas, the linear terms pH, Time and Dose had a positive influence which posses synergistic effect indicate that with an increase of these factors there will be an increase in response (Singh et al., 2011) i.e removal percentage of MY.

5.4.3. Analysis of variance (ANOVA)

ANOVA was performed to verify the satisfactoriness of the developed quadratic model. The model and model terms are regarded as significant only when the values of Prob>F are less than 0.0003. The terms with higher F-value and lower p-value have greater

importance to produce an impact on response (removal percentage). The P-value and F-value of model were found to be <0.0002 and 126.30, respectively, which implies that the model is highly significant and better, co-relate the experimental data with statistical model. Among all the parameters the linear terms (A, B, C), interaction term (A×B) and (A×C) , and square terms, A^2 and B^2 , showed most significant effect on response, having P-value <0.002 table no 5.16 ANOVA (significant and not significant) terms. The model shows a reasonable acceptable value between model R^2 (0.9274) and predicted R^2 (0.8645), adjusted R^2 value (0.8821) was obtained by ANOVA study. From this analysis it was found that developed quadratic model was found to be suitable for representing the experimental data of adsorption of MY by GONC.

Table no 5.15 Fit summery of different model:

Source	Linear	2FI	Quadratic	Cubic
Sum of squares	425.62	353.51	347.50	4.25
Mean square	3.86	4.41	1.46	2.53
F-value	285.436	58.528	785.23	145.23
Lack of fit P-value	<0.006	0.042	<0.0001	0.0215
Std. Dev.	6.31	8.48	0.085	4.34
R^2	0.5794	0.4710	0.9274	0.7832
Adjusted R^2	0.5005	0.3364	0.8821	0.6225
Predicted R^2	0.4262	0.2435	0.8645	0.4932
PRESS	63.97	108.81	339.41	76.31
Remarks			Suggested	Aliased

Table no 5.14 Model experimental analysis Data:

Run	Factor 1 A: pH	Factor 2B: Adsorbent dose (mg)	Factor 3 C: Time (min)	Response (Removal percentage)
1	10.00	200.00	150.00	50.11
2	6.00	34.66	82.50	40.21
3	2.00	200.00	150.00	98.84
4	10.00	25.00	15.00	22.32
5	2.00	25.00	15.00	42.89
6	6.00	112.50	82.50	89.96
7	6.00	112.50	31.02	72.21
8	2.00	200.00	15.00	91.88
9	6.00	259.66	82.50	80.11
10	12.73	112.50	82.50	38.52
11	1.00	112.50	82.50	88.52
12	10.00	25.00	150.00	52.52
13	6.00	112.50	82.50	89.96
14	6.00	112.50	82.50	89.96
15	6.00	112.50	196.02	81.53
16	6.00	112.50	82.50	89.96
17	6.00	112.50	82.50	89.96
18	10.00	200.00	200.00	54.62
19	6.00	112.50	112.50	89.96
20	2.00	25.00	25.00	77.78

The analysis of statistical properties of the model was also performed by normal percentage probability plot of the residuals, a system for assessing the better relationship between the set of observed values with the theoretical distribution (Bingol et al., 2010). Approximately linear data points indicated the process was followed normal distribution (Figure no 5.45). Furthermore, a high value of R^2 (0.9274) and a realistic agreement of predicted R^2 (0.8645) with adj. R^2 value (0.8821) verified the capability of the fitted quadratic model for MY adsorption. Thus all of these statistical tests showed that the developed quadratic model was suitable for representing the data and reasonably able to interpret the relationship between the process variables and response. Figure no 5.47 and 5.48 shows the % probability verses internally studentized residuals, predicted verses actual R^2 respectively.

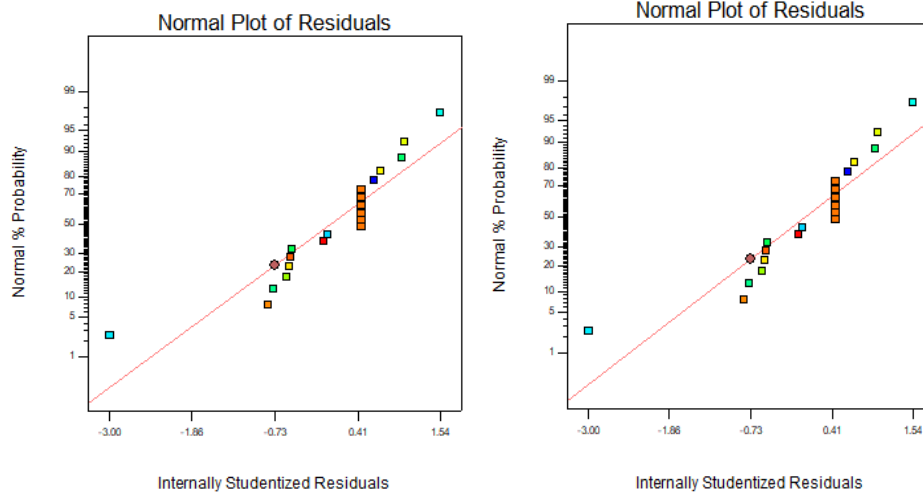


Figure no 5.47 Normal % probability Vs Residual **Figure no 5.48 Predicted Vs Actual**

5.4.5. Graphical interpretation of models by 3D response surface and contour plots: Interaction effects of process variables on response

The graphical representation was generated by Design expert software (version 7.2.0) of the individual parameter and their interactive effects of process variables on response (removal percentage) within the experimental range were obtained through three dimensional responses surface and contour plots.

5.4.5.1. Effect of adsorbent dose (GONC) and pH of the solution:

From the figure no 5.49 and 5.50, it was observed that the mutual effect of pH of the solution and adsorbent dose on process response at constant time (82.50 min). An increase in pH of the solution correspond to the increase in response function up to certain limit after that the response function shows reverse trend. The reason may be due to the fact that the accessibility of active sites enhances with the increase the pH up to certain limit beyond that the negative trend was observed. These observations were consistence with the batch study experiment.

Table no 5.16 ANOVA table (significant and not significant terms):

Source	Sum-of Square	DF	Mean Square	F value	P-value prob> F	Remarks
Model	321.36	9	11.48	126.3	< 0.0001	Significant
A-pH	4.1218	1	4.21	56.24	< 0.0001	Significant
B-Dose	2.5641	1	8.75	23.54	< 0.0001	Significant
C-Time	1.5421	1	5.21	36.46	< 0.0002	Significant
AB	0.2278	1	0.561	2.51	< 0.0002	Significant
AC	0.3241	1	0.412	5.36	< 0.0001	Significant
BC	0.2142	1	0.174	3.23	0.3145	
A²	0.2324	1	0.2143	244.23	< 0.0002	Significant
B²	25.32	1	25.324	425.14	< 0.0001	Significant
C²	32.62	1	32.621	1.52	0.5213	
Residual	0.0549	10	0.0652			
Lack of Fit	0.3842	5	0.0024	2.514	0.4421	
Pure error	0.0322	5	0.109			Not Significant

5.4.5.2. Effect of pH of the solution and reaction time (min):

The pH of the solution and reaction time (min) were considered for the process. From the figure no 5.51 and 5.52, it was observed that the effect of pH of the solution was directly related with the reaction time for the process response at constant adsorbent dose (112.50 mg). An increase in pH of the solution corresponds to the increase in response function with time increase. The reason may be due to the fact that the pH of the solution was increased with the reaction time. These observations were better consistence with the batch study experimental data.

5.4.5.3. Effect of adsorbent dose (mg) and reaction time (min):

The mutual effect of adsorbent dose and reaction time was analyzed in the figure no 5.53 and 5.54. The response function i.e, percentage removal was increased with the increase of adsorbent dose with time. The accessibility of active site of the adsorbent was enhanced with the reaction time at constant pH (6.00) of the solution. The dye molecules get more attached with the functional group of the adsorbent and hence increase the response for the process. The experimental data was better correlate with the model result.

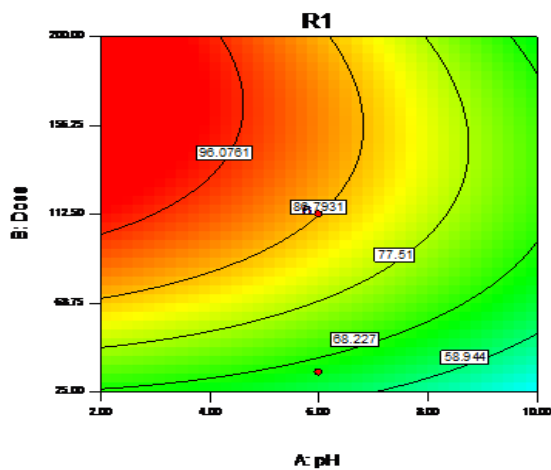


Figure no 5.49 Contour plot of Dose and pH

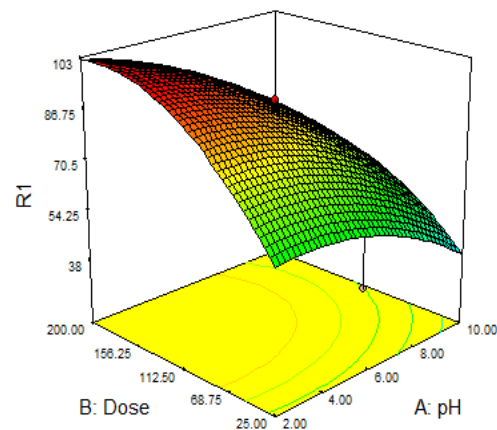


Figure no 5.45 3D surface of Dose and pH

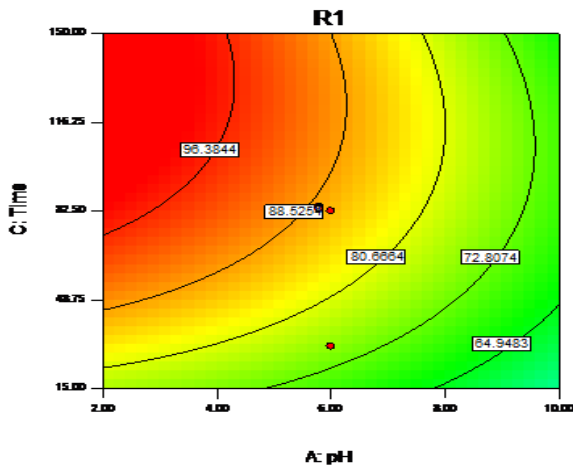


Figure no 5.51 Contour plot of Time and pH

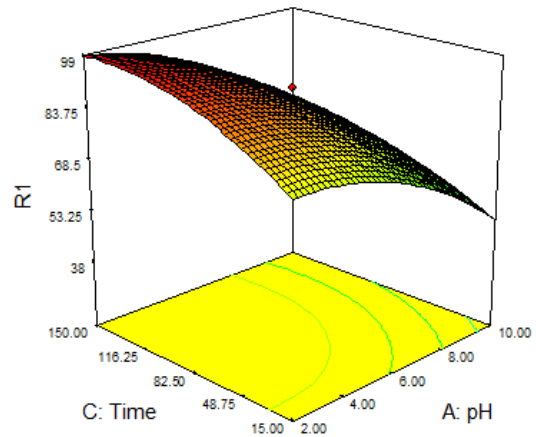


Figure no 5.52 3D surface of Time and pH

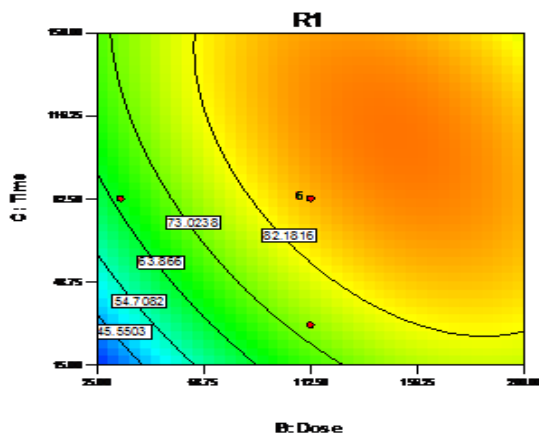


Figure no 5.53 Contour plot of Time and Dose

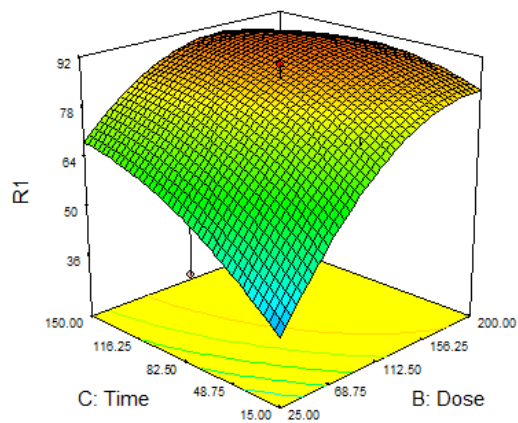


Figure no 5.54 3D surface of Time and Dose

5.5. Optimization and confirmation of reaction condition:

Design Expert software (version 7.2.0) generated a set of results to predict optimum reaction conditions using the quadratic model. To achieve maximum removal percentage (91.88), from process optimization modeling the optimum initial pH, adsorbent dose and reaction time were found to be 6.00, 112.00 mg, 82.50 min respectively. A good agreement was observed between the predicted R^2 and the corresponding R^2 obtained from the experimental data, which indicates the suitability of the model for predicting the response as well as to optimize the process conditions.

5.6. Column study:

5.6.1. Effect of various parameters on column performance:

The effects of various parameters like bed height, flow rate and influent dye concentration were evaluated for the column mode adsorption process of MY by GONC. The breakthrough curves (C_t/C_0 versus t) obtained during this study did not match with the theoretical column mode 'S' shaped. The reason behind the deviation of appearance can be endorsed by the two primary factors. Firstly, the slow adsorption rate kinetics of dyes molecules and secondly, the use of small lab-scale column equipments makes the breakthrough faster which leads to an incomplete 'S' shape of the plot (Al-Degs et al., 2009).

5.6.2. Effect of bed depth

The effect of MY adsorption by various bed heights (2, 3 and 5 cm) were evaluated during this experiment which were obtained when the column was packed with 4, 6 and 8 g of dried GONC respectively. Adsorption breakthrough curves (Figure no 5.52) for different bed depths at constant input flow rate (5 ml/min) with input concentration of MY 100 mg/ml were considered by plotting C/C_0 versus t . The data obtained from the experiment were presented in table no 5.17 and it was observed that the amount of total dye adsorbed (m_{ad}) increased with the bed height increased at exhaustion time. The better performance was obtained at highest bed height. This is due to the fact that as the column bed height increases, the surface area of adsorbent also increases. As a result the contact time of dye molecules with active sites of adsorbent is increased which give rise in the removal percentage of MY on GONC (Han et al., 2008). Thus, when the column bed depth was increased from 2 to 5 cm t_b and t_e increased from 152 to 280 min and 210 to 322 min, respectively.

Table no 5.17 Effect of different bed height, concentration and flow rate on column adsorption:

Z (cm)	F (ml/min)	C ₀ (mg/l)	t _b (min)	t _e (min)	m _{ad} (mg)	q _{e,exp} (mg/g)
2	5	100	152	280	42.16	10.54
3	5	100	170	310	55.32	9.22
5	5	100	210	322	60.35	7.54
3	10	100	165	305	33.64	8.41
3	15	100	155	260	26.43	6.60
3	5	150	145	250	20.56	5.14

5.6.3 Effect of flow rate:

The performance of the column was dependent on input adsorbate flow rate at fixed bed height and concentration (3 cm, 100 mg/l). Figure no 5.53 represent the relationship between C_t/C_0 with time t at different flow rate (5, 10, 15 ml/min). The break through time and the exhaustion time are decreased from 170 to 155 min and 310 to 260 min respectively when flow rate was increased from 5 to 15 ml/min. The reason behind this phenomenon is that the residence time of the dye molecules on the adsorbent surface was decreased when the flow rate was increased. As a result the removal efficiency and break through time are decreased along with exhaustion time (Uddin et al., 2009).

5.6.3. Effect of initial dye concentration:

The influent dye concentrations have significant effect to the column performance. The performance of column evaluated at various influent dye concentrations (100, 150 mg/l) during this study. From the figure no 5.54 (concentration) and 5.55 (exp. study), it was clearly observed that the break through time and exhaustion time was decreased from 155 to 145 min and 260 to 250 min when concentration of dye increased from 100 to 150 mg/l respectively. At higher concentration the gradient of concentration increased the diffusion coefficient and fast saturation of active sites of the adsorbents which may leads to the decrease of break through time and exhaustion time respectively (Han et al., 2009).

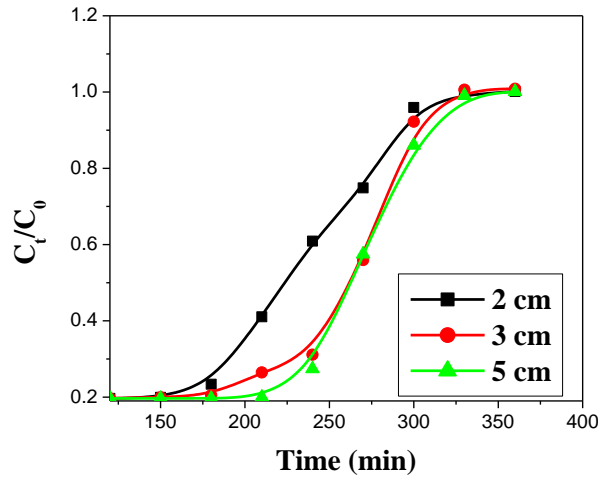


Figure no 5.52 Column study (bed height) of MY

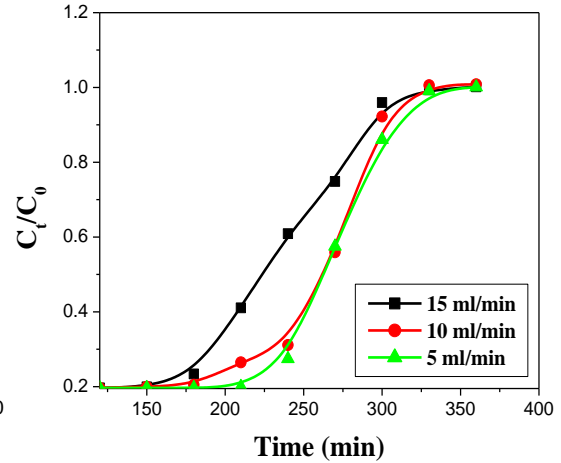


Figure no 5.53 Column study of MY flow rate

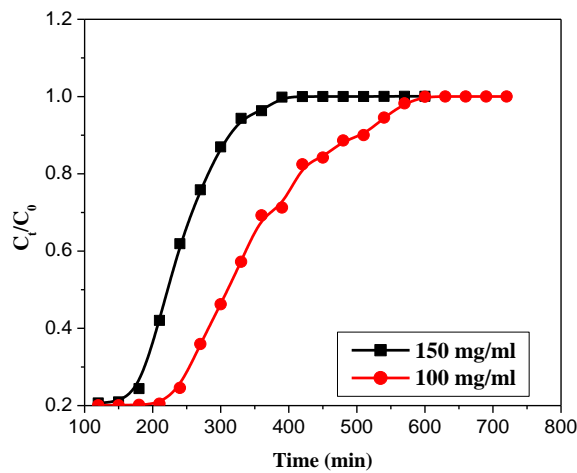


Figure no 5.54 Column study concentration of MY



Figure no 5.55 Column study (set-up)

5.6.4. Modeling of column data:

5.6.4.1. Thomas model:

The experimental data were obtained and analyzed by Thomas and BDST model. The data at C_t/C_0 values was taken higher than 0.05 and lower than 0.98 were considered for modeling the experimental value. Thomas rate constant (K_{th}) and adsorption capacity (q_e) were obtained from the slope and intercept, obtained using linear regression (Uddin et al., 2009). Thomas model parameters are presented in table no 5.18. The R^2 values were obtained ranging from 0.84 to 0.90, evaluated from regression coefficient analysis. The increase in the initial dye concentration at constant bed height (3cm) and flow rate (5ml/min) the value of q_e decreased along with the value of K_{th} decreased. Thus, better column performance can be achieved with lower flow rate, lower concentration at constant bed height. It is evident from Table 5.19 that the experimental and calculated

adsorption capacities are close at all the operating conditions studied it evident the experimental data satisfy the column model.

Table no. 5.18 Thomas model constant value:

C_0 (mg/l)	Q (ml/min)	K_{Th} (ml. min./mg)	q_e exp (mg/g)	q_e cal (mg/g)	R^2
100	5	0.0466	9.81	9.22	0.9025
150	10	0.0315	6.54	5.14	0.8464

5.6.4.2. BDST model:

The ability of BDST model to predict column performance different concentration and unknown flow rate was investigated utilizing experimental data obtained from column experiment. The constants, N_0 and K_a , were calculated from t_s vs. Z plots for different column bed depth of 2, 3 and 5 cm. The high R^2 values ranging from 0.943 to 0.988 demonstrates the validity of BDST model and better represent the experimental data compare to Thomas model. The value of N_0 , K_a , a and b were calculated from the equation and listed in table no 5.19. The lower adsorption capacity at low breakthrough and low concentration than that at exhausted condition of column bed is due to the un-saturation of several adsorbent active sites by the dye molecules. Table no 5.20 represented the breakthrough time using BDST constant for new flow rate or new concentration.

Table no. 5.19 BDST model constant value:

Bed depth Z (cm)	a (min/cm)	b (min)	K_a (l/mg/min)	N_0 (mg/l)	R^2
2	3.41	-0.865	0.0006	172.83	0.9432
3	15.11	36.42	0.00353	255.56	0.9588
5	18.25	38.50	0.00226	276.32	0.9883

Table no 5.20 Breakthrough time calculated using BDST constant for new flow rate or new concentration:

C_t/C_0	a (min/cm)	b (min)	t_{cal} (min)	t_{exp} (min)
F= 3 ml/min C ₀ = 75 mg/l	F= 3ml/min C ₀ = 75 mg/l	F= 3ml/min C ₀ = 75 mg/l	F= 3ml/min C ₀ = 75 mg/l	F= 3ml/min C ₀ = 75 mg/l
0.2	5.832	0.651	63	75
0.9	44.56	3.12	276	285
F= 20ml/min C ₀ = 200 mg/l	F= 20ml/min C ₀ = 200 mg/l	F= 20ml/min C ₀ = 200 mg/l	F= 20ml/min C ₀ = 200 mg/l	F= 20ml/min C ₀ = 200 mg/l
0.2	1.782	0.826	52	65
0.9	6.852	0.035	175	188

5.7. Crystal violet:

5.7.1. Batch adsorption study:

The removal efficiency of CV by GO, R-GO and GONC at various operational parameters were analyzed during this experimental study. The aqueous CV solution of 100 ml was taken in 250 ml conical flask with varying one operational parameters keeping others parameter constant to evaluate the varying parameters optimum point.

5.7.2. Effect of adsorbent dose:

The adsorbent dose plays a very vital role to adsorption. The CV removal efficiency of adsorbents were increased with the amount of adsorbent increase up to 0.10 g/l after that for higher dose no drastic change in removal percentage of CV was observed. The increase in amount of adsorbents leads to the increase the surface area which may leads to the increase the active sites present in the adsorbent thus boost up the interaction between adsorbents and dyes molecules presents in aqueous phase (Ahmed et al., 2009). Form the figure no 5.56, 5.57, 5.58, it was clearly observed that GONC shows better removal efficiency than R-GO and GO due to the more number of potential active sites presents in its structure than R-GO and GO.

5.7.3. Effect of initial dye concentration:

Initial dye concentration has adverse effect on adsorption capacity of adsorbents (GO, R-GO, GONC). It is evident from the figure no 5.59, 5.60, 5.61 that the removal percentage of R-GO, GO and GONC were decreasing with the increasing initial dye concentration from 10-100 mg/l. At constant adsorbent dose fixed numbers of active sites become saturated by the dye molecules easily and further increase the concentration leads to the decrease in removal efficiency. Further increase the concentration the more number of dye molecules get un-reacted and hence decrease the removal percentage (Ahmad et al., 2009). The GONC shows the better removal efficiency comparing with R-GO and GO, because large number of active sites presents in its structure.

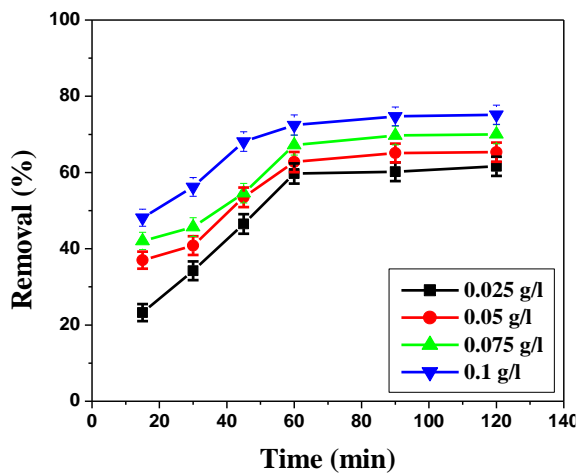


Figure no 5.56 removal of CV by R-GO

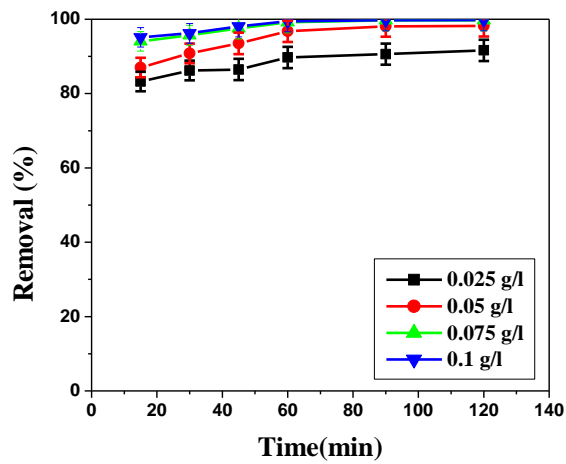


Figure no 5.57 removal of CV by GO

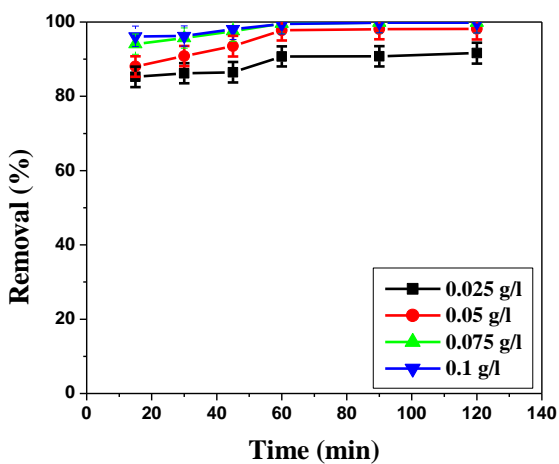


Figure no 5.58 removal of CV by GONC

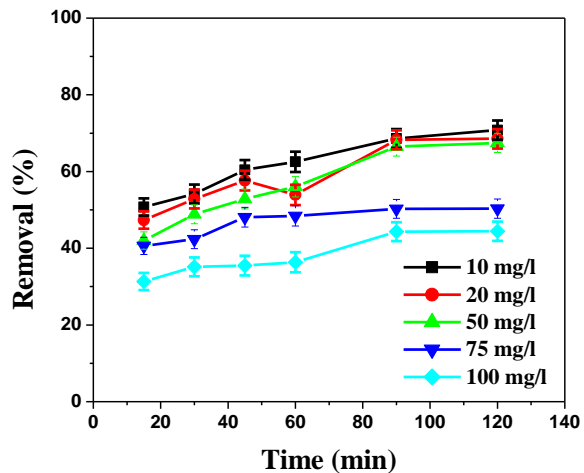


Figure no 5.59 removal of CV by R-GO at Conc.

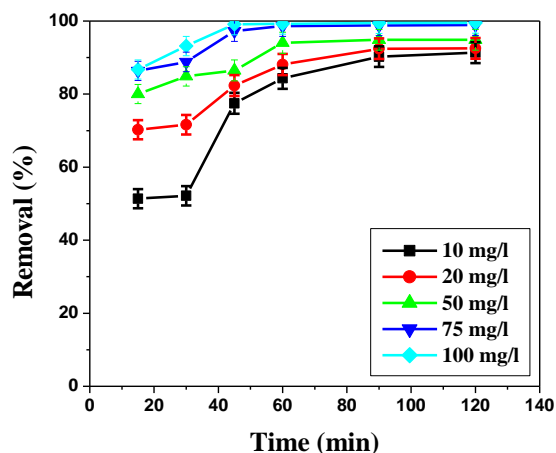


Figure no 5.60 removal of CV by GO at Conc.

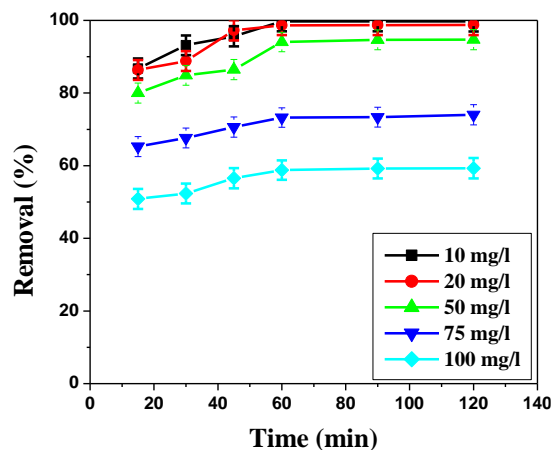


Figure no 5.61 removal of CV by GONC at Conc.

5.7.4. Effect of pH of the solution:

The pH of the medium will control the magnitude of the electro-static charges that are produced by the ionized dye molecules (Khan et al., 2013). In the figure no 5.62, 5.63, 5.64 shows the percentage removal of CV at different pH with respect to time for R-GO, GO and GONC were evaluated during this study. The removal percentage of CV was increased with the increase of pH of the solution for all adsorbents. At pH 10 the removal efficiency was more for all adsorbents. Though CV is a basic in nature, at dissociation its colour containing groups (chromophoric groups) are positively charged which attract negatively charged oxygen containing groups present in the adsorbents. The removal efficiency was better for GONC compare with R-GO and GO due to the large number of oxygen containing active group's presents into GONC structure which attract more number of ionized dye molecules present into the solution.

5.7.5. Effect of temperature on dye adsorption:

The impact of temperature on adsorption process is very important for dye adsorption as shown on figure no 5.65, 5.66, and 5.67. The removal percentage of CV were increased with the increasing the temperature from 20 °C to 40 °C for all adsorbent. If the percentage removal of dye molecules increases with increasing temperature then the adsorption is an endothermic in nature (Senthil kumar et al.2006). At higher temperature the mobility between the CV molecules increased which leads to the better interaction between active sites of adsorbents. The increasing trend was observed up to 40 °C beyond that the percentage removal decreased. The reason behind this phenomenon as suggested by (Chatterjee et al., 2007) (Chiou et. al., 2005) at high temperature weakening the physical bonds between the adsorbate molecules and active sites which may leads to the

decrease in adsorption efficiency. The removal efficiency of GONC was better than R-GO and GO.

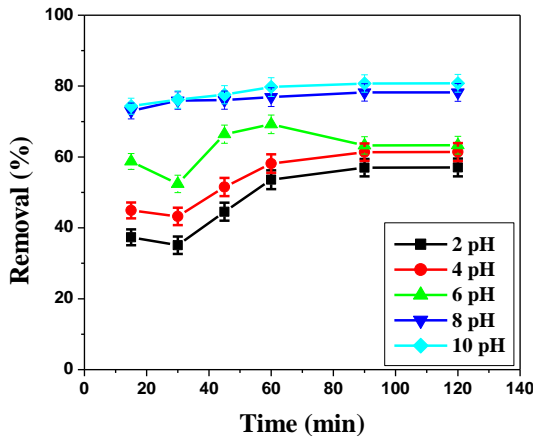


Figure no 5.62 removal of CV by R-GO at pH

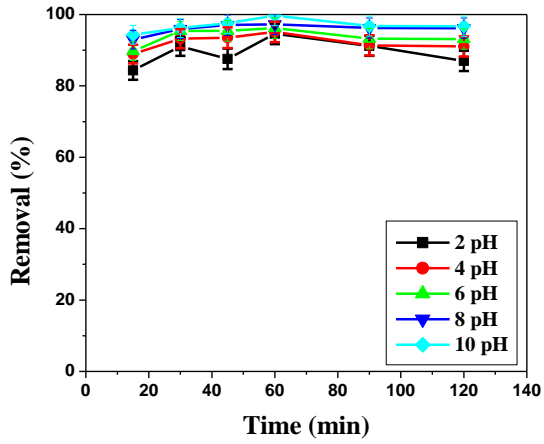


Figure no 5.63 removal of CV by GO at pH

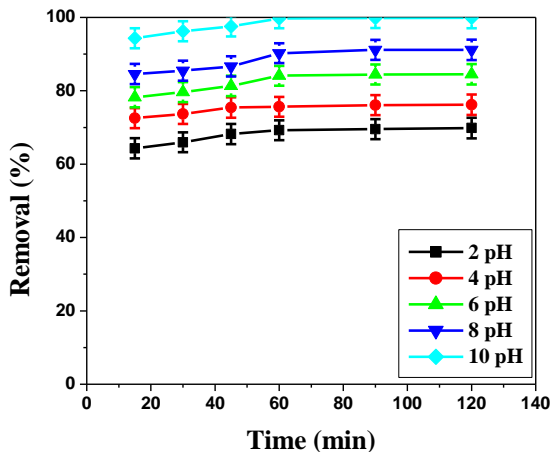


Figure no 5.64 removal of CV by GONC at pH

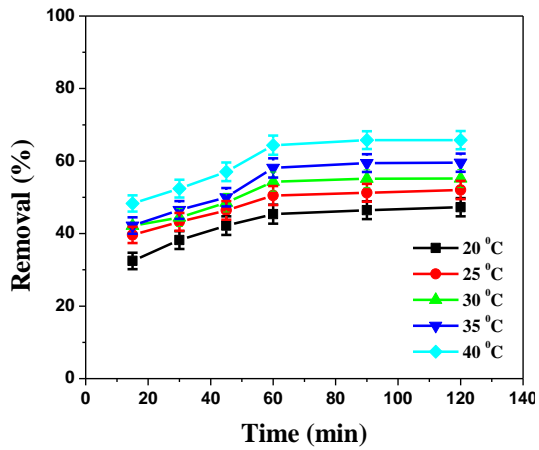


Figure no 5.65 removal of CV by R-GO at Temp

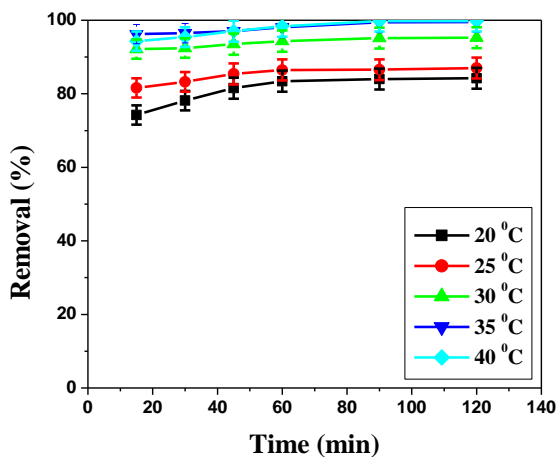


Figure no 5.66 removal of CV by GO at Temp

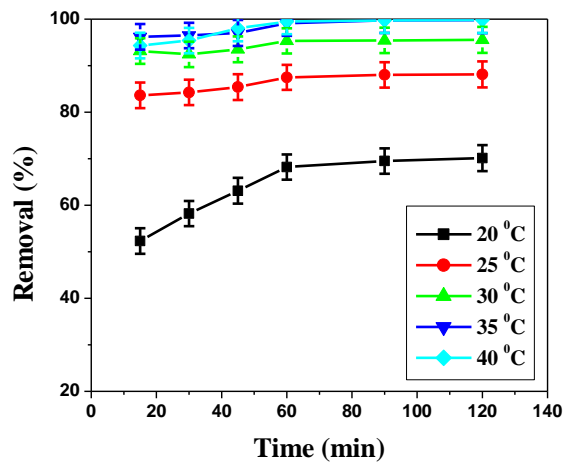


Figure no 5.67 removal of CV by GONC at Temp

5.7.6 Equilibrium study of CV by GONC:

To evaluate the effect of all operational parameters together on CV removal by GONC was investigated during this experiment (Figure no 5.70). All the operational parameters i.e., pH of the solution, adsorbent dose, initial dye concentration and temperature kept at its optimum point (adsorbent dose – 0.1 g/l, solution pH- 10, temperature- 40 °C and initial dye concentration-50 mg/l). Figure no 5.68 (equilibrium study), 5.69, 5.70, 5.71 (experimental image) shows that up to 45 min the increasing trend was observed beyond that the removal was constant. It was evident that more than ninety percent of CV molecules were removed from its aqueous phase by GONC effectively at approximately 60 min.

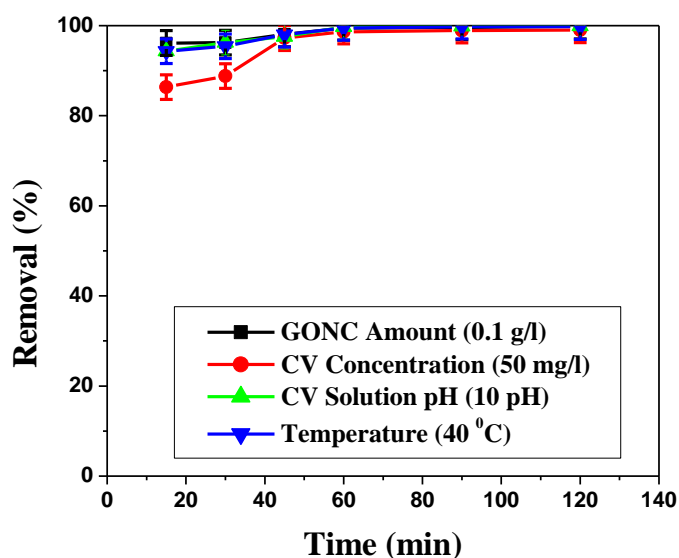


Figure no 5.68 Equilibrium study of CV by GONC



Figure no 5.69 CV remove by R-GO



Figure 5.70 CV remove by GO



Figure 5.71 CV remove by GONC

5.7.7. Adsorption Isotherms:

Experimental data were analyzed by the Langmuir, Freundlich and Temkin isotherms models. The adsorption capacity of adsorbents (R-GO, GO and GONC) for removal of CV from its aqueous phase was calculated from the models equations listed in table no 5.21.

Langmuir isotherms model describe the monolayer adsorption process with homogeneous distribution of dye molecules onto the adsorbent surface (Sajab et al., 2011). The Langmuir parameters q_0 and b was calculated from slope and intercept of linearized plot of C_e/q_e vs C_e . Furthermore the high R^2 value and small χ^2 indicate the applicability of the model. The R^2 of GONC ($R^2= 1.0$) is higher compare with R-GO ($R^2= 0.95$) and GO ($R^2= 0.98$) along with small χ^2 value which reflects the Langmuir model was better represent the experimental data.

Freundlich isotherms co-relate with multilayer adsorption process, where dye molecules interact with heterogeneous adsorbent surface. The Freundlich model constant parameters K_F and n was calculated from the slop and intercept of the linear plots $\ln q_e$ vs $\ln C_e$, for R-GO, GO and GONC. The surface of adsorbents is more heterogeneous when the value of n is close to zero (Haghsresh et al., 2005). The value of R^2 and χ^2 indicates the applicability of the model.

Temkin isotherms model assumes that the heat of adsorption process decreases linearly with the increase in coverage area of adsorbent surface (Limousin et al., 2007). The model constant parameter B_T and K_T was calculated from slope and intercept of the linearized plot q_e vs $\ln C_e$.

Among the three models Langmuir model was better represent the experimental data with highest R^2 value and smallest χ^2 value for GONC comparing with the R-GO and GO.

5.7.8. Adsorption kinetics:

The reaction rate and mechanism of process is an important step to be considered and evaluated by the adsorption kinetics. The three kinetics model viz., Pseudo-first-order, Pseudo-second-order and Inter particle diffusion model were consider to finding out the experimental adsorption rate constant. The dye adsorption process can be considered as a quasi-instantaneous diffusion process (Oladoja and Akinlabi, 2009). For the pseudo-first

order, linear plot of $\ln(q_e - q_t)$ vs t provides poor R^2 value and large χ^2 value and shows high disparity between experimental adsorption capacity and calculated one for R-GO, GO and GONC were listed in tabulated form (Table no 5.22).

Pseudo-second-order kinetics model is the most significant and acceptable kinetics model which correlate the diffusion of liquid film on to the adsorbent surface. The linear plot of t/q_t vs t with greater R^2 value and small χ^2 value depict the model acceptability (Saeed et al., 2010). The reaction rate constant K_2 and q_e (adsorption capacity) were calculated from the intercept and slope of the equation (table no 5.22). The chi-square (χ^2) value was small for GONC compare with R-GO and GO predicted that GONC better represent the second-order kinetics model.

Adsorption process not only governed by the surface phenomenon but also intra-molecular diffusion or combination of both, this phenomenon was stated in intra-particle diffusion model (Mall et al., 2005). The value of R^2 and χ^2 depict the feasibility of adsorption process were listed in table 5.22. From the table it was observed that GONC posses high R^2 value than R-GO and GO but comparing less with its pseudo-second-order kinetics model value.

5.7.9. Adsorption Thermodynamics:

The activation energy (E_a kJ/mol) is determine the nature of the adsorption process the value of E_a (GO-82.43, RGO- 46.63, GONC- 96.24 kJ/mol) obtained from the linear plot of $\ln K$ versus $1/T$ indicating that the adsorption process is physisorption in nature (Anirudhan and Radhakrishnan, 2008). The values of ΔH^0 and ΔS^0 were calculated from slope and intercept of the linear plot $\ln K_d$ versus $1/T$. The positive value of ΔH^0 (R-GO- 28.34, GO-36.15 and GONC- 68.25 kJ/mol) indicates the process is endothermic in nature and positive value of ΔS^0 suggested that (R-GO-1.19, GO-2.23 and GONC- 3.26 kJ/mol) the increased randomness between solid-solute interface. The value of ΔH^0 and ΔS^0 for GONC is higher than GO and R-GO. The value of Gibbs free energy (ΔG^0) determines the nature of process whether it is physisorption or chemisorption in nature. The negative value of ΔG^0 various temperatures correspond to the spontaneous nature of adsorption (Liu et al., 2012). The values of ΔG^0 , ΔH^0 , ΔS^0 for GO, R-GO, GONC were listed in table no 5.23.

5.7.10. Response surface methodology used for optimization of CR adsorption by GONC:

5.7.10.1. Model verification and develop regression model equation:

For establish a relationship between mathematical and statistical model response surface methodology have been used (Anderson and Whitcomb, 2005).

From the batch experiment and different process model it was established that GONC posses better remove efficiency of CV from its aqueous mode than GO and R-GO. RSM study of CV was analyzed for GONC with three independent process parameters viz..., adsorbent dose (mg), pH of the CV solution, reaction time (min) and their impact on the response (removal percentage) were investigated. The model was suggested twenty experiments listed in table no 5.24.

Table no 5.21 Isotherms models constant values of CV by R-GO, GO, GONC:

Isotherms models	Parameters	Adsorbents		
		R-GO	GO	GONC
Langmuir model	q_0 (mg/g)	217.3	229.3	249.9
	B (l/mg)	0.003	0.004	0.207
	R^2	0.9525	0.9865	1.0
	χ^2	18.52	12.53	9.14
Freundlich model	K_F (mg/g (l/mg) ^{1/n})	227.1	228..5	229.3
	$1/n$	0.0164	0.0154	0.0148
	R^2	0.9376	0.9519	0.9818
	χ^2	22.36	19.12	15.34
Temkin model	B_T (l/g)	35.77	36.17	37.75
	K_T	1.25	1.80	3.06
	R^2	0.9275	0.9533	0.9804
	χ^2	26.21	23.31	18.56

The best fitted polynomial quadratic equation for describing response (removal percentage). All the parameters value was listed in table no 5.25. The polynomial quadratic equation with their actual variables were expressed as –

$$\begin{aligned} \text{Response (Removal Percentage)} = & -162.67 + 17.58 * \text{pH} + 9.56 * \text{Time} \\ & + 69.83 * \text{Adsorbent dose} + 0.034 * \text{pH} \\ & * \text{Time} + 0.35 * \text{pH} * \text{Adsorbent dose} + 0.62 * \\ & \text{Time} * \text{Adsorbent dose} - 1.15 * \text{pH}^2 \\ & - 0.16 * \text{Temperature}^2 - 51.09 * \text{Adsorbent dose}^2 \end{aligned}$$

The constant -162.67 was independent and negative for all factors and interaction between them shows decreasing trends. The independent terms (pH, Time, Adsorbent dose) and interaction terms (pH*Dose), (pH* Time), (Dose*Time) should possess positive sign leads to synergistic effect on response i.e the response will increase as the value of these terms increase. Whereas, the second order terms pH, Time and Dose had a negative influence which possesses antagonistic effect indicate that with an increase of these factors there will be an decrease in response (Singh et al., 2011) i.e removal percentage of CV.

Table no 5.22 Adsorption Kinetics parameters:

Kinetics models	Parameters	Adsorbents					
		R-GO		GO		GONC	
		Q _e exp	Q _e cal	Q _e exp	Q _e cal	Q _e exp	Q _e cal
Pseudo-first-order	q _e (mg/g)	23.25	22.11	25.79	25.25	36.23	39.23
	K ₁ (h)	0.263		0.276		0.376	
	R ²	0.9411		0.9445		0.9769	
	χ ²	32.12		28.56		22.53	
Pseudo-second-order	q _e (mg/g)	133.1	137.5	254.2	257.6	358.2	362.3
	K ₂ (g g/h)	0.185		0.069		0.025	
	R ²	0.9528		0.989		0.9983	
	χ ²	27.35		23.11		15.21	
Intra-particle Diffusion	C	2.47		3.216		3.73	
	K _{diff} (mg/g h ^{1/2})	11.24		14.02		14.81	
	R ²	0.9234		0.9492		0.9888	
	χ ²	36.45		33.36		28.42	

Table no 5.23 Thermodynamics parameters for removal of CV by R-GO, GO and GONC.

Temperature	Parameters	Adsorbents		
		R-GO	GO	GONC
303 K	ΔG^0 (kJ/mol)	-1.094	-1.54	-2.52
	ΔH^0 (kJ/mol)	28.34	36.15	68.25
	ΔS^0 (J/mol K)	1.19	2.23	3.26
308 K	ΔG^0 (kJ/mol)	-1.62	-2.23	-3.42
	ΔH^0 (kJ/mol)	28.34	36.15	68.25
	ΔS^0 (J/mol K)	1.19	2.23	3.26
313 K	ΔG^0 (kJ/mol)	-2.93	-3.17	-4.21
	ΔH^0 (kJ/mol)	28.34	36.15	68.25
	ΔS^0 (J/mol K)	1.19	2.23	3.26

5.7.10.2. Analysis of variance (ANOVA)

ANOVA was performed to verify the satisfactoriness of the developed quadratic model. The model and model terms are regarded as significant only when the P values (Prob>F) are less than 0.0002 with high F value 174.23. Among all the parameters the linear terms (A, B, C), interaction term (A×C), (AxB) and square terms B² showed most significant effect on response, having P-value <0.0002 to < 0.0001 table no 5.26 represent ANOVA model. The model shows a reasonable acceptable value between model R² (0.9965) and predicted R² (0.9622), adjusted R² value (0.9933) was obtained by ANOVA model. From this analysis it was found that developed quadratic model was found to be suitable for representing the experimental data of adsorption of CV by GONC.

Table no 5.24 Model experimental analysis:

Run	Factor 1 A: pH	Factor 2B: Adsorbent dose (g/l)	Factor 3 C: Time (min)	Response (Removal percentage)
1	12.73	0.63	32.50	80.12
2	6.73	0.63	32.50	99.82
3	6.73	0.63	32.50	99.82
4	10.29	1.00	25.00	86.72
5	6.73	0.63	32.50	99.82
6	10.29	0.26	40.00	73.14
7	3.13	0.26	40.00	48.17
8	6.73	0.63	20.00	70.87
9	10.29	1.00	40.00	97.29
10	6.73	0.63	45.11	80.82
11	6.73	0.63	32.50	99.82
12	6.73	0.01	32.50	60.14
13	6.73	1.26	32.50	99.87
14	3.16	1.00	25.00	63.54
15	3.16	0.26	25.00	48.14
16	1.20	0.63	32.50	45.49
17	3.16	0.63	32.50	99.82
18	6.73	1.00	40.00	68.14
19	6.00	0.26	32.50	99.82
20	10.29	0.63	25.00	77.72

Table no 5.26 ANOVA model:

Source	Sum-of Square	DF	Mean Square	F value	P-value prob> F	Remarks
Model	168.65	9	15.84	174.23	< 0.0001	Significant
A-pH	3.1218	1	4.21	65.24	< 0.0002	Significant
B-Dose	2.5641	1	8.75	32.54	< 0.0001	Significant
C-Time	1.5421	1	5.21	30.46	< 0.0002	Significant
AB	0.2005	1	0.214	3.52	< 0.0002	Significant
AC	0.2541	1	0.452	6.32	< 0.0001	Significant
BC	0.2142	1	0.555	4.23	0.3145	
A²	0.4215	1	0.2321	0.452	0.2541	
B²	25.32	1	25.324	322.14	< 0.0002	Significant
C²	0.3214	1	32.621	401.52	0.1842	
Residual	0.0549	10	0.0622			
Lack of Fit	0.3842	5	0.0542	3.2145	0.6241	
Pure error	0.0322	5	0.125			Not Significant

Table no 5.25 Fit summary of different model:

Source	Linear	2FI	Quadratic	Cubic
Sum of squares	3964.93	3932.78	25.64	0.00
Mean square	360.45	491.6	5.13	0.00
F-value	78.53	86.58	866.23	24.32
Lack of fit P-value	<0.003	0.046	<0.0001	0.0325
Std. Dev.	15.74	17.39	1.60	0.00
R²	0.4581	0.4624	0.9965	0.8632
Adjusted R²	0.3564	0.2143	0.9933	0.7734
Predicted R²	0.2484	0.2061	0.9622	0.6821
PRESS	5499.08	10434.66	203.46	56.24
Remarks			Suggested	Aliased

The analysis of statistical properties of the model was also performed by normal percentage probability plot of the residuals, a system for assessing the better relationship between the set of observed values with the theoretical distribution (Bingol et al., 2010). Approximately linear data points indicated the process was followed normal distribution (Figure no 5.73). Furthermore, a high value of R^2 (0.9965) and a realistic agreement of predicted R^2 (0.9722) with adj. R^2 value (0.9933) verified the capability of the fitted quadratic model for CV adsorption. Thus all of these statistical tests showed that the developed quadratic model was suitable for representing the data. Figure 5.72 and 5.73

shows the % probability verses internally studentized residuals, predicted verses actual R^2 respectively.

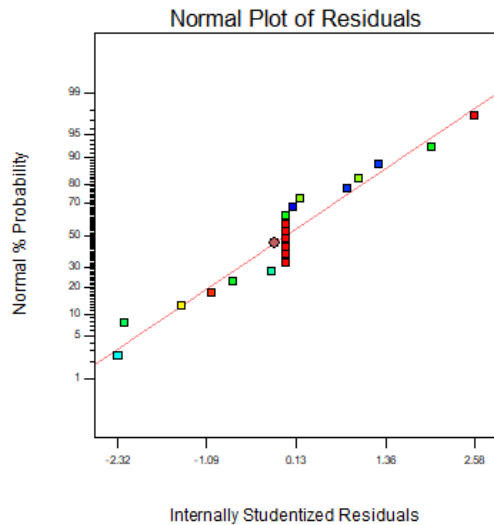


Figure 5.72 Normal % probability Vs Residual (CV)

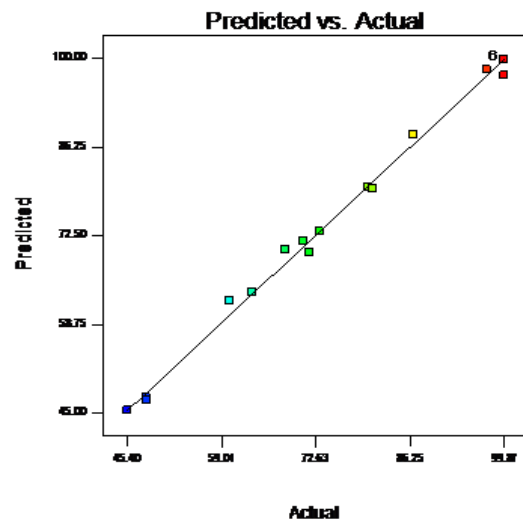


Figure 5.73 Predicted Vs Actual (CV)

5.7.11. Graphical interpretation of models by 3D response surface and contour plots: Interaction effects of process variables on response

The statistical model analysis generated by Design expert software (version 7.2.0) of the individual parameter (adsorbent dose, solution pH and reaction time) and their interactive effects of process variables on response (removal percentage) within the experimental range were obtained through three dimensional responses surface and contour plots.

5.7.11.1. Effect of adsorbent dose (GONC) and pH of the solution:

From the figure 5.73, 5.74 it was showed that the mutual effect of pH of the solution and adsorbent dose on process response at constant time (32.50 min). An increase in pH of the solution correspond to the increase in response function i.e, removal percentage up to certain limit after that the response function does not show any significant trend. The reason may be due to the fact that the accessibility of active sites enhances with the increase the pH up to certain limit beyond that the constant trend was observed. These observations were better to co-relate the experimental data.

5.7.11.2. Effect of pH of the solution and reaction time (min):

The pH of the solution and reaction time (min) were considered one of the interactive parameters for the process. From the figure 5.75, 5.76, it was observed that the effect of pH of the solution was directly related with the reaction time for the process response at constant adsorbent dose (63.50 mg). The pH of the solution increase with the increase of response function with time increases. The reason may be due to the fact that the pH of the solution was increased with the reaction time. These observations were better consistence with the batch study experimental data.

5.7.11.3. Effect of adsorbent dose (mg) and reaction time (min):

The communal effect of adsorbent dose and reaction time was analyzed in the figure no 5.77, 5.78. The response function i.e, percentage removal was increased with the increase of adsorbent dose with time. The accessibility of active site of the adsorbent was enhanced with the reaction time at constant pH (8.73) of the solution. The dye molecules get more attached with the functional group of the adsorbent and hence increase the response for the process. The experimental data was better correlate with the model result.

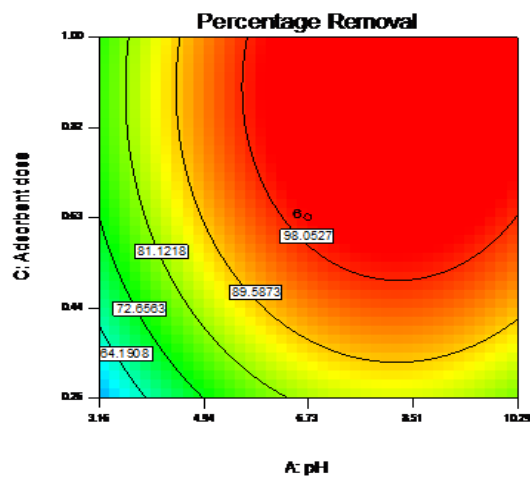


Figure no 5.73 Contour plot (CV) Dose and pH

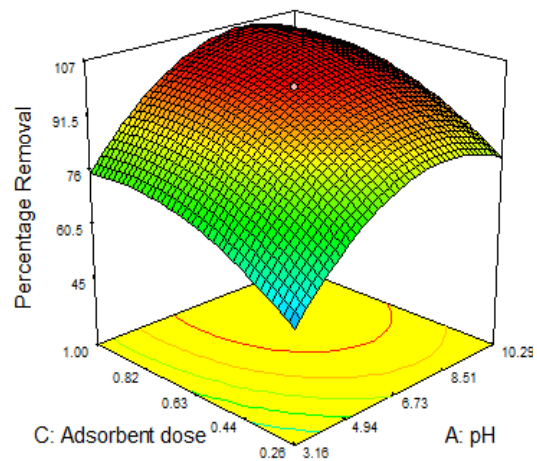


Figure 5.74 3D surface (CV) Dose and pH

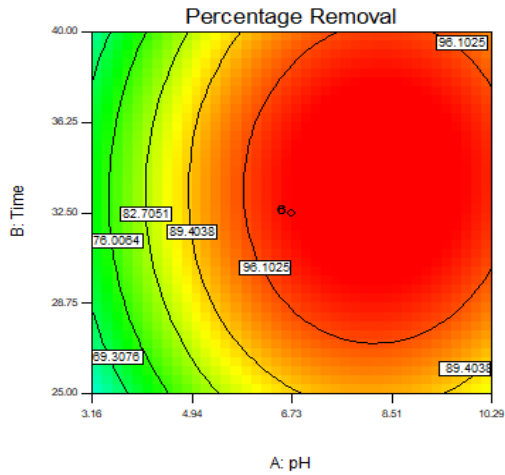


Figure 5.75 Contour plot (CV) of Time and pH

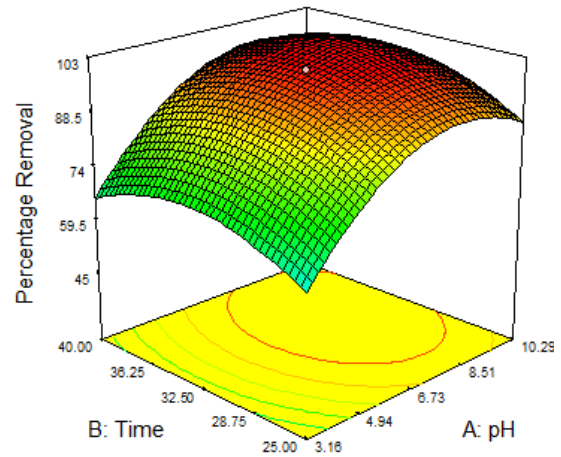


Figure 5.76 3D surface (CV) of Time and pH

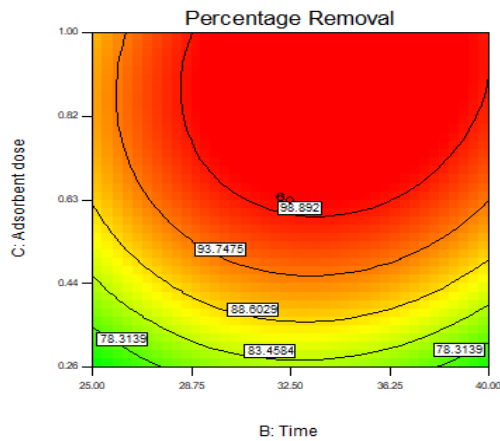


Figure 5.77 Contour plot (CV) of Time and Dose

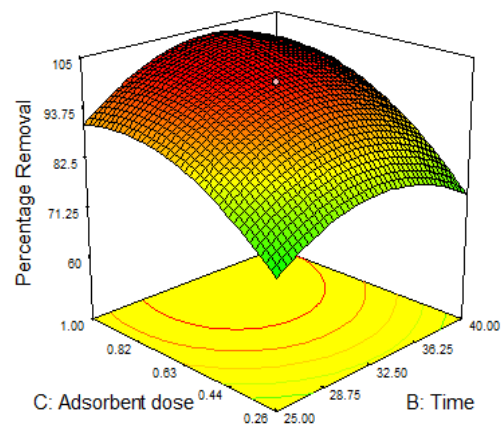


Figure 5.78 3D surface (CV) of Time and Dose

5.7.12. Optimization and confirmation of reaction condition:

Design Expert software (version 7.2.0) generated a set of results to predict optimum reaction conditions using the quadratic model. To achieve maximum removal percentage (99.82), from process optimization modeling the optimum initial pH, adsorbent dose and reaction time were found to be 8.73, 63.50 mg, 32.50 min respectively. A good agreement was observed between the predicted R^2 and adjusted R^2 obtained with the experimental R^2 , which indicates the suitability of the model for predicting the response as well as to optimize the process conditions.

5.7.13. Column study:

5.7.13.1. Effect of various parameters on column performance:

The effects of various parameters like bed height, flow rate and influent dye concentration were varying to evaluate the column mode adsorption process performance of CV by GONC. The breakthrough curves (C_t/C_0 versus t) obtained during this study did not thoroughly match with the theoretical column mode 'S' shaped curved. The reason behind the deviation of appearance can be endorsed by the two main factors – 1. The slow adsorption rate kinetics plays a vital role between dye molecules and GONC, 2. The use of small lab-scale column equipments makes the breakthrough faster which leads to an incomplete 'S' shape of the plot (Al-Degs et al., 2009).

5.7.13.2. Effect of bed depth

The effect of performance of GONC on adsorption depends on various bed heights (2, 3 and 5 cm) when the column was packed with 4, 6 and 8 g of dried GONC respectively. Adsorption breakthrough curves (Figure 5.79) was obtained for different bed depths at constant input flow rate (5 ml/min) with input CV concentration 100 mg/ml was considered by plotting c_t/c_o versus t . The data obtained from the experiment were presented in table no 5.27 and it was observed that at exhaustion time the amount of total dye adsorbed (m_{ad}) increased with the bed height increased. The better performance was obtained at highest bed height. This is due to the fact that as the column bed height increases, the surface area of active sites presents in the adsorbent increase. At reaction time the dye molecules gets attached with the active sites of adsorbent and hence increases the removal percentage of CV on GONC (Han et al., 2008). Thus, when the column bed depth was increased from 2 to 5 cm t_b and t_e increased from 125 to 370 min and 360 to 490 min, respectively (Figure no 5.79).

Table no 5.27 Effect of different bed height, concentration and flow rate on column adsorption

Z (cm)	F (ml/min)	C ₀ (mg/l)	t _b (min)	t _e (min)	m _{ad} (mg)	q _{e,exp} (mg/g)
2	5	100	125	360	52.41	13.10
3	5	100	250	410	56.34	9.39
5	5	100	210	322	64.06	8.00
3	10	100	180	380	30.53	7.32
3	15	100	130	310	22.11	6.60
3	5	150	80	230	18.44	5.06

5.7.13.3. Effect of flow rate:

The performance of the column was dependent on input adsorbate flow rate at fixed bed height and concentration (3 cm, 100 mg/l). Figure 5.84 represent the relationship between C_t/C_0 with time t at different flow rate (5, 10, 15 ml/min). The exhaustion time increased from 230 to 310 min when flow rate was increased from 5 to 15 ml/min respectively. The reason behind this phenomenon that the residence time of the dye molecules on the adsorbent surface decreased when the flow rate was increased which leads to decreased the removal efficiency and break through time along with exhaustion time simultaneously (Uddin et al., 2009).

5.7.13.4. Effect of initial dye concentration:

The influent dye concentration leads to the detrimental effect on the column performance. The performance of column evaluated at various influent dye concentrations (100, 150 mg/l) during this study. From the figure no 5.85 and 5.86 (exp. Setup), it was clearly observed that the break through time and exhaustion time was decreased from 180 to 80 min and 370 to 280 min when concentration of dye increased from 100 to 150 mg/l respectively. At higher concentration the gradient of concentration increased the diffusion coefficient and fast saturation of active sites of the adsorbents which may leads to the decrease of break through time and exhaustion time respectively (Han et al., 2009).

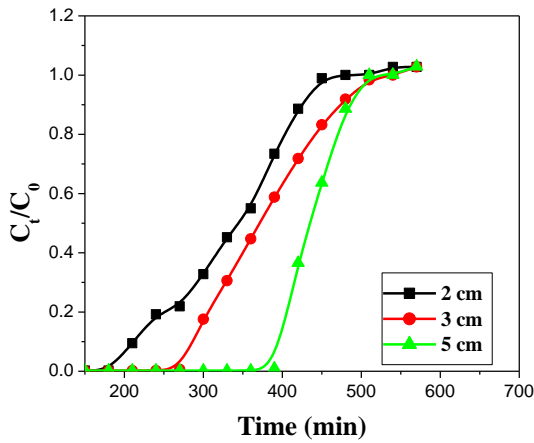


Figure 5.79 Column study (bed height) of CV

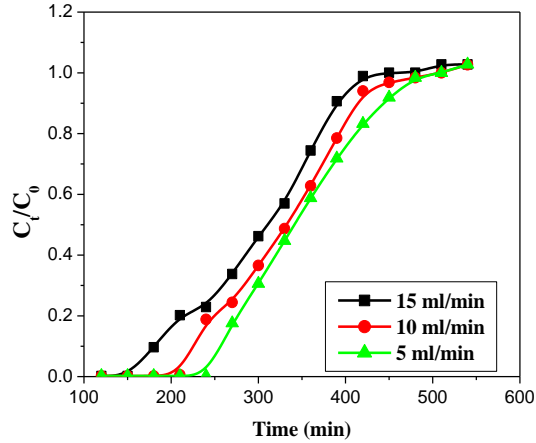


Figure 5.80 Column study (flow rate) of CV

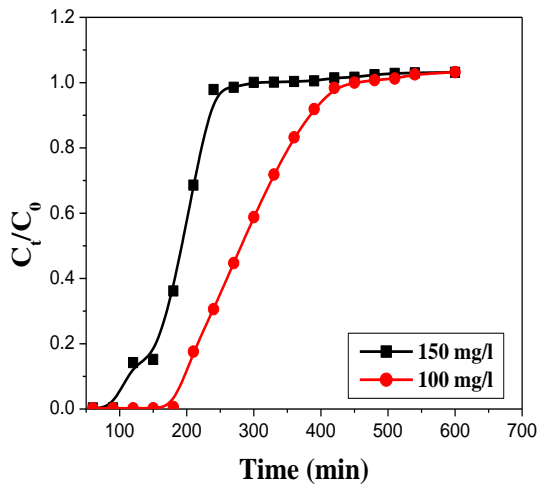


Figure no 5.81 Column study (influent concentration) of CV



Figure 5.82 Column study (set-up)

5.7.14. Modeling of column data:

5.7.14.1. Thomas model:

The experimental data were obtained from column experiments and analyzed by Thomas and BDST model. The data at C_t/C_o values was taken higher than 0.03 and lower than 0.98 were considered for modeling the experimental value. Thomas rate constant (K_{Th}) and adsorption capacity (q_e) were obtained from the slope and intercept (Uddin et al., 2009). Thomas model parameters are presented in table no 5.28. The R^2 values were obtained ranging from 0.84 to 0.90, evaluated from regression coefficient analysis. The increase in the initial dye concentration at constant bed height (3cm) and flow rate (5ml/min) the value of q_e decreased along with the value of k_{Th} decreased. Thus, better column performance can be achieved with lower flow rate, lower concentration at constant bed height. It is evident from Table 3.11 that the experimental and calculated

adsorption capacities are close at all the operating conditions studied it evident the experimental data satisfy the column model.

Table no 5.28 Thomas model constant values:

C_0 (mg/l)	Q (ml/min)	K_{Th} (ml. min./mg)	q_e (mg/g) exp	q_e cal (mg/g)	R^2
100	5	0.06466	9.81	7.32	0.9235
150	10	0.04325	6.54	5.06	0.8244

5.7.14.2. BDST model:

The ability of BDST model to predict column performance different concentration and unknown flow rate was investigated utilizing experimental data obtained from column experiment. The constants, N_0 and K_a , were calculated from t_s vs. Z plots for different column bed depth of 2, 3 and 5 cm. The high R^2 values ranging from 0.956 to 0.989 demonstrates the validity of BDST model and better represent the experimental data compare to Thomas model. The value of N_0 , K_a , a (ml/cm) and b were calculated from the equation and listed in table no 5.29. The lower adsorption capacity at low breakthrough and low concentration than that at exhausted condition of column bed is due to the un-saturation of several adsorbent active sites by the dye molecules. Table no 5.30 represented the breakthrough time using BDST constant for new flow rate or new concentration.

Table no 5.29 BDST model constant values:

Bed depth Z (cm)	a (min/cm)	b (min)	K_a (l/mg/min)	N_0 (mg/l)	R^2
2	5.34	-0.760	0.0008	184.38	0.9562
3	17.36	44.42	0.00453	264.30	0.9643
5	20.52	46.35	0.00326	282.11	0.9891

Table no 5.30 Breakthrough time calculated using BDST constant for (CV) new flow rate or new concentration:

C_t/C_0	a (min/cm)	b (min)	t_{cal} (min)	t_{exp} (min)
F= 3 ml/min C ₀ = 75 mg/l	F= 3ml/min C ₀ = 75 mg/l	F= 3ml/min C ₀ = 75 mg/l	F= 3ml/min C ₀ = 75 mg/l	F= 3ml/min C ₀ = 75 mg/l
0.2	7.856	0.542	78	90
0.9	55.64	4.35	323	335
F= 20ml/min C ₀ = 200 mg/l	F= 20ml/min C ₀ = 200 mg/l	F= 20ml/min C ₀ = 200 mg/l	F= 20ml/min C ₀ = 200 mg/l	F= 20ml/min C ₀ = 200 mg/l
0.2	2.453	0.752	63	75
0.9	9.634	0.046	160	175

5.8. Poly Aromatic Hydrocarbons:

5.8.1. Phenol (PH):

5.8.2. Batch adsorption study:

The removal efficiency of PH by GO, R-GO and GONC at changing of various parameters were analyzed during this adsorption study. The aqueous PH (Phenol) solution of 100 ml was taken in 250 ml conical flask with varying one operational parameter keeping other parameters constant in BOD incubator shaker at constant 120 rpm.

5.8.2.1. Effect of adsorbent dose:

The uptake capacity of the adsorbent was determined by the adsorbent dose analysis. The PH removal efficiency of three adsorbents (GO, R-GO, GONC) were increased with the amount of adsorbent dose increase up to 0.2 g/l after that no drastic change in removal percentage was shown. The increase the amount of adsorbents leads to the increase the surface area which may leads to the increase the active sites present in the adsorbent which boost up the interaction between adsorbents with PH molecules presents in aqueous phase (Ahmed et al., 2009). Form the figure no 5.83, 5.84, 5.85, it was clearly observed that GONC shows better removal efficiency than R-GO and GO due to the more number of potential active sites presents in its structure than R-GO and GO.

5.8.2.2. Effect of initial phenol concentration:

Initial dye concentration have inverse effect on removal efficiency of PH by GO, R-GO and GONC. It is evident from the figure no 5.86, 5.87, 5.88 that the removal percentage

of PH by R-GO, GO and GONC shows increasing trend with the increase initial dye concentration from 10-100 mg/l. The maximum removal was observed at 10 mg/l increasing trend was observed up to 50 mg/l after that the removal efficiency was lowered at this point all the active sites presents in the adsorbents being covered by the PH molecules. Further increase the concentration the more number of dye molecules get un-reacted and hence decrease the removal percentage (H. Catherine et al., 2017). The GONC shows the better removal efficiency comparing with R-GO and GO because large number of active sites presents in its structure.

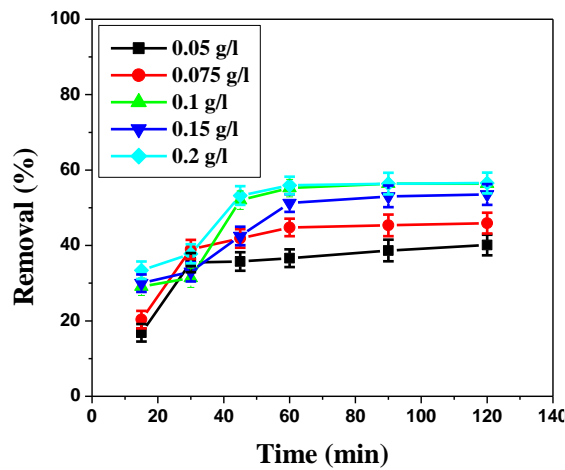


Figure no 5.83 removal of PH by R-GO

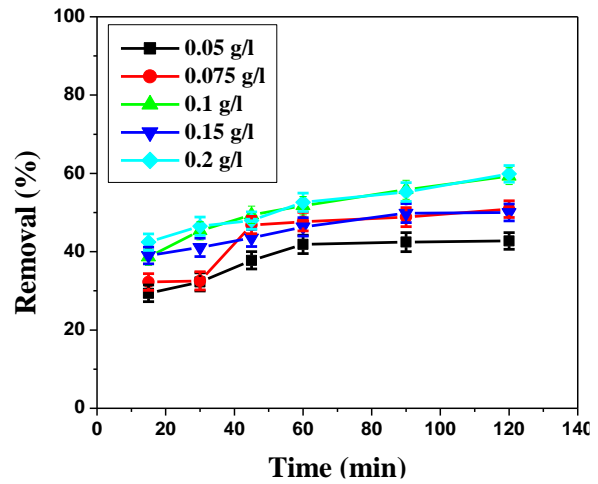


Figure no 5.84 removal of PH by GO

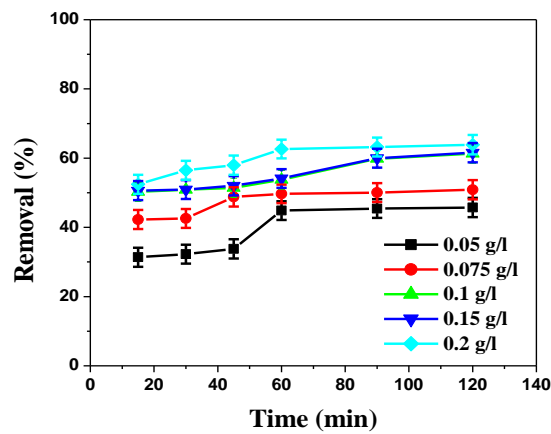


Figure no 5.85 removal of PH by GONC

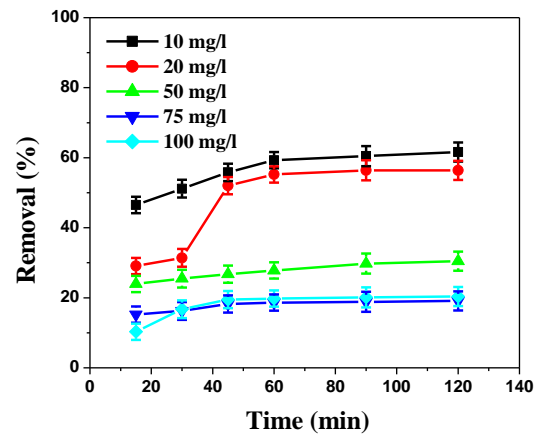


Figure no 5.86 removal of PH by R-GO at Conc.

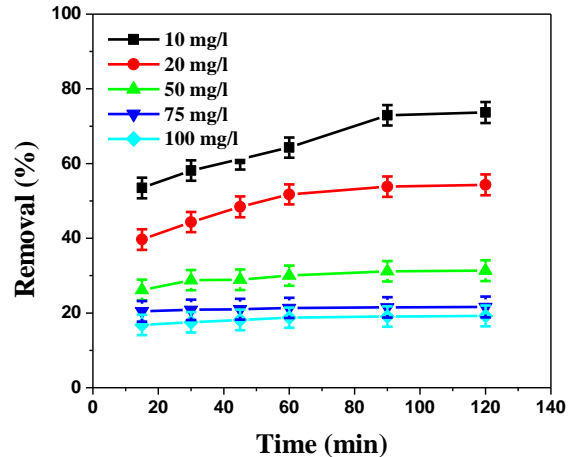
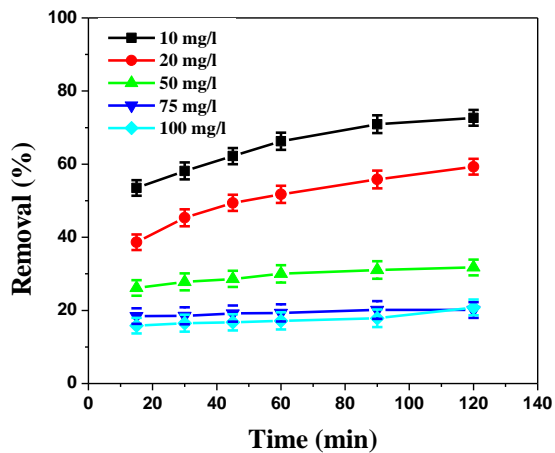


Figure no 5.87 removal of PH by GO at Conc. Figure no 5.88 removal of PH by GONC at Conc.

5.8.2.3. Effect of pH of the solution:

The pH of the medium will control the PH removal by controlling the magnitude of the electro-static charges that are produced by the ionized dye molecules (Khan et al., 2013). In the figure 5.89, 5.90, 5.91 shows the removal percentage of PH at different solution pH with respect to time by R-GO, GO and GONC were analyzed during this study. From the figure it was observed that at lower pH the removal percentage was less due to the strong repulsion force present between solution H^+ and phenolic H^+ ions. This repulsion force strongly hinders the dissociation of phenol. The removal percentage was gradually increase between pH-4 to 6 probably the dissociation factors which helps to dissociate the phenol into phenate ions and gets attached by the actives sites presents into the adsorbent, beyond pH 6 the removal was decreased due to the large number of phenate groups presents in basic pH which oppose the force of attraction (Y.Wu et al., 2014). The removal efficiency was better for GONC compare with R-GO and GO due to the large number of oxygen containing active group's presents into GONC structure which attract more number of phenate groups present into the solution.

5.8.2.4. Effect of temperature on dye adsorption:

The temperature of the system was regulated the removal efficiency of phenol. From the following figure 5.92, 5.93, 5.94 it was clearly observed that the removal percentage of PH were increased with the increasing the temperature $20^{\circ}C$ to $35^{\circ}C$ for all adsorbent beyond that the removal percentage was decreased. The mobility of molecules of PH was increased with the temperature increased up to $35^{\circ}C$ for these the molecules of PH gets more reacted with the active sites of the adsorbents beyond that the efficiency was decreased because at high temperature weakening the physical interaction bond between

active sites and the PH molecules which leads to the decrease in removal efficiency (Rathour et al., 2016). The removal efficiency of GONC was better than R-GO and GO.

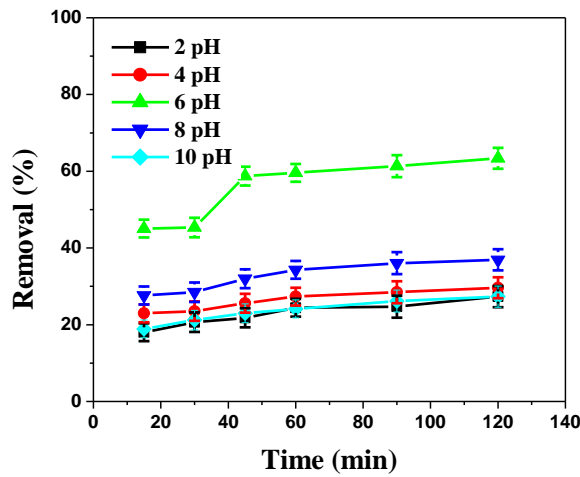


Figure no 5.89 removal of PH by R-GO at pH

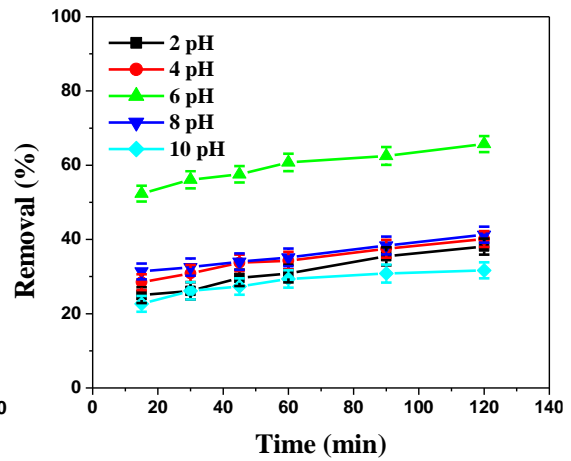


Figure no 5.90 removal of PH by GO at pH

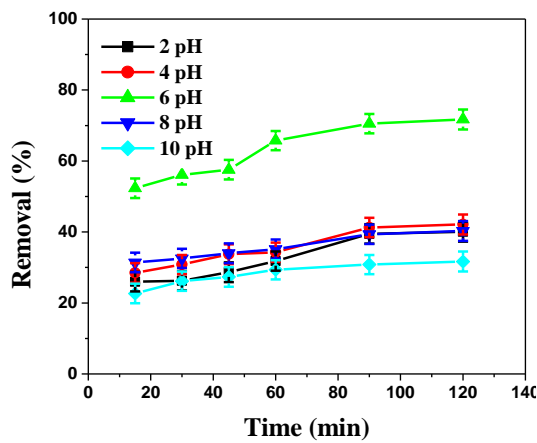


Figure no. 5.91 removal of PH by GONC at pH

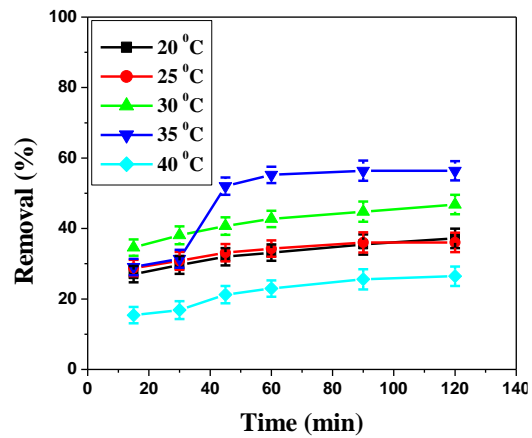


Figure no 5.92 removal of PH by R-GO at temp

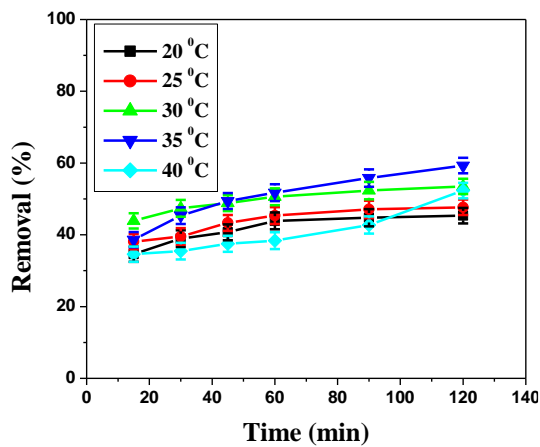


Figure no 5.93 removal of PH by GO at temp

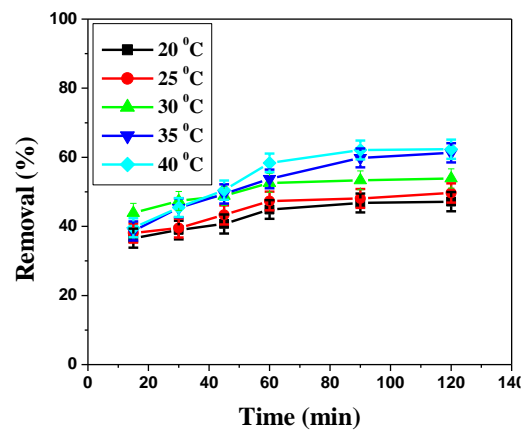


Figure no 5.94 removal of PH by GONC at temp

5.8.3. Equilibrium study of PH by GONC:

To evaluate the effect of all operational parameters together on PH removal by GONC was investigated during this experiment. All the operational parameters i.e., pH of the solution, adsorbent dose, initial dye concentration and temperature kept at its highest point (adsorbent dose – 0.1 g/l, pH of the solution- 6, temperature- 35 °C and initial PH concentration-10 mg/l). Figure no.5.95 shows that up to 60 min the increasing trend was observed beyond that the removal was constant due to the saturation of active sites present in the GONC structure.

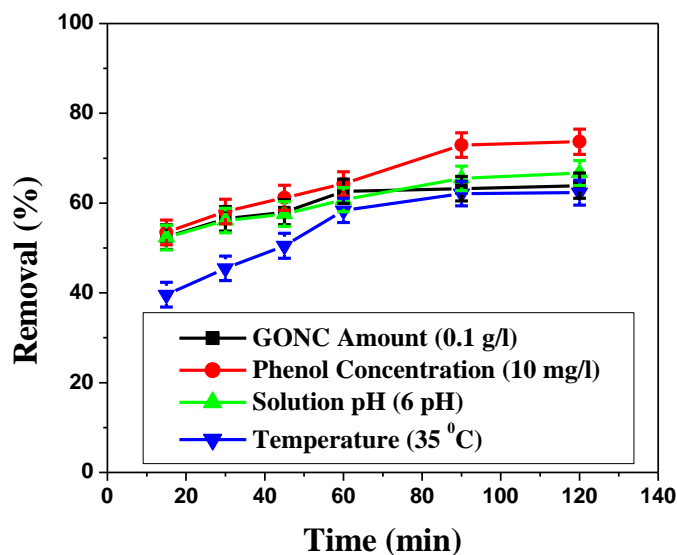


Figure no 5.95 Equilibrium study of PH by GONC

5.8.4. Adsorption Isotherms:

Experimental data were analyzed by the Langmuir, Freundlich and Temkin isotherms models. The adsorption capacity of adsorbents R-GO, GO and GONC for removal of PH from its aqueous phase was calculated from the models equations.

Langmuir isotherms model describe the monolayer adsorption process with homogeneous distribution of PH molecules onto the adsorbent surface (Xiaobo.et al, 2014). The Langmuir parameters constant and error chi square (χ^2) were represented in table no 5.31.

Freundlich isotherms co-relate with multilayer adsorption process, where PH molecules interact with heterogeneous adsorbent surface (Y.Wu.et al, 2014). The Freundlich model constant parameters K_F and n was calculated from the slop and intercept of the linear plots $\ln q_e$ vs $\ln C_e$, for R-GO, GO and GONC, the values were listed in table no 5.31.

Temkin isotherms model assumes that the heat of adsorption process decreases linearly with the increase in coverage area of adsorbent surface (Limousin et al., 2007). The model constant parameters B_T and K_T was calculated from slope and intercept of the linearized plot q_e vs $\ln C_e$, listed in table no 5.31.

Among the three models Langmuir model was better represent the experimental data with highest R^2 value and smallest χ^2 value for GONC comparing with the GR-GO and GO.

Table no 5.31 Isotherms models constant values of PH by R-GO, GO, GONC:

Isotherms models	Parameters	Adsorbents		
		R-GO	GO	GONC
Langmuir model	q_0 (mg/g)	82.45	98.25	99.62
	B (l/mg)	1.005	1.60	1.64
	R^2	0.9825	0.9996	1.0
	χ^2	28.63	25.34	22.10
Freundlich model	K_F (mg/g (l/mg) ^{1/n})	192.5	194.9	195.1
	$1/n$	0.68	0.54	0.52
	R^2	0.976	0.984	0.988
	χ^2	35.57	32.16	26.61
Temkin model	B_T (l/g)	11.02	11.76	12.06
	K_T	4.66	4.87	5.120
	R^2	0.924	0.974	0.978
	χ^2	23.56	22.14	22.10

5.8.5. Adsorption kinetics:

The reaction rate and mechanism of process is an important step to be considered and evaluated by the adsorption kinetics. The three kinetics model viz., Pseudo-first-order, Pseudo-second-order and Inter particle diffusion model were consider to finding out the experimental adsorption rate constant. For the pseudo-first order linear plot of $\ln (q_e - q_t)$ vs t provides poor R^2 value and large χ^2 value and shows high disparity between experimental adsorption capacity and calculated one for R-GO, GO and GONC were listed in tabulated form (Table. 5.32).

Pseudo-second-order kinetics model is the most significant and acceptable kinetics model in adsorption process. The linear plot of t/q_t vs t with greater R^2 value and small χ^2 value depict the model acceptability (Y.Wu.et al, 2014). The reaction rate constant K_2 and q_e (adsorption capacity) for R-GO, GO and GONC were calculated from the intercept and slope of the equation and listed in table no 5.32.

Adsorption process not only governed by the surface phenomenon but also intra-molecular diffusion or combination of both, this phenomenon was stated in intra-particle diffusion model. The linear plot qt vs $t^{1/2}$ provides the complexity nature of adsorption process (Mall et al., 2005). The rate constant K_{diff} was calculated from the slope of the graph, all the process constant values for R-GO, GO, GONC were listed in table no 5.29.

5.8.6. Adsorption Thermodynamics:

The activation energy (E_a kJ/mol) is establish the nature of the adsorption process the value of E_a (GO-54.43, RGO- 41.36, GONC- 75.42 kJ/mol) obtained from the linear plot of $\ln K$ versus $1/T$ indicating that the adsorption process is physisorption in nature (Y. Wu et al., 2014) (Anirudhan and Radhakrishnan, 2008). The values of enthalpy (ΔH^0) and entropy (ΔS^0) were calculated from slope and intercept of the linear plot $\ln K_d$ versus $1/T$. The positive value of ΔH^0 (R-GO- 29.68, GO-57.37 and GONC- 66.85 kJ/mol) indicates the process is endothermic in nature and positive value of ΔS^0 indicated that (R-GO-1.91, GO-2.32 and GONC- 6.45 kJ/mol) the increased randomness between solid-solute interface. The value of ΔH^0 and ΔS^0 for GONC is higher than GO and R-GO. The value of Gibbs free energy (ΔG^0) determines the nature of process whether it is physisorption or chemisorption in nature. The negative value of ΔG^0 for various temperatures corresponds to the spontaneous nature of adsorption (T.Liu et al., 2012) (Y.Wu.et al, 2014). The values of ΔG^0 , ΔH^0 , ΔS^0 for GO, R-GO and GONC were listed in table no.5.33.

Table no. 5.33 Adsorption Thermodynamics parameters:

Temperature	Parameters	Adsorbents		
		R-GO	GO	GONC
303 K	ΔG^0 (kJ/mol)	-1.64	-1.98	-3.55
	ΔH^0 (kJ/mol)	29.68	57.37	66.85
	ΔS^0 (J/mol K)	1.91	2.23	6.45
308 K	ΔG^0 (kJ/mol)	-2.11	-2.58	-4.85
	ΔH^0 (kJ/mol)	29.68	57.37	66.85
	ΔS^0 (J/mol K)	1.91	2.23	6.45
313 K	ΔG^0 (kJ/mol)	-2.59	-2.94	-5.93
	ΔH^0 (kJ/mol)	29.68	57.37	66.85
	ΔS^0 (J/mol K)	1.91	2.23	6.45

Table no. 5.32 Adsorption kinetics model:

Kinetics models	Parameters	Adsorbents					
		R-GO		GO		GONC	
		q_e exp	q_e cal	q_e exp	q_e cal	q_e exp	q_e cal
Pseudo-first-order	q_e (mg/g)	20.23	26.45	25.41	29.34	28.64	31.65
	K_1 (h)	0.0098		0.0129		0.00138	
	R^2	0.888		0.9526		0.9890	
	χ^2	27.34		24.23		22.15	
Pseudo-second-order	q_e (mg/g)	172.5	177.3	252.1	255.3	345.25	346.63
	K_2 (g g/h)	0.034		0.045		0.077	
	R^2	0.960		0.993		0.999	
	χ^2	23.63		18.45		15.53	
Intraparticle Diffusion	C	13.2		15.7		17.6	
	K_{diff} (mg/g h ^{1/2})	17.5		12.5		20.1	
	R^2	0.845		0.9012		0.963	
	χ^2	29.13		26.14		24.16	

5.8.7. Response surface methodology used for optimization of PH adsorption by GONC:

5.8.7.1. Model verification and develop regression model equation:

Response surface methodology has been used for establishing the relationship between mathematical and statistical model (Anderson and Whitcomb, 2005).

From the batch experiment and different process model it was established that GONC posses better remove efficiency of PH from its aqueous mode than GO and R-GO. RSM study of PH was analyzed for GONC with three independent process parameters viz..., adsorbent dose (mg), pH of the PH solution, reaction time (min) and their impact on the

response (removal percentage) were investigated. The model was suggested twenty experiments listed in table no 5.34.

The best fitted polynomial quadratic equation for describing response (removal percentage). All the model parameters value was listed in table no 5.35. The polynomial quadratic equation with their actual variables were expressed as –

$$\begin{aligned} \text{Response (Removal Percentage)} = & -165.04 + 48.19 * \text{pH} + 1.53 * \text{Time} \\ & + 0.28 * \text{Adsorbent dose} - 0.032 * \text{pH} \\ & * \text{Time} - 0.03 * \text{pH} * \text{Adsorbent dose} \\ & - 0.45 * \text{Time} * \text{Adsorbent dose} + 3.28 * \text{pH}^2 \\ & - 0.010 * \text{Temperature}^2 - 1.85 * \text{Adsorbent dose}^2 \end{aligned}$$

The constant -165.03 was independent and negative for all factors shows decreasing trends. The interaction terms (pH*Time), (pH*Adsorbent Dose), (Adsorbent Dose*Time) along with second order terms (pH and Adsorbent Dose) should possess negative sign leads to antagonistic effect on response function i.e the response will decrease as the value of these parameters increase. Whereas, the linear terms (Time, Adsorbent Dose and pH) with the second order term pH had a positive influence which possesses synergistic effect indicate that with an increase of these factors there will be an increase in response (Singh et al., 2011) i.e removal percentage of PH. Different models have been analyzed and listed in table no. 5.35, shows the quadratic model was suggested.

5.8.7.2. Analysis of variance (ANOVA)

ANOVA was performed to verify the suitability of the developed quadratic model. The model and model terms are regarded as significant only when the values of F is high and less P value (Prob>F) 121.62 and P value less than 0.0003 respectively. Among all the parameters the linear terms (A,B,C), interaction term (AxB) and square terms A² and B² showed most significant effect on response, having P-value <0.0002 to < 0.0001 table no 5.36 represents ANOVA model. The model shows a reasonable acceptable value between model R² (0.9462) and predicted R² (0.8995), adjusted R² value (0.9045) was obtained by ANOVA model. From this analysis it was found that developed quadratic model was found to be suitable for representing the experimental data.

Table 5.35 Fit Summary of different model:

Source	Linear	2FI	Quadratic	Cubic
Sum of squares	1064.49	968.79	129.75	0.000
Mean square	96.77	121.10	25.95	16.32
F-value	47.77	59.78	254.26	12.8
Lack of fit P-value	0.0486	0.0324	<0.003	0.0045
Std. Dev.	8.54	9.07	0.481	4.50
R ²	0.3809	0.4317	0.9462	0.8443
Adjusted R ²	0.2015	0.3548	0.9045	0.6542
Predicted R ²	0.2245	0.3342	0.8995	0.5214
PRESS	186.25	261.35	154.32	291.54
Remarks			Suggested	Aliased

The analysis of statistical properties of the model was also performed by normal percentage probability plot of the residuals, a system for assessing the better relationship between the set of observed values with the theoretical distribution (Bingol et al., 2010). Approximately linear data points indicated the process was followed normal distribution (Figure no 5.100). Furthermore, a high value of R² (0.9462) and a realistic agreement of predicted R² (0.8995) with adj. R² value (0.9045) verified the capability of the fitted quadratic model for PH adsorption. Thus all of these statistical tests showed that the developed quadratic model was suitable for representing the data. Figure 5.96 and 5.97 shows the % probability verses internally studentized residuals, predicted verses actual R² respectively.

Table 5.34 RSM Model experimental analysis:

Run	Factor 1 A: pH	Factor 2B: Adsorbent dose (g/l)	Factor 3 C: Time (min)	Response (Removal percentage)
1	6.50	175.00	45.00	48.84
2	6.50	175.00	45.00	48.84
3	5.00	250.00	30.00	52.32
4	6.50	301.00	45.00	60.17
5	3.98	175.00	45.00	32.56
6	8.00	250.00	30.00	35.76
7	5.00	100.00	60.00	42.02
8	6.50	175.00	45.00	48.84
9	5.00	100.00	30.00	34.88
10	8.00	250.00	60.00	38.95
11	9.00	175.00	45.00	30.23
12	6.50	175.00	70.00	56.69
13	6.50	175.00	45.00	48.84
14	6.50	175.00	19.77	32.56
15	6.50	48.88	45.00	36.92
16	8.00	100.00	30.00	32.86
17	8.00	100.00	60.00	36.52
18	5.00	250.00	60.00	57.56
19	6.50	175.00	45.00	57.56
20	6.50	175.00	45.00	57.56

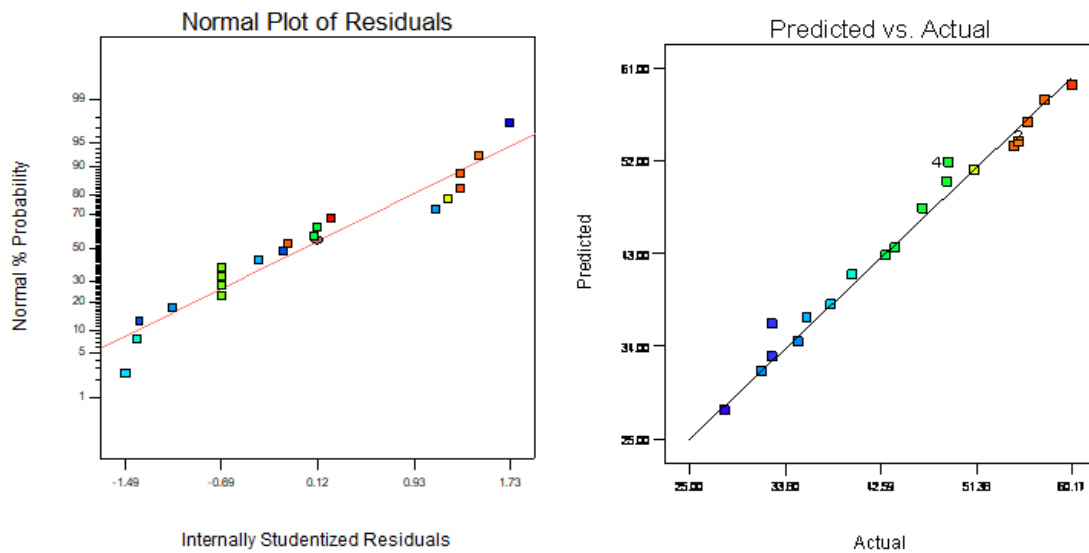


Figure no 5.96 Normal % probability verses Residual

Figure no. 5.97 Predicted Vs Actual

5.9. Graphical interpretation of models by 3D response surface and contour plots: Interaction effects of process variables on response

The statistical model analysis generated by Design expert software (version 7.2.0) of the individual parameter (adsorbent dose, solution pH and reaction time) and their interactive effects on response (removal percentage) within the experimental range were obtained through three dimensional responses surface and contour plots.

5.9.1. Effect of adsorbent dose (GONC) and pH of the solution:

From the figure 5.98, 5.99, it was showed that the mutual effect of pH of the solution and adsorbent dose on process response at constant time (37.50 min). An increase in pH of the solution corresponds to the increase in response function. The reason may be due to the fact that the accessibility of active sites enhances with the increase the pH up to certain limit beyond that the constant trend was observed.

5.9.2. Effect of pH of the solution and reaction time (min):

From the figure 5.100, 5.101, it was observed that the effect of pH of the solution was directly related with the reaction time for the process response at constant adsorbent dose (125.00 mg). An increase in pH of the solution with the increase in response function

with time increases. The reason may be due to the fact that the pH of the solution was increased with the reaction time.

Table no 5.36 ANOVA model:

Source	Sum-of Square	DF	Mean Square	F value	P-value prob> F	Remarks
Model	142.35	9	13.52	121.62	< 0.0001	Significant
A-pH	3.3241	1	4.21	65.24	< 0.0002	Significant
B-Dose	2.6410	1	6.66	32.54	< 0.0002	Significant
C-Time	1.4253	1	5.21	30.46	< 0.0002	Significant
AB	0.2478	1	0.782	5.21	< 0.0002	Significant
AC	0.2258	1	0.354	2.51	0.2425	
BC	0.2142	1	0.741	4.23	< 0.0002	
A²	34.23	1	22.46	256.85	< 0.0001	Significant
B²	25.32	1	25.324	322.14	< 0.0002	Significant
C²	0.2450	1	0.3524	1.562	0.20452	
Residual	0.0549	10	0.07824			
Lack of Fit	0.3842	5	0.0365	3.2145	0.5421	
Pure error	0.0322	5	0.113			Not Significant

5.9.3. Effect of adsorbent dose (mg) and reaction time (min):

The communal effect of adsorbent dose and reaction time (min) was analyzed in the figure no 5.102, 5.103. The response function i.e, percentage removal was increased with the increase of adsorbent dose with time. The accessibility of active site of the adsorbent was enhanced with the reaction time at constant pH (6.00) of the solution. The PH molecules get more attached with the functional group of the adsorbent and hence increase the response for the process. The experimental data was better correlate with the model result.

5.9.4. Optimization and confirmation of reaction condition:

From the above observation it was observed that the experimental data better co relate the statistical data. To achieve maximum removal percentage (60.17), from process optimization modeling the optimum initial pH, adsorbent dose and reaction time were found to be 6.00, 125.00 mg, 35.50 min respectively. A good agreement was observed between the predicted R^2 and adjusted R^2 obtained with the experimental R^2 , which

indicates the suitability of the model for predicting the response as well as to optimize the process conditions.

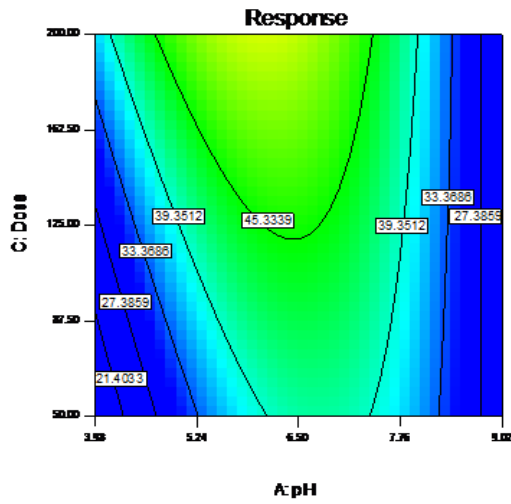


Figure 5.98 Contour plot (PH) of Dose and pH

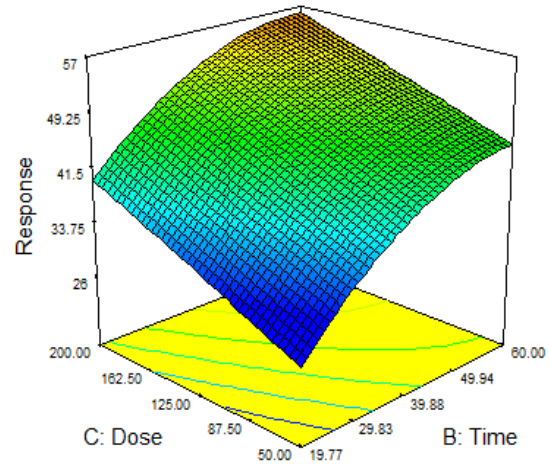


Figure no 5.99 3D surface (PH) of Dose and pH

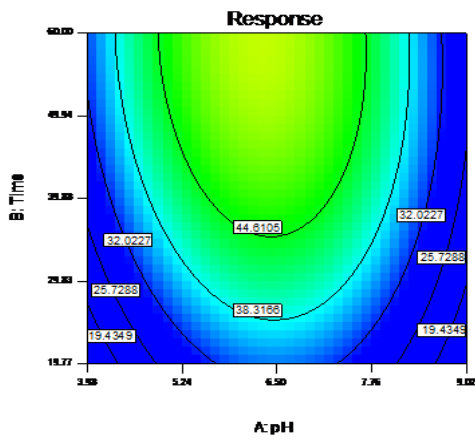


Figure no 5.100 Contour plot (PH) of Time Vs pH

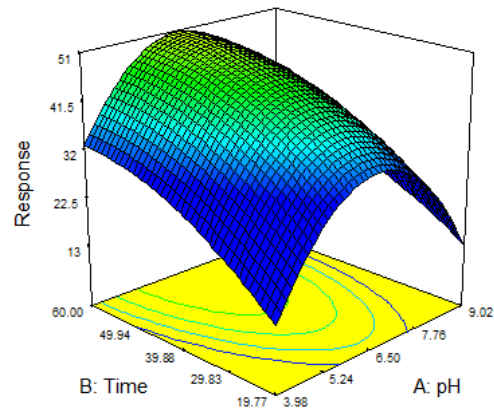


Figure no 5.101 3D surface (PH) of Time and pH

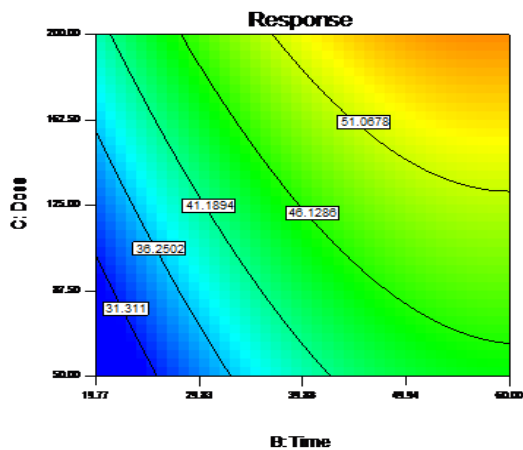


Figure no 5.102 Contour plot (PH) of Time and Dose

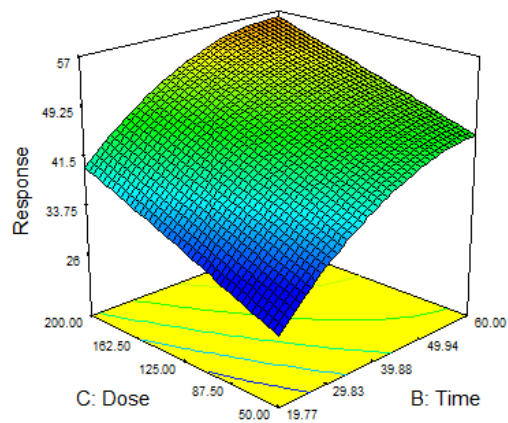


Figure no 5.103 3D surface (PH) of Time and Dose

5.10. Column study:

5.10.1. Effect of various parameters on column performance:

To evaluate the efficiency of GONC in large scale application column mode was apply. The effects of various parameters like bed height, flow rate and influent PH concentration were varying to evaluate the column mode adsorption process of PH. The breakthrough curves (C_t/C_0 verses t) obtained during this study did not thoroughly match with the theoretical column mode 'S' shaped curved. The reason behind the deviation of appearance can be endorsed by the two main factors –

1. The slow adsorption rate kinetics plays a vital role between PH molecules and GONC.
2. The use of small lab-scale column equipments makes the breakthrough faster which leads to an incomplete 'S' shape of the plot (Al-Degs et al., 2009).

5.10.2. Effect of bed depth:

The outcome of performance of GONC on adsorption depends on various bed heights (2, 3 and 5 cm) when the column was packed with 4, 6 and 8 g of dried GONC respectively. Adsorption breakthrough curves (figure no 5.104) was obtained for different bed depths at constant input flow rate (5 ml/min) with input PH concentration 50 mg/ml was considered. The data obtained from the experiment were presented in table no 5.37 and it was observed that at exhaustion time the amount of total dye adsorbed (m_{ad}) increased with the bed height increased. The better performance was obtained at highest bed height. This is due to the fact that as the column bed height increases, the active sites presents in the adsorbent increase. At reaction time the PH molecules gets attached with the active sites of adsorbent and hence increases the removal percentage of PH on GONC (Han et al., 2008).

5.10.3. Effect of flow rate:

The performance of the column was dependent on input adsorbate flow rate at fixed bed height and concentration (3 cm, 50 mg/l). Figure 5.109 represent the relationship between C_t/C_0 with time t at different flow rate (5, 10, 15 ml/min). The exhaustion time decreased from 420 to 380 min when flow rate was increased from 5 to 15 ml/min respectively. The reason behind this phenomenon that the residence time of the PH molecules on the adsorbent surface decreased when the flow rate was increased (Uddin et al., 2009).

5.10.4. Effect of initial dye concentration:

The influent PH concentrations lead to the detrimental effect on the column performance. The performance of column evaluated at various influent dye concentrations (50, 100 mg/l) during this study. From the figure 5.105, it was clearly observed that the break through time and exhaustion time was decreased from 300 to 240 min and 420 to 370 min when concentration of PH increased from 50 to 100 mg/l respectively. At higher concentration the concentration gradient increased the diffusion coefficient and fast saturation of active sites of the adsorbents takes place (Han et al., 2009).

Table no 5.37 Effect of different bed height, concentration and flow rate on column adsorption:

Z (cm)	F (ml/min)	C ₀ (mg/l)	t _b (min)	t _e (min)	m _{ad} (mg)	q _{e,exp} (mg/g)
2	5	50	140	370	33.04	8.26
3	5	50	230	410	45.23	7.53
5	5	50	290	430	65.11	8.13
3	10	50	210	390	29.32	7.33
3	15	50	150	375	22.43	5.60
3	5	100	260	390	16.55	4.13

5.10.5. Modeling of column data:

5.10.5.1. Thomas model:

The experimental data were obtained from column experiments and analyzed by Thomas and BDST model. The data at C_t/C_0 values was taken higher than 0.82 and lower than 0.97 were considered for modeling the experimental value. Thomas rate constant (K_{Th}) and adsorption capacity (q_e) were obtained from the slope and intercept (Uddin et al., 2009). Thomas model parameters are presented in table no 5.38. The R^2 values were obtained ranging from 0.86 to 0.92, evaluated from regression coefficient analysis. The increase in the initial PH concentration at constant bed height (3cm) and flow rate (5ml/min) the value of q_e decreased along with the value of k_{Th} decreased. Thus, better column performance can be achieved with lower flow rate, lower concentration at constant bed height. It is evident from Table 5.38 that the experimental and calculated adsorption capacities are close at all the operating conditions studied it evident the experimental data satisfy the column model.

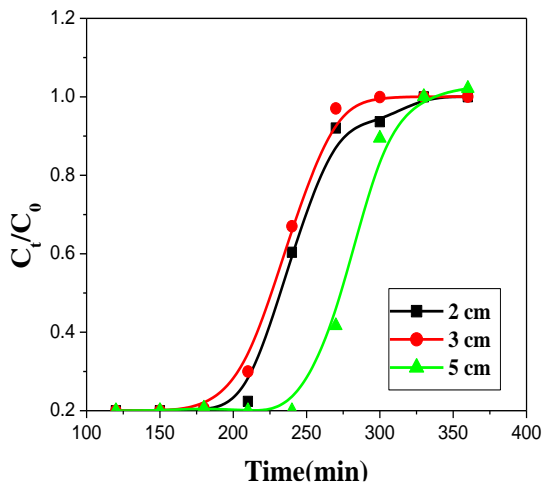


Figure 5.108 Column study (bed height) of PH

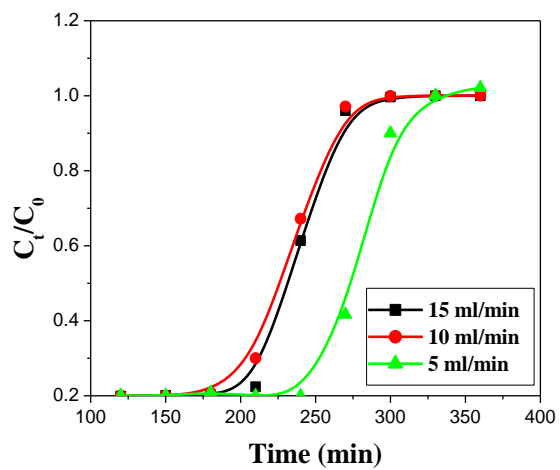


Figure 5.109 Column study (flow rate) of PH

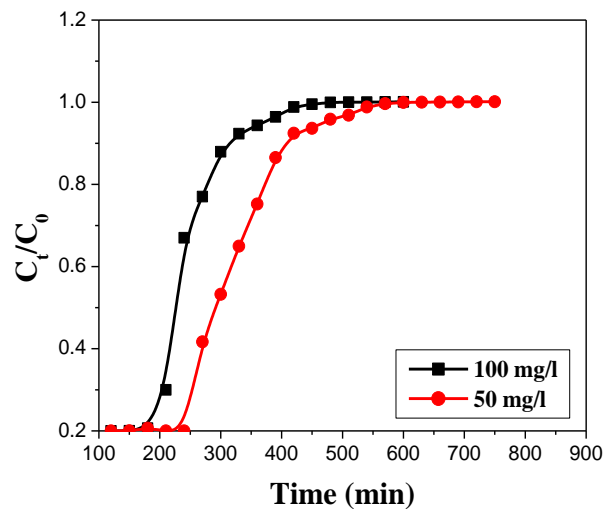


Figure 5.110 Column study (influent concentration) of PH

5.10.5.2. BDST model:

The ability of BDST model to predict column performance different concentration and unknown flow rate was investigated utilizing experimental constant value obtained from column experiment. The constants, N_0 and K_a , were calculated from t_s vs. Z plots for different column bed depth of 2, 3 and 5 cm. The high R^2 values ranging from 0.88 to 0.95 demonstrates the validity of BDST model. The value of N_0 , K_a , a , b were calculated from the equation and listed in table no 5.39. Table no 5.40 represented the breakthrough time using BDST constant for new flow rate or new concentration.

Table no 5.38 Thomas model constant values:

C₀ (mg/l)	Q (ml/min)	K_{Th}(ml. min./mg)	q_e exp (mg/g)	q_e cal (mg/g)	R²
50	5	0.0542	5.60	5.16	0.9213
150	5	0.0365	4.13	3.52	0.8611

Table no 5.39 BDST model constant values:

Bed depth Z (cm)	a (min/cm)	b (min)	K_a (l/mg/min)	N₀ (mg/l)	R²
2	11.59	0.352	0.0272	118.6	0.8832
3	16.42	0.418	0.0558	132.12	0.9213
5	16.82	0.452	0.0581	133.66	0.9511

Table no 5.40 Breakthrough time calculated using BDST constant for (CV) new flow rate or new concentration:

C_t/C₀	a (min/cm)	b (min)	t_{cal} (min)	t_{exp} (min)
F= 3 ml/min C ₀ = 25 mg/l	F= 3 ml/min C ₀ = 25 mg/l	F= 3 ml/min C ₀ = 25 mg/l	F= 3 ml/min C ₀ = 25 mg/l	F= 3 ml/min C ₀ = 25 mg/l
0.2	3.754	0.369	62	75
0.9	37.63	2.59	240	255
F= 20ml/min C ₀ = 125 mg/l	F= 20ml/min C ₀ = 125 mg/l	F= 20ml/min C ₀ = 125 mg/l	F= 20ml/min C ₀ = 125 mg/l	F= 20ml/min C ₀ = 125 mg/l
0.2	1.854	0.546	55	68
0.9	6.632	0.146	150	168

5.11. Naphthalene:

5.11.1. Batch adsorption study:

The removal efficiency of NAP by GO, R-GO and GONC at various experimental parameters were analyzed during this adsorption study. The aqueous NAP solution of 100 ml was taken in 250 ml conical flask with variation in one operational parameters and keeping other parameters constant in BOD incubator shaker at constant 120 rpm. The solution was taken out from the flask after predetermined time intervals and residual concentration of NAP was measured by UV-VIS spectrophotometer at 219 nm.

5.11.1.1. Effect of adsorbent dose:

The uptake capacity of the adsorbent was determined by the adsorbent dose analysis. The NAP removal efficiency of three adsorbents (GO, R-GO, GONC) were increased with the amount of adsorbent dose increase up to 0.10 g/l after that no drastic change was shown. The increase the amount of adsorbents leads to the increase the active sites presents in the adsorbents, which boost up the interaction between active sites with NAP molecules presents in aqueous phase (Ahmed et al., 2009). Form the figure 5.106, 5.107, 5.108 it was clearly observed that GONC shows better removal efficiency than R-GO and GO due to the more number of potential active sites presents in its structure than R-GO and GO.

5.11.1.2. Effect of initial NAP concentration:

Initial NAP concentration have inverse effect on removal efficiency of NAP by R-GO, GO and GONC. It is evident from the fig 5.109, 5.110, 5.111, that the removal percentage of NAP by R-GO, GO and GONC shows decreasing trend with the increase initial NAP concentration form 5-25 mg/l. The maximum removal was almost similar for 5 and 10 mg/l. The reasons behind this phenomenon was at low concentration the all active sites being saturated by the NAP molecules but when the concentration was increase amount of NAP molecules was increase but the limited number of active sites the removal efficiency was not increase (H. Catherine et al., 2017). The GONC shows the better removal efficiency comparing with R-GO and GO because large number of active sites presents in its structure.

5.11.1.3. Effect of pH of the solution:

The pH of the medium will control the NAP removal by controlling the magnitude of the electro-static charges that are produced by the ionized adsorbate molecules (Khan et al., 2013). In the figure 5.112, 5.113, 5.114 shows the removal percentage of NAP at different solution pH with respect to time by R-GO, GO and GONC were analyzed during this study. From the figure it was observed that at lower pH the removal percentage was less due to the strong electro-static repulsion force present between active sites and ionized NAP molecules. The removal percentage was gradually increase between pH-4 to 6 probably the dissociation factors which helps to neutralize the repulsion force, beyond pH 6 almost remains unchanged (Xu et.al., 2012). The removal efficiency was better for GONC compare with R-GO and GO due to the large number of oxygen containing active groups presents into GONC structure which attract more numbers ionized NAP molecules.

5.11.1.4. Effect of temperature on dye adsorption:

The removal efficiency of NAP also governed by solution temperatures. From the following figure 5.115, 5.116, 5.117 it was clearly observed that the removal percentage of NAP were increased with the increasing the temperature 20 °C to 40 °C. The mobility of molecules of NAP was increased with the temperature increased hence gets more reacted with the active sites of the adsorbents beyond that the efficiency was decreased because at high temperature weakening the bonds between adsorbent and adsorbate molecules (X.Yang et al., 2013). The removal efficiency of GONC was better than R-GO and GO.

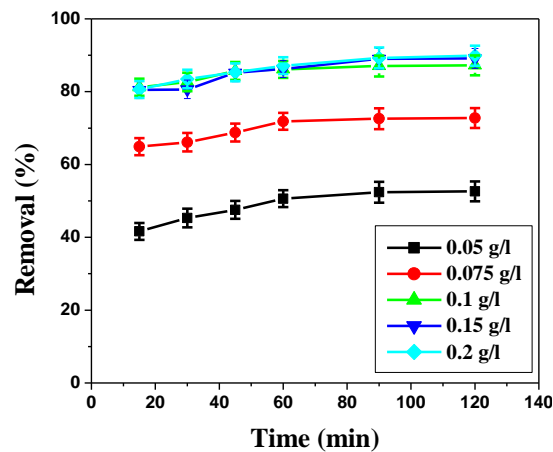


Figure no 5.106 NAP removal by R-GO

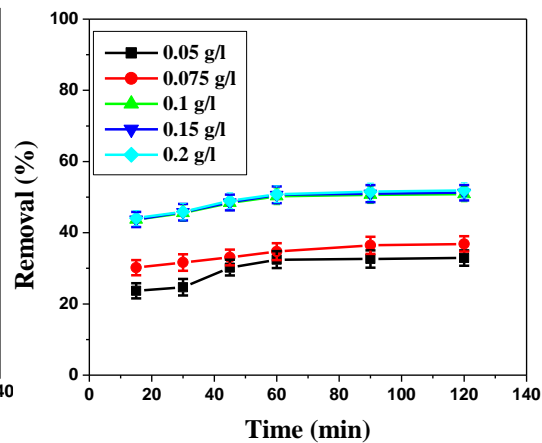


Figure no 5.107 NAP removal by GO

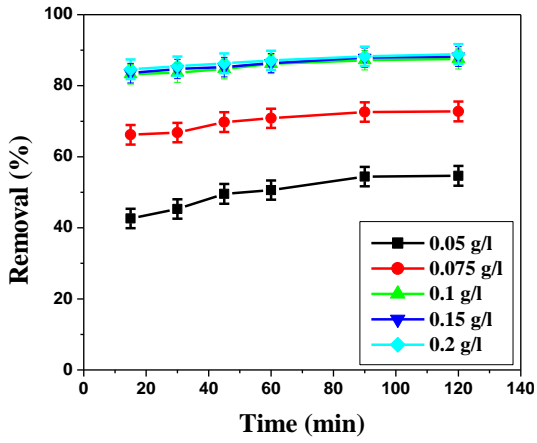


Figure no 5.108 NAP removal by GONC.

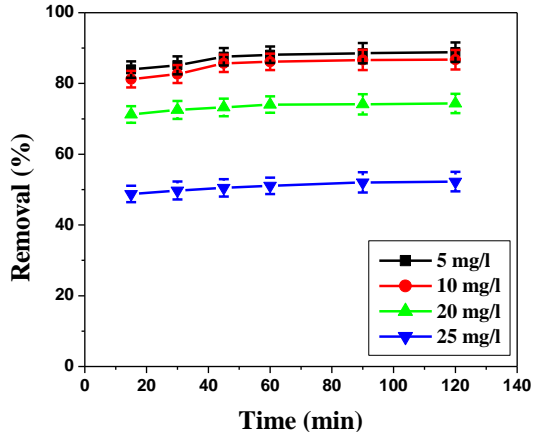


Figure no 5.109 NAP removal by R-GO at conc

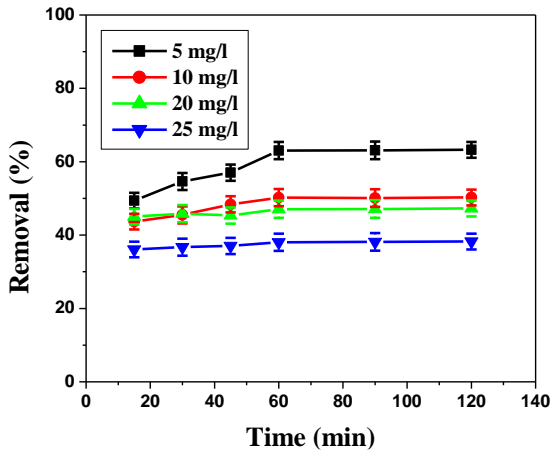


Figure no 5.110 NAP removal by GO at Conc

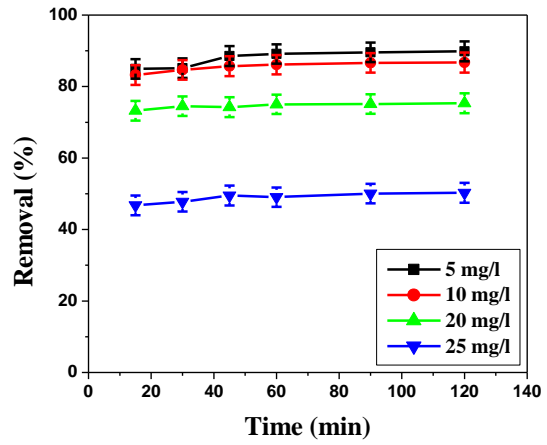


Figure no.5.111 NAP removal by GONC at Conc

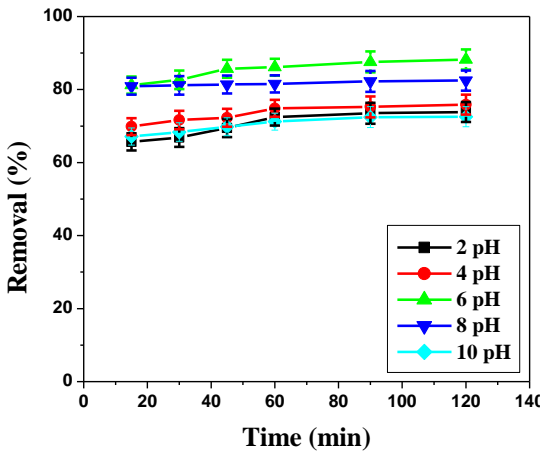


Figure no. 5.112 removal of NAP by R-GO at pH

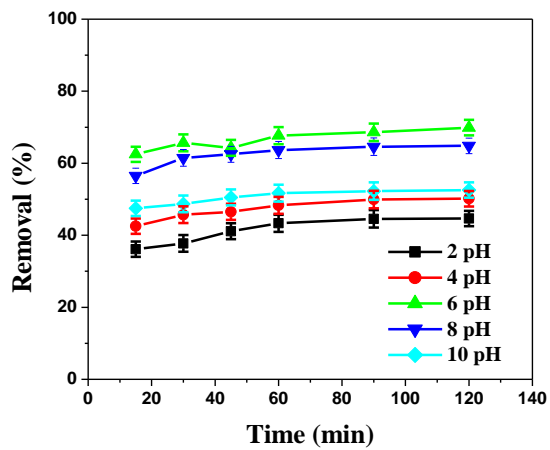


Figure no 5.113 removal of NAP by GO at pH

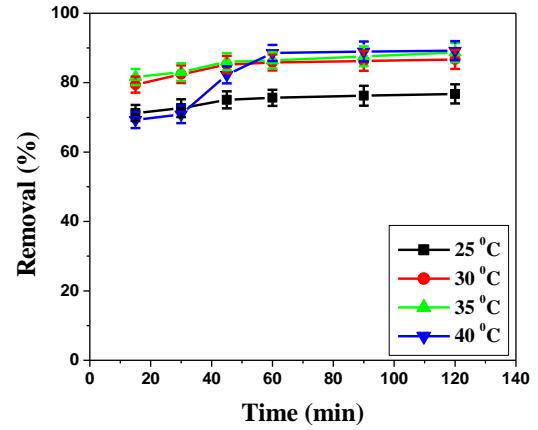
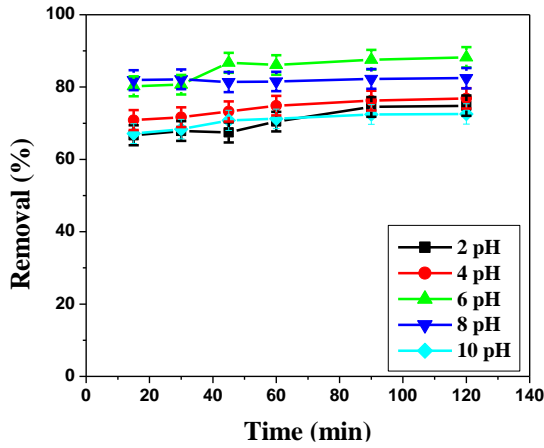


Figure no. 5.114 removal of NAP by GONC at pH. Figure no 5.115 removal of NAP by R-GO at temp

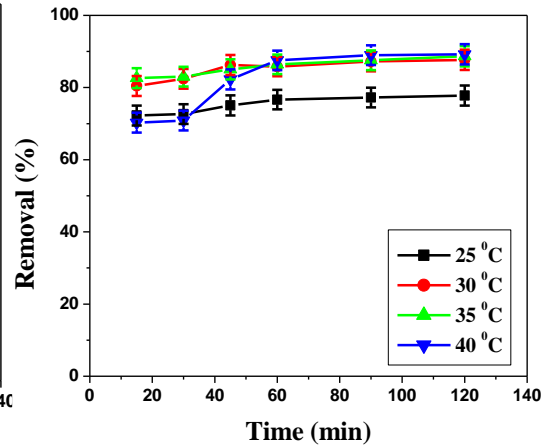
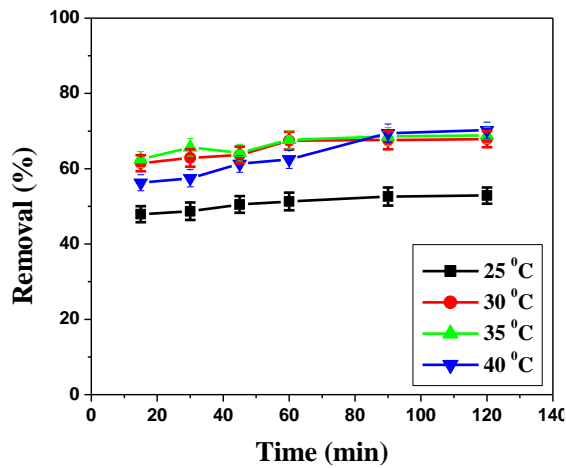


Figure 5.116 removal of NAP by GO at temp

Figure no 5.117 removal of NAP by GONC at temp

5.12.2. Equilibrium study of NAP by GONC:

To evaluate the effect of all operational parameters together on NAP removal by GONC was investigated during this adsorption experiment. All the operational parameters i.e., adsorbent dose, solution pH, initial NAP concentration and temperature kept at their optimum point (adsorbent dose – 0.1 g/l, pH of the solution- 6, temperature- 40 °C and initial NAP concentration-10 mg/l). Figure no.5.118 shows that up to 50 min the removal percentage was increasing beyond that the removal efficiency of GONC was constant due to the saturation of active sites.

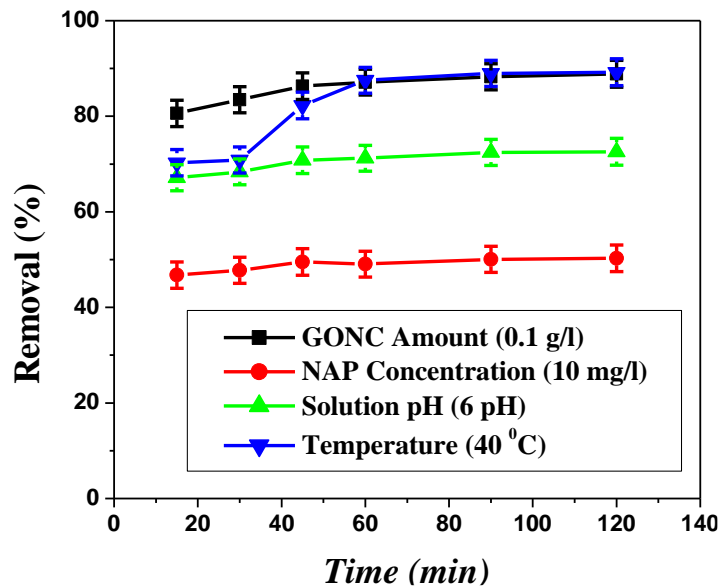


Figure no 5.118 Equilibrium study of NAP by GONC

5.12.3. Adsorption Isotherms:

The interaction between adsorbent surface and adsorbate molecules were investigated during adsorption isotherms experiments. Experimental data were analyzed by the Langmuir, Freundlich and Temkin isotherms models. The adsorption capacity of adsorbents GR-GO, GO and GONC for removal of NAP from its aqueous phase was calculated from the models equations.

Langmuir isotherms model describe the monolayer adsorption process with homogeneous distribution of adsorbate molecules onto the adsorbent solid surface (Sajab et al., 2011) (Xu et al., 2012). All the parameters constant value along with regression coefficient listed in table no 5.41.

Freundlich isotherms co-relate with multilayer adsorption process, where adsorbate molecules interact with heterogeneous surface of adsorbent (Haghseresh et al., 2005) (Z. Pei et al., 2013). The Freundlich model constant parameters K_F and n along with regression coefficient listed in table no 5.41.

Temkin isotherms model assumes that the heat of adsorption process decreases linearly with the increase in coverage area of adsorbent surface (Limousin et al., 2007). The model constant parameter B_T and K_T was calculated from slope and intercept of the linearized plot q_e vs $\ln C_e$.

Among the three models Langmuir model was better represent the experimental data with high regression coefficient and smallest linear error (χ^2) value for GONC comparing with the R-GO and GO.

5.12.4. Adsorption kinetics:

The three kinetics model viz., Pseudo-first-order, Pseudo-second-order and Inter particle diffusion model were consider find out the experimental adsorption rate constant. The NAP adsorption process can be considered as a quasi-instantaneous diffusion process. All the model constant values listed in table no 5.42.

Pseudo-second-order kinetics model is the most significant and acceptable kinetics model which correlate the diffusion of liquid film on to the adsorbent surface (Saeed et al., 2010) (Xu et al., 2012). Table no 5.42 shows the less disparity between experimental and calculated one. The chi-square (χ^2) value was smaller for GONC than R-GO and GO as depicted that GONC better represent the second-order kinetics model.

Adsorption process not only governed by the surface phenomenon but also intra-molecular diffusion or combination of both, this phenomenon was stated in intra-particle diffusion model (Mall et al., 2005). The value of R^2 and χ^2 depict the feasibility of adsorption process were listed in table no 5.42.

From the table it was observed that GONC posses high R^2 value and small χ^2 value than R-GO and GO for pseudo-second-order kinetics model.

5.12.5. Adsorption Thermodynamics:

Thermodynamics analysis of adsorption process decides the endothermic or exothermic nature of the adsorption process (Anirudhan and Radhakrishnan, 2008). The values of ΔH^0 and ΔS^0 were calculated from slope and intercept of the linear plot $\ln K_d$ versus $1/T$. The positive value of ΔH^0 indicates the process is endothermic in nature and positive value of ΔS^0 suggested that the increased randomness between solid-solute interface. The value of ΔH^0 and ΔS^0 for GONC is higher than GO and R-GO. The value of gibbs free energy (ΔG^0) determines the nature of process whether it is physisorption or chemisorption in nature. The negative values of ΔG^0 for various temperatures correspond to the spontaneous nature of adsorption (Liu et al., 2012). The values of ΔG^0 , ΔH^0 , ΔS^0 for GO, R-GO, GONC were listed in table no 5.43.

Table no 5.41 Isotherms parameters value of NAP:

Isotherms models	Parameters	Adsorbents		
		R-GO	GO	GONC
Langmuir model	q_0 (mg/g)	62.5	88.4	95.4
	B (l/mg)	5.54	3.04	8.16
	R^2	0.996	0.9436	0.9998
	χ^2	28.21	26.64	23.52
Freundlich model	K_F (mg/g (l/mg) ^{1/n})	99.15	96.3	101.96
	$1/n$	0.296	0.670	0.275
	R^2	0.9012	0.888	0.9354
	χ^2	41.84	35.36	33.51
Temkin model	B_T (l/g)	26.34	15.42	26.67
	K_T	7.96	5.23	8.39
	R^2	0.982	0.875	0.989
	χ^2	34.32	27.54	29.41

Table no 5.42 Kinetics parameters value of NAP:

Kinetics models	Parameters	Adsorbents					
		R-GO		GO		GONC	
		q_e exp	q_e cal	q_e exp	q_e cal	q_e exp	q_e cal
Pseudo-first-order	q_e (mg/g)	35.65	37.36	20.42	23.12	38.15	40.22
	K_1 (h)	0.0616		0.0172		0.0681	
	R^2	0.946		0.845		0.982	
	χ^2	37.21		35.45		28.24	
Pseudo-second-order	q_e (mg/g)	382.6	383.6	275.6	278.3	393.5	395.4
	K_2 (g g/h)	0.058		0.024		0.061	
	R^2	0.992		0.958		1.0	
	χ^2	18.52		16.34		12.35	
Intraparticle Diffusion	C	22.56		14.56		24.01	
	K_{diff} (mg/g h ^{1/2})	18.26		10.65		19.63	
	R^2	0.946		0.9223		0.978	
	χ^2	28.45		26.63		23.54	

Table no 5.43 Activation energy parameters for removal of NAP by R-GO, GO and GONC:

Temperature	Parameters	Adsorbents		
		R-GO	GO	GONC
303 K	ΔG^0 (kJ/mol)	-1.46	-1.13	-1.86
	ΔH^0 (kJ/mol)	66.35	50.89	73.54
	ΔS^0 (J/mol K)	1.64	1.21	2.40
308 K	ΔG^0 (kJ/mol)	-1.88	-1.54	-2.31
	ΔH^0 (kJ/mol)	66.35	50.89	73.54
	ΔS^0 (J/mol K)	1.64	1.21	2.40
313 K	ΔG^0 (kJ/mol)	-2.12	-1.72	-2.42
	ΔH^0 (kJ/mol)	66.35	50.89	73.54
	ΔS^0 (J/mol K)	1.64	1.21	2.40

5.12.6. Response surface methodology used for optimization of CR adsorption by GONC:**5.12.6.1. Model verification and develop regression model equation:**

For establish a relationship between mathematical and statistical model response surface methodology have been used (Anderson and Whitcomb, 2005).

From the batch experiment and different process model it was observed that GONC posses better remove efficiency of NAP from its aqueous mode than GO and R-GO. RSM study of NAP was analyzed for GONC with three independent process parameters viz..., adsorbent dose (mg), pH of the solution, reaction time (min) and their impact on the response (removal percentage) were investigated. The model was suggested twenty experiments listed in table no 5.44. The polynomial quadratic model was best describing response function (removal percentage). All the parameters value was listed in table no 5.45. The polynomial quadratic equation with their actual variables were expressed as –

$$\begin{aligned} \text{Response (Removal Percentage)} = & -170.82 + 46.92 * \text{pH} + 0.89 * \text{Time} \\ & + 0.65 * \text{Adsorbent dose} + 0.019 * \text{pH} \\ & * \text{Time} - 0.06 * \text{pH} * \text{Adsorbent dose} \\ & - 0.25 * \text{Time} * \text{Adsorbent dose} - 3.06 * \text{pH}^2 \\ & - 0.012 * \text{Temperature}^2 - 0.83 * \text{Adsorbent dose}^2 \end{aligned}$$

The constant -170.82 was independent and negative sign shows decreasing trends for all factors and interaction between them. The interaction terms (Time*Adsorbent dose)

(pH*Dose) should possess negative sign leads to antagonistic effect on response i.e the response will decrease as the value of these terms increase. Whereas, the independent terms (pH, Adsorbent dose, Time) and interaction terms (pH*Time) and second order terms (pH, Time and Adsorbent Dose) had a positive influence which possesses synergistic effect indicate that with an increase of these factors directly proportional to response (Singh et al., 2011) i.e removal percentage of NAP.

5.12.6.2. Analysis of variance (ANOVA)

ANOVA was performed to verify the satisfactoriness of the developed quadratic model. The model terms are regarded as significant only with high F value and P value (Prob>F) are 112.4 less than 0.0002. Among all the parameters the linear terms (A, B, C), interaction term (AxB) and square terms A^2 B^2 showed most significant effect on response, having P-value <0.0002 to < 0.001 table no 5.46 represent ANOVA model. The model shows a reasonable acceptable value between model R^2 (0.9062) and predicted R^2 (0.8661), adjusted R^2 value (0.8752) was obtained by ANOVA model. From this analysis it was found that developed quadratic model was found to be suitable for representing the experimental data of adsorption of NAP by GONC.

Table 5.45 Fit summary of different model

Source	Linear	2FI	Quadratic	Cubic
Sum of squares	1994.21	1626.59	677.64	0.00
Mean square	181.29	203.32	5.53	0.00
F-value	56.34	152.42	354.63	78.89
Lack of fit P-value	<0.005	0.245	<0.0002	0.0263
Std. Dev.	23.64	14.21	6.34	0.00
R^2	0.4362	0.5401	0.9062	0.3245
Adjusted R^2	0.3524	0.4125	0.8752	0.2115
Predicted R^2	0.3212	0.3951	0.8661	0.1852
PRESS	325.24	474.4	159.79 (Suggested)	204.64 (Aliased)

Table 5.44 RSM Model experimental analysis:

Run	Factor 1 A: pH	Factor 2B: Adsorbent dose (g/l)	Factor 3 C: Time (min)	Response (Removal percentage)
1	6.50	175.00	45.00	71.7292
2	6.50	175.00	45.00	71.7292
3	5.00	250.00	30.00	63.9167
4	6.50	301.00	45.00	78.3333
5	3.98	175.00	45.00	65.1042
6	8.00	25.00	30.00	52.3125
7	5.00	100.00	60.00	46.3333
8	6.50	175.00	45.00	71.7292
9	5.00	100.00	30.00	42.7917
10	8.00	250.00	60.00	68.8125
11	9.02	175.00	45.00	35.6667
12	6.50	175.00	70.00	76.1875
13	6.50	175.00	45.00	71.7292
14	6.50	175.00	19.77	48.3542
15	6.50	48.88	45.00	35.0417
16	8.00	100.00	30.00	61.3333
17	8.00	100.00	60.00	61.0208
18	5.00	250.00	60.00	73.1875
19	6.50	175.00	45.00	71.7292
20	6.50	175.00	45.00	71.7292

The analysis of statistical properties of the model was also performed by normal percentage probability plot of the residuals, a system for assessing the better relationship between the set of observed values with the theoretical distribution (Bingol et al., 2010). Approximately linear data points indicated the process was followed normal distribution (Figure no 5.119). Furthermore, a high value of R^2 (0.9062) and a realistic agreement of predicted R^2 (0.8661) with adj. R^2 value (0.8751) verified the capability of the fitted quadratic model for NAP adsorption. Thus all of these statistical tests showed that the developed quadratic model was suitable for representing the data. Figure 5.119 and 5.120 shows the % probability verses internally studentized residuals, predicted verses actual R^2 respectively.

5.12.7. Graphical interpretation of models by 3D response surface and contour plots: Interaction effects of process variables on response

The statistical model analysis generated by Design expert software (version 7.2.0) of the individual parameter (adsorbent dose, solution pH and reaction time) and their interactive effects of process variables on response (removal percentage) within the experimental range were obtained through three dimensional responses surface and contour plots.

Table no 5.46 ANOVA model:

Source	Sum-of Square	DF	Mean Square	F value	P-value prob> F	Remarks
Model	118.52	9	14.52	112.4	< 0.0001	Significant
A-pH	4.6351	1	5.02	60.45	< 0.0001	Significant
B-Dose	3.5421	1	7.76	37.56	< 0.0001	Significant
C-Time	1.8652	1	6.21	29.86	< 0.0001	Significant
AB	0.3254	1	0.778	5.21	< 0.0002	Significant
AC	0.2258	1	0.241	2.51	0.2425	
BC	0.2142	1	0.471	4.23	0.3145	
A²	28.54	1	26.41	285.52	< 0.0002	Significant
B²	25.32	1	22.95	322.14	< 0.0001	Significant
C²	0.241	1	0.245	4.021	0.5421	
Residual	0.0549	10	0.07824			
Lack of Fit	0.3842	5	0.0365	3.2145	0.5421	
Pure error	0.0322	5	0.113			Not Significant

5.12.7.1. Effect of adsorbent dose (GONC) and pH of the solution:

From the figure 5.121, 5.122 it was showed that the mutual effect of pH of the solution and adsorbent dose on process response at constant time (37.50 min). An increase in pH of the solution correspond to the increase in response function i.e, removal percentage up to certain limit after that the response function show constant effect on response. The reason may be due to the fact that the accessibility of active sites enhances with the increase. These observations were better to co-relate the experimental data.

5.12.7.2. Effect of pH of the solution and reaction time (min):

The pH of the solution and reaction time (min) were considered one of the interactive parameters for the process. From the figure 5.123, 5.124 it was observed that the effect of pH of the solution was directly related with the reaction time for the process response at constant adsorbent dose (125.00 mg). An increase in pH of the solution with the increase in response function with time increases. The reason may be due to the fact that the pH of the solution was increased with the reaction time. These observations were better consistence with the batch study experimental data.

5.12.10.3. Effect of adsorbent dose (mg) and reaction time (min):

The communal effect of adsorbent dose and reaction time was analyzed in the figure 5.125, 5.126. The response function i.e, percentage removal was increased with the increase of adsorbent dose with time. The accessibility of active site of the adsorbent was enhanced with the reaction time at constant pH (6.00) of the solution. The NAP molecules get more attached with the functional group of the adsorbent and hence increase the response for the process. The experimental data was better correlate with the model result.

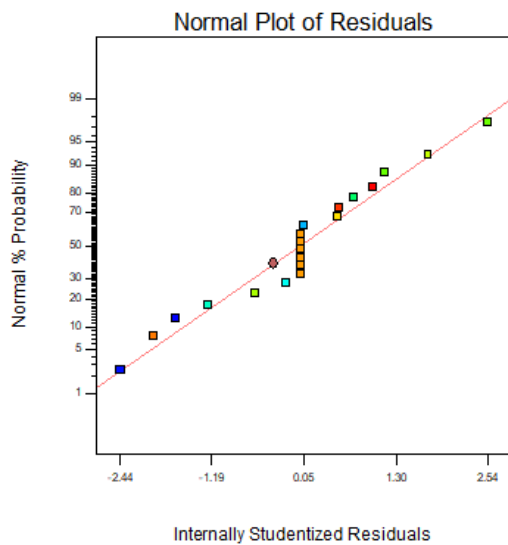


Figure 5.119 Normal % probability versus Residual (NAP)

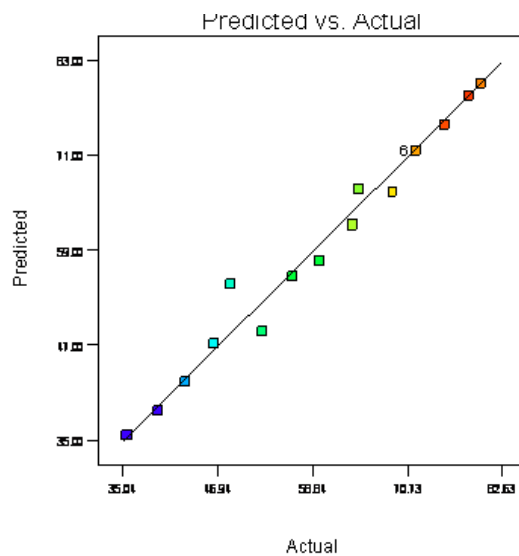


Figure 5.120 Predicted versus Actual (NAP)

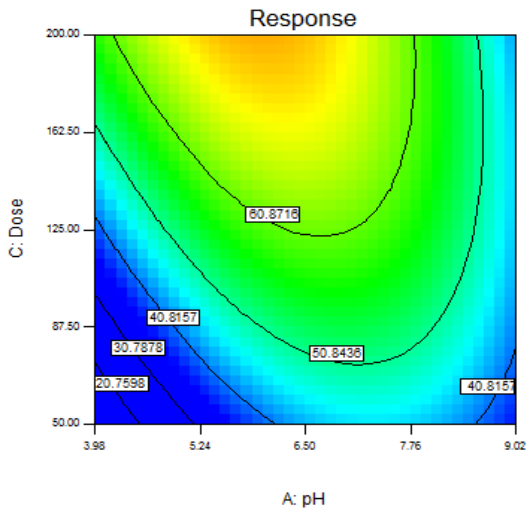


Figure 5.121 Contour plot (NAP) of Dose and pH of the solution

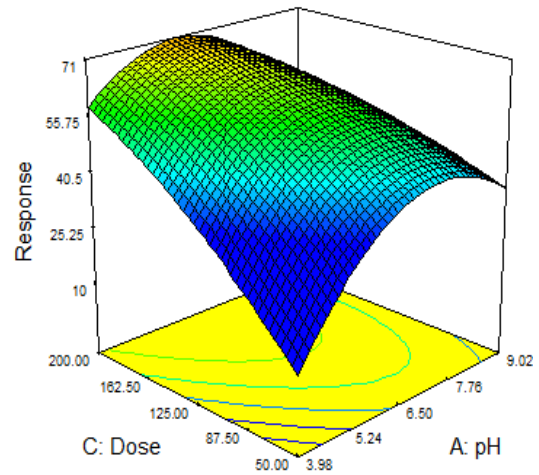


Figure 5.122 3D surface (NAP) of Dose and pH

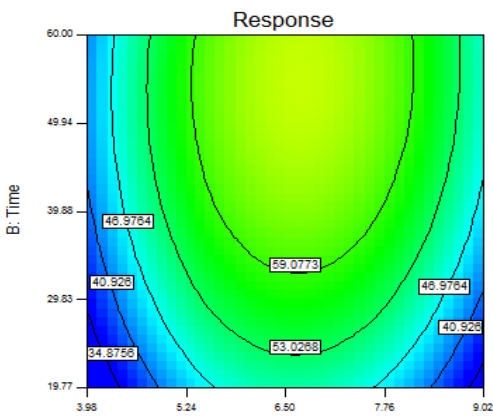


Figure 5.123 Contour plot (NAP) of Time and pH of the solution

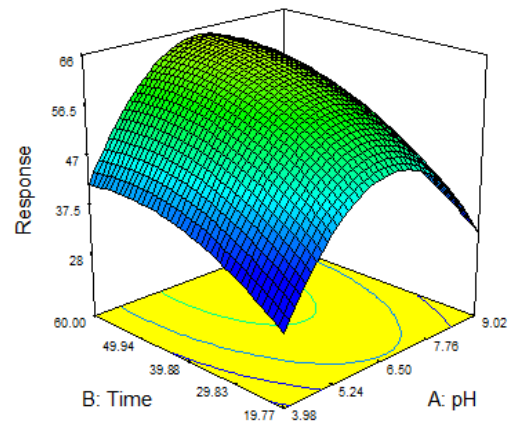


Figure 5.124 3D surface (NAP) of Time and pH

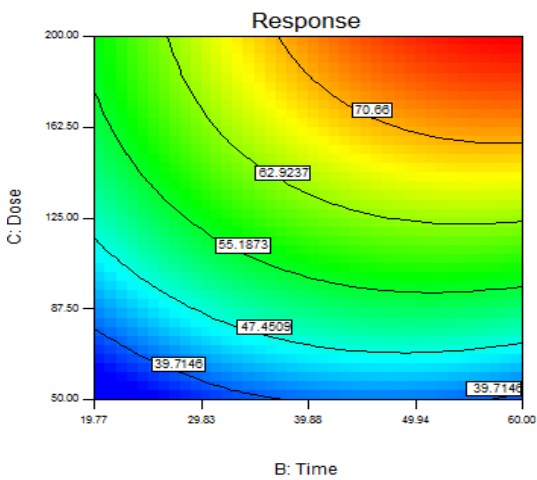


Figure 5.125 Contour plot (NAP) of Time and Dose

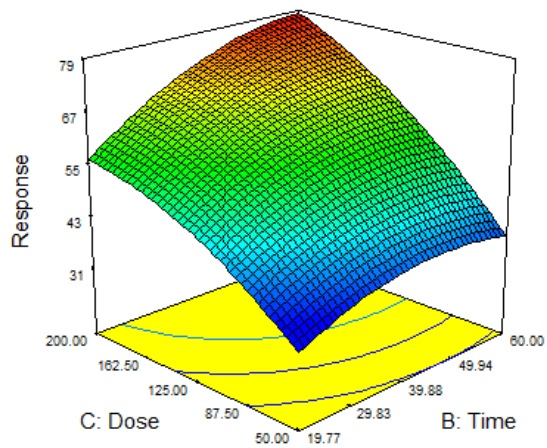


Figure 5.126 3D surface (NAP) of Time and Dose

5.12.8. Optimization and confirmation of reaction condition:

Design Expert software (version 7.2.0) generated a set of results to predict optimum reaction conditions using the quadratic model. To achieve maximum removal percentage (78.33), from process optimization modeling the optimum initial pH, adsorbent dose and reaction time were found to be 6.00, 125.0 mg, 37.50 min respectively. A good agreement was observed between the predicted R^2 and adjusted R^2 obtained with the experimental R^2 , which indicates the suitability of the model for predicting the response as well as to optimize the process conditions.

5.13. Column study:

5.13.1. Effect of various parameters on column performance:

The effects of various parameters like bed height, flow rate and influent NAP concentration were varying to evaluate the large scale (column mode) adsorption process by GONC investigated. The breakthrough curves (C_t/C_0 versus t) obtained during this study did not thoroughly match with the theoretical column mode 'S' shaped curved. The reason behind the deviation of appearance can be endorsed by the two main factors –

1. The slow adsorption rate kinetics plays a vital role between NAP molecules and GONC.
2. The use of small lab-scale column equipments makes the breakthrough faster which leads to an incomplete 'S' shape of the plot (Al-Degs et al., 2009).

5.13.2. Effect of bed depth

The effect of performance of GONC on adsorption depends on various bed heights (2, 3 and 5 cm) when the column was packed with 4, 6 and 8 g of dried GONC respectively. Adsorption breakthrough curves (Figure 5.127) was obtained for different bed depths at constant input flow rate (5 ml/min) with input NAP concentration 50 mg/ml was considered by plotting c_t/c_0 versus t . The data obtained from the experiment were presented in table no 5.47 and it was observed that at exhaustion time the amount of total dye adsorbed (m_{ad}) increased with the bed height increased. The better performance was

obtained at highest bed height. This is due to the fact that as the column bed height increases, the active sites presents in the adsorbent increase which leads to the increase the removal percentage (Han et al., 2008). Thus, when the column bed depth was increased from 2 to 5 cm t_b and t_e increased from 130 to 290 min and 330 to 450 min, respectively.

Table no: 5.47 Effect of different bed height, concentration and flow rate on column adsorption:

Z (cm)	F (ml/min)	C ₀ (mg/l)	t _b (min)	t _e (min)	m _{ad} (mg)	q _{e,exp} (mg/g)
2	5	50	130	330	25.40	6.35
3	5	50	225	380	39.22	6.53
5	5	50	290	450	69.51	8.68
3	10	50	210	345	24.63	6.12
3	15	50	110	290	17.79	4.44
3	5	100	120	230	20.65	5.14

5.13.3. Effect of flow rate:

The performance of the column was reliant on input NAP flow rate at fixed bed height and concentration (3 cm, 50 mg/l). Figure 5.131 represent the relationship between C_t/C_0 with time t at different flow rate (5, 10, 15 ml/min). The exhaustion time decreased from 430 to 380 min when flow rate was increased from 5 to 15 ml/min respectively (Figure no 5.128). The reason behind this phenomenon that the residence time of the NAP molecules on the adsorbent surface decreased when the flow rate was increased which leads to decreased the removal efficiency and break through time along with exhaustion time simultaneously (Uddin et al., 2009).

5.13.4. Effect of initial dye concentration:

The influent NAP concentrations lead to the detrimental effect on the column performance. The performance of column evaluated at various influent dye concentrations (50, 100 mg/l) during this study. From the figure no 5.129 it was clearly observed that the break through time (t_b) and exhaustion time (t_e) was decreased from 245 to 140 min and 475 to 280 min when concentration of NAP increased from 50 to 100 mg/l respectively. At higher concentration the gradient of concentration increased the

diffusion coefficient and fast saturation of active sites of the adsorbents which may leads to the decrease of break through time and exhaustion time respectively (Han et al., 2009).

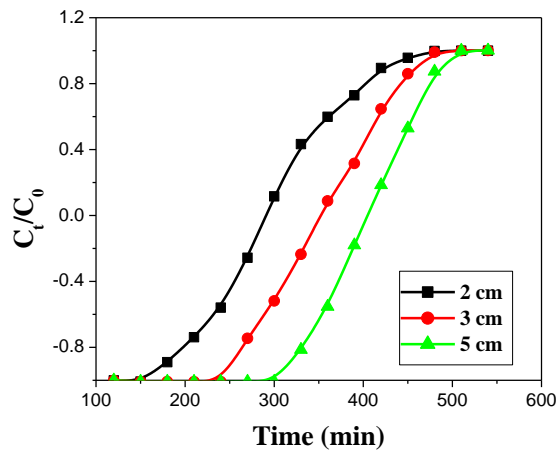


Figure no 5.127 Column study (bed height) of NAP

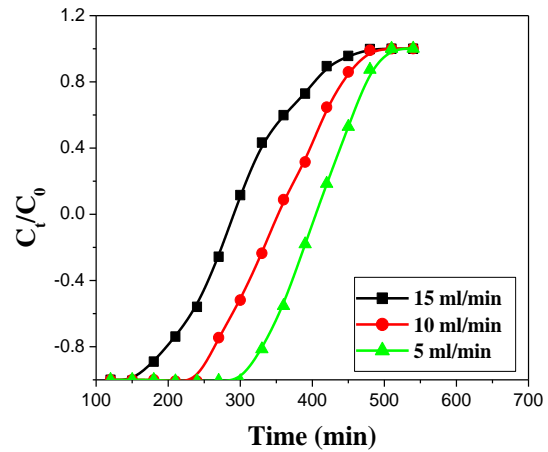


Figure 5.128 Column study (flow rate) of NAP

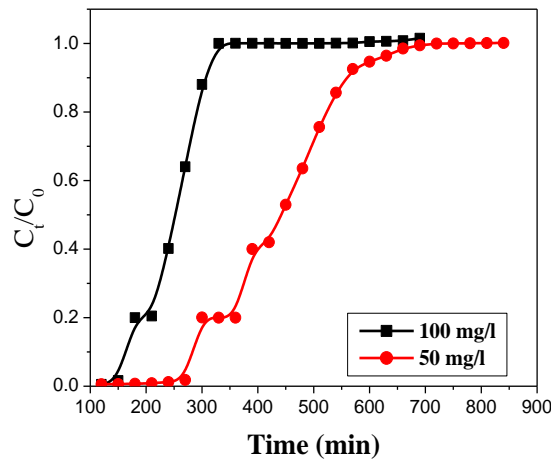


Figure 5.129 Column study (influent concentration) of NAP

5.14.. Modeling of column data:

5.14.1. Thomas model:

The experimental data were obtained from column experiments and analyzed by Thomas and BDST model. The data at C_t/C_o values was taken higher than 0.06 and lower than 0.94 were considered for modeling the experimental value. Thomas rate constant (K_{Th}) and adsorption capacity (q_e) were obtained from the slope and intercept (Uddin et al., 2009). Thomas model parameters are presented in table 5.48. The R^2 value was obtained ranging from 0.85 to 0.90, evaluated from regression coefficient analysis. The increase in the initial NAP concentration at constant bed height (3cm) and flow rate (5ml/min) the

value of q_e decreased along with the value of K_{Th} decreased. Thus, better column performance can be achieved with lower flow rate, lower concentration at constant bed height. It is evident from Table 5.48 that the experimental and calculated adsorption capacities are close at all the operating conditions studied it evident the experimental data satisfy the column model.

Table no 5.48 Thomas model constant values:

C_0 (mg/l)	Q (ml/min)	K_{Th} (ml. min./mg)	q_e (mg/g) _{exp}	q_e cal (mg/g)	R^2
100	5	0.06425	6.35	5.22	0.8540
150	10	0.05352	6.12	5.13	0.9013

5.14.2. BDST model:

The ability of BDST model to predict column performance unknown concentration and unknown flow rate was investigated utilizing experimental data obtained from column experiment. The constants, N_0 and K_a , were calculated from t_s vs. Z plots for different column bed depth of 2, 3 and 5 cm. The high R^2 values ranging from 0.92 to 0.96 demonstrates the validity of BDST model. The value of N_0 , K_a , a and b were calculated from the equation and listed in table no 5.49 The lower adsorption capacity at low breakthrough and low concentration than that at exhausted condition of column bed is due to the un-saturation of several adsorbent active sites by the dye molecules. Table no 5.50 represented the breakthrough time using BDST constant for new flow rate or new concentration.

Table no. 5.49 BDST model constant value:

Bed depth Z (cm)	a (min/cm)	b (min)	K_a (l/mg/min)	N_0 (mg/l)	R^2
2	11.59	0.352	0.0272	118.6	0.9213
3	16.42	0.418	0.0558	132.12	0.9448
5	16.85	0.452	0.0581	133.66	0.9623

Table no. 5.50 Breakthrough time calculated using BDST constant for (NAP) new flow rate or new concentration:

C_t/C_0	a (min/cm)	b (min)	t_{cal} (min)	t_{exp} (min)
F= 3 ml/min C ₀ = 25 mg/l	F= 3ml/min C ₀ = 25 mg/l	F= 3ml/min C ₀ = 25 mg/l	F= 3ml/min C ₀ = 25 mg/l	F= 3ml/min C ₀ = 25 mg/l
0.2	3.754	0.369	62	75
0.9	37.63	2.59	240	255
F= 20ml/min C ₀ = 150 mg/l	F= 20ml/min C ₀ = 150 mg/l	F= 20ml/min C ₀ = 150 mg/l	F= 20ml/min C ₀ = 150 mg/l	F= 20ml/min C ₀ = 150 mg/l
0.2	1.854	0.546	55	68
0.9	6.632	0.146	150	168

5.15. Toxicological analysis:

Toxicological analysis was done for CR, MY, CV, PH and NAP by *Cicer arietinum* seeds. Batch experimental data conclude that removal efficiency of GONC was better for all adsorbate solution comparing with R-GO and GO. Three set of experiment was carried out such as untreated solution (for all adsorbate) treated solution (by GONC) and one control distilled water solutions (Roy et al., 2018). The root- shoot length of *Cicer arietinum* seeds for 6 days analysis was measured and shows that the root length was increased day by day for treated solution comparing with untreated one. Figure no 5.130, 5.132, 5.134, 5.136, 5.138 shows the root length for untreated and treated solutions of CR, MY, CV, PH and NAP by GONC respectively and figure no 5.131, 5.133, 5.135, 5.137, 5.139 shows the bar graphs of root length analysis of CR, MY, CV, PH, NAP respectively.



Figure no 5.130 Toxicological analysis of CR

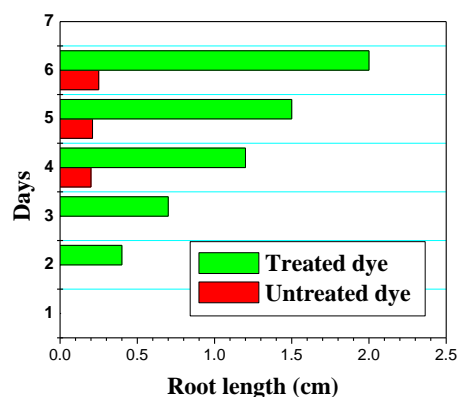


Figure no 5.131 Root length analysis of CR



Figure no 5.132 Toxicological analysis of MY

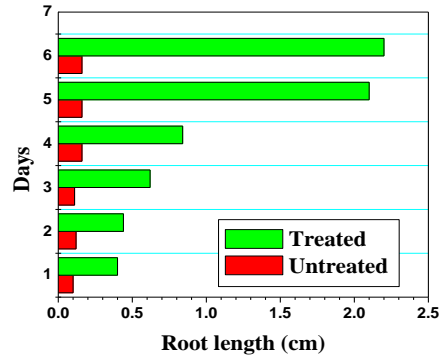


Figure no 5.133 Root length analysis of MY



Figure no 5.134 Toxicological analysis of CV

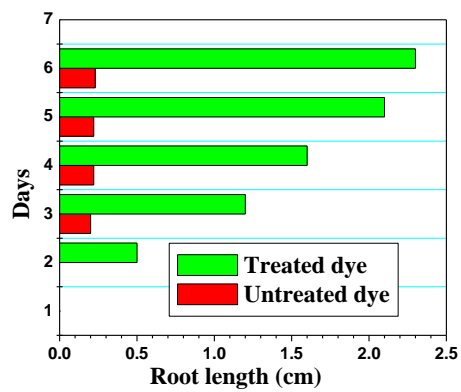


Figure no 5.135 Root length analysis of CV



Figure no 5.136 Toxicological analysis of PH

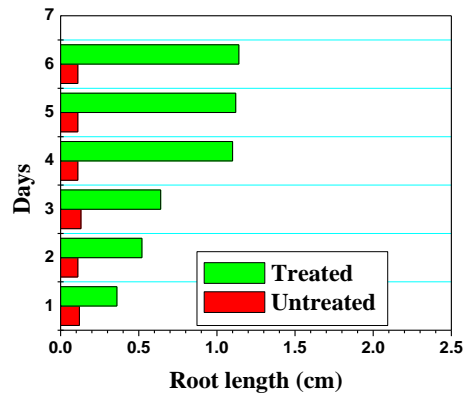


Figure no 5.137 Root length analysis of PH



Figure no 5.138 Toxicological analysis of NAP

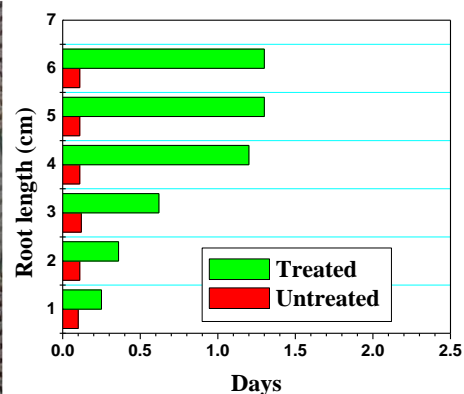


Figure no 5.139 Root length analysis of NAP

5.16. Regeneration study:

The regeneration study of GONC was done by 1 N HCl and or 1 N NaOH solution depends up on the treated adsorbate solution pH. GONC particles were separated by vacuum filtration technique using membrane filter (Milipore 0.45 μ m) and dried in hot air-oven at 60 $^{\circ}$ C for 3 h. Regeneration study was performed by GO for dye and PAH reported in literature (Yu et al., 2017) (Tahir et al., 2017). Regeneration study was conducted up to third adsorption–desorption cycle. The equilibrium study was conducted for all adsorbate solution (CR, MY, CV, PH and NAP) at their optimum parameter range and adsorbed again by regenerated GONC. The removal efficiency was observed for CR that around 92 % for first cycle, 72 % for second cycle and 60 % for third cycle (Figure no 5.145). For MY removal by regenerated GONC around 90 % for first cycle, 75 % for second cycle, 60 % for third cycle was observed (Figure no 5.146). Removal efficiency of GONC for CV 91 % for first cycle, 78 % for second cycle and 65 % for third cycle was observed (Figure no 5.147). The equilibrium study of PH was done again by regenerated GONC and was shown that around 88 % for first cycle, 70 % for second cycle and 60 % for third cycle (Figure no 5.148). For NAP the removal efficiency around 65 % for first cycle, 50 % for second cycle and 43 % for third cycle was observed (Figure no 5.149). Result shows that GONC has potential capacity for the removal of all the adsorbate molecules from its solution second and third tie efficiently and most of the properties of freshly prepared materials. More than ninety percent all the absorbed molecules removed by applying 1N HCl or 1N NaoH so it was conclude that mostly physisorption takes place during the experiment.

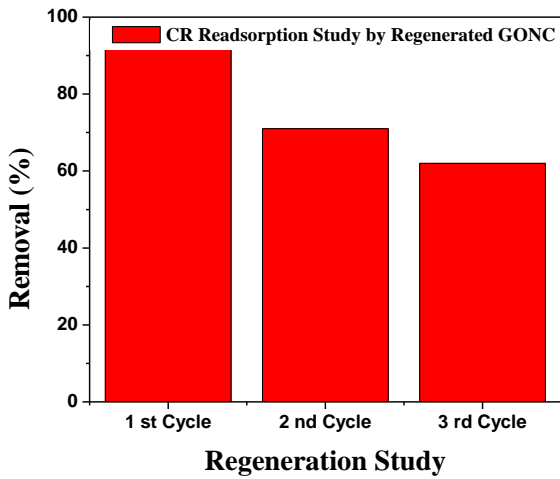


Figure no 5.141 Regeneration study of CR

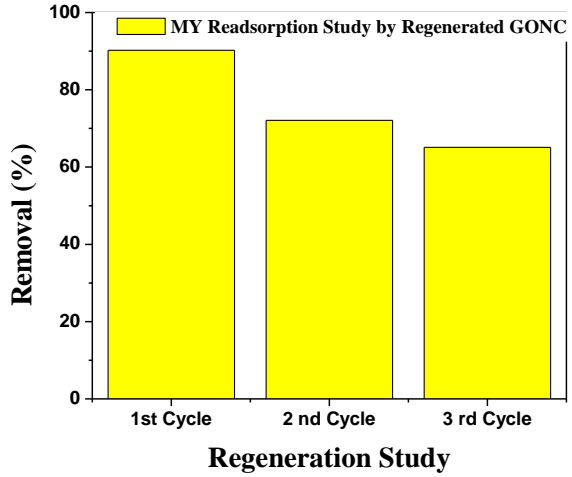


Figure no 5.142 Regeneration study of MY

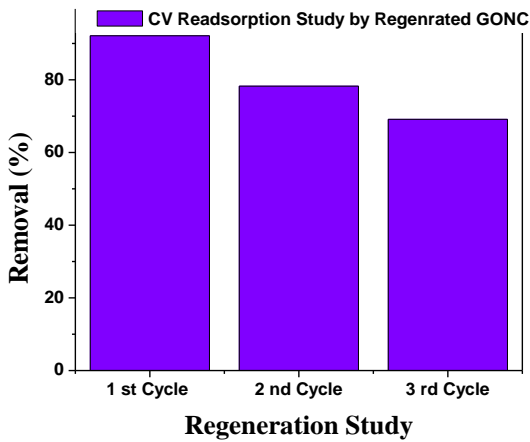


Figure no 5.143 Regeneration study of CV

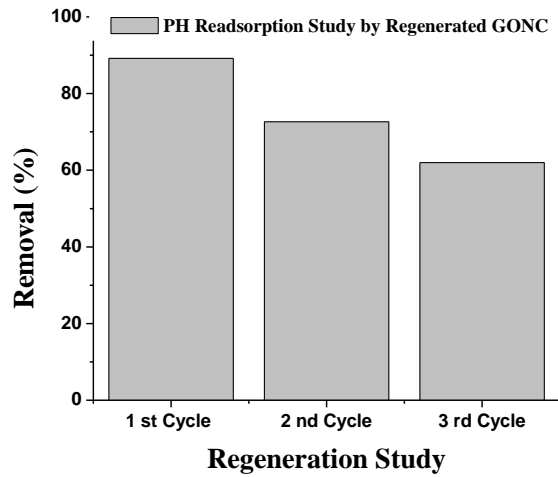


Figure no 5.144 Regeneration study of PH

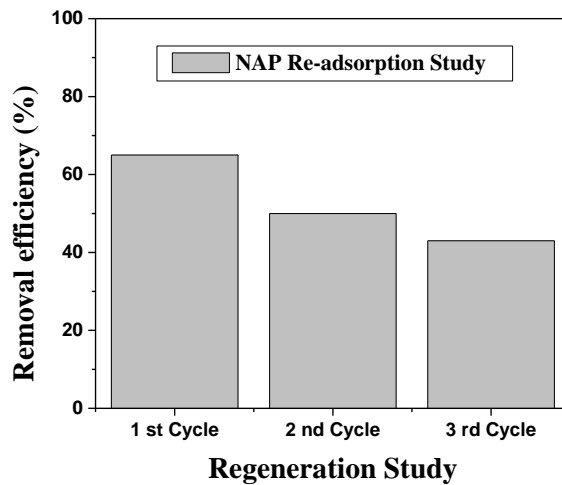


Figure no 5.145 Regeneration study of NAP

CHAPTER 6

REACTION MECHANISM, SUMMARY AND CONCLUSIONS

6.1 Reaction Mechanism:

Experimental analysis conclude that GONC has potential efficiency to remove dyes and PAH from aqueous solution as well as wastewater. The reaction mechanisms between adsorbate (dyes and PAH's) and GONC are discussed in this section.

6.1.1 Congo red (CR) adsorption mechanism:

Result presented in the preceding section indicates that the removal efficiency was maximum for GONC than R-GO and GO. The reaction mechanism between CR and GONC molecules is described in this section. The ionized CR molecules were captured by GONC powdered accomplished through hydrogen bonds (Wu et al., 2008), van der Waal force and London dispersion force of interaction (Figure no 6.1).

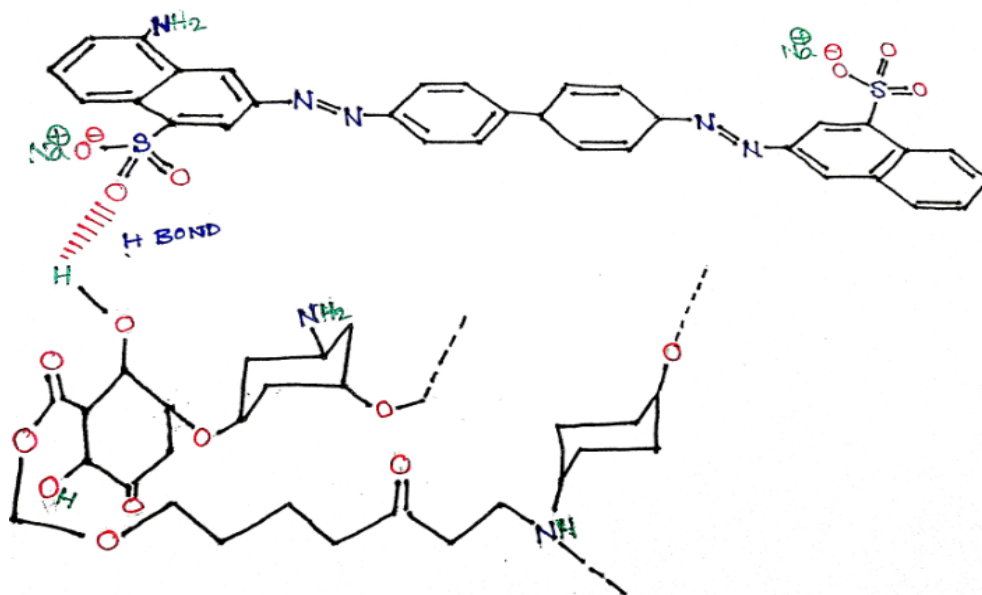


Figure no 6.1. Schematic diagram of CR removal by GONC

However, at pH 6 the CR molecules was slightly acidic in nature which imparts the positive ions into the solution and makes a mainly hydrogen bonds with the oxygen atoms presented

in GONC structure. The more number of oxygen atoms presented in GONC structure was evident by EDX analysis presented in the chapter no 3 section no 3.3. The positive value of ΔH^0 (GONC- 67.30 kJ/mol) indicates the process is endothermic in nature and positive value of ΔS^0 (GONC- 3.97 kJ/mol) demonstrate the increased randomness between solid-solute interface. The experimental result shows that Langmuir and pseudo second order was better to relate the data. So GONC effectively removed CR from its aqueous solution.

6.1.2 Metanil Yellow (MY) adsorption mechanism:

Experimental data reveals that the removal of MY by GONC was more than R-GO and GO. The adsorption reaction mechanism reveals that mainly physical bonds such as hydrogen bonds, dipole-dipole interaction and van der Waals force of attraction were responsible for MY removal from its aqueous solution (Figure no 6.2).

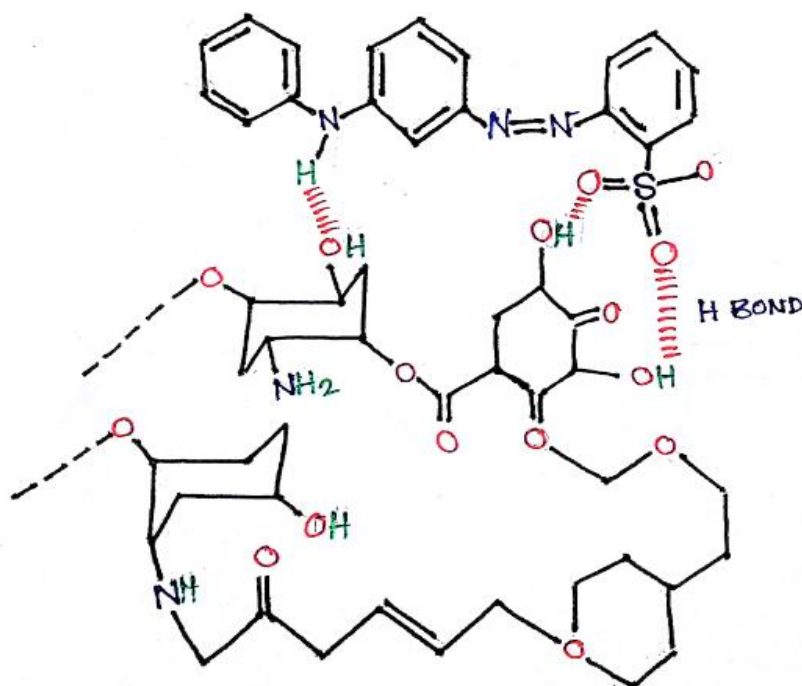


Figure no 6.2. Schematic diagram of MY removal by GONC

At pH 2 the solution was acidic in nature which imparts the positive charge and gets attracted by the oxygen atoms presents in the GONC structure evident by EDX image. Another physical force i.e, the dipole-dipole interaction takes place between N (δ^-) present into the MY and H (δ^+) presents in to the GO (Guo et al., 2013) containing in GONC

structure. The positive value of ΔH^0 (GONC- 73.80 kJ/mol) indicates the process is endothermic in nature and positive value of ΔS^0 suggested that (GONC- 3.14 kJ/mol) the increased randomness between solid-solute interface.

6.1.3 Crystal Violet (CV) adsorption mechanism:

The physisorption was take place between CV and GONC molecules accomplish with hydrogen bond and dipole-dipole interaction. The mainly hydrogen bonds and dipole-dipole interaction force were responsible for the CV removal from its aqueous solution (Figure no 6.3).

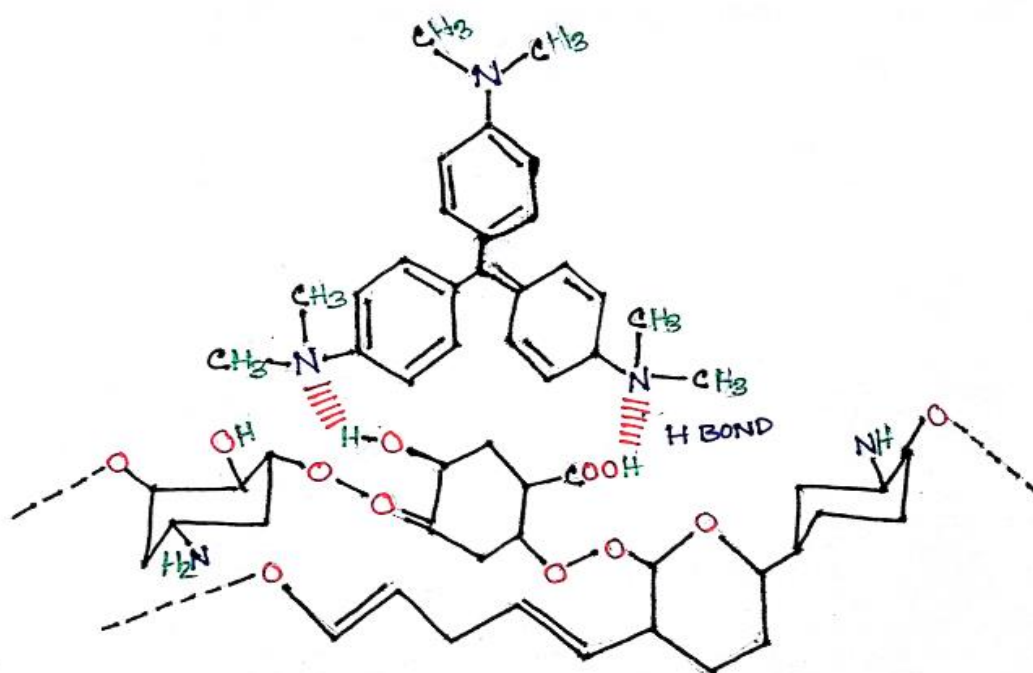


Figure no 6.3. Schematic diagram of CV removal by GONC

Experimental data shows that GONC possesses the better removal efficiency than R-GO and GO because of more number of charged oxygen atoms present into its structure accomplished by EDX analysis. The strong hydrogen bonds acted between N (δ^-) of CV and H (δ^+) of GO (Gopi et al., 2016) present into the GONC structure. The positive value of ΔH^0 (GONC-

68.25 kJ/mol) indicates the process is endothermic in nature and positive value of ΔS^0 suggested that (GONC- 3.26 kJ/mol) the increased randomness between solid-solute interface

6.1.4 Phenol (PH) adsorption mechanism:

Adsorption experimental result shows that physisorption takes place between GONC and phenol molecules (Figure no 6.4), rate of adsorption was maximum than R-GO and GO.

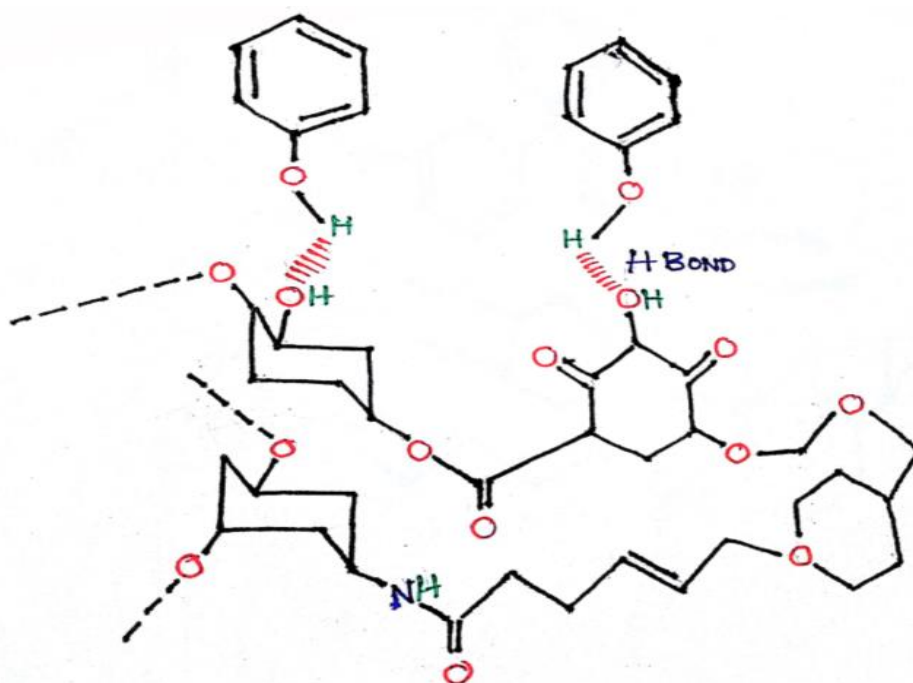


Figure no 6.4. Schematic diagram of PH removal by GONC

Phenol acidic in nature at pH 6 an electro static interaction force and hydrogen bonds acted between adsorbate and adsorbent molecules (Guocheng et al., 2011). GONC posses large number of oxygen containing groups than R-GO and GO was evident by FTIR and EDX image which leads generate strong interaction force towards phenol presents into the solution. The positive value of ΔH^0 (GONC- 66.85 kJ/mol) indicates the process is endothermic in nature and positive value of ΔS^0 indicated that (GONC- 6.45 kJ/mol) the increased randomness between solid-solute interface.

6.1.5 Naphthalene adsorption mechanism:

Experimental data reveals that physisorption was occurred between the GONC and NAP molecules. Apart from hydrogen bonds the van der Waal force, London dispersion force,

intra molecular attraction force and other physical bonds were acted between naphthalene and GONC molecules (Ania et al., 2006). GONC posses higher removal efficiency of NAP than R-GO and GO from its aqueous solution. At higher temperature a driving force was acted between NAP molecules and GONC which leads to the showing higher removal efficiency. The positive value of ΔH^0 indicates the process is endothermic in nature and positive value of ΔS^0 suggested that the increased randomness between solid-solute interface. The value of ΔH^0 and ΔS^0 for GONC is higher. The value of Gibbs free energy (ΔG^0) determines the nature of process whether it is physisorption or chemisorption in nature.

6.2. Comparison between adsorption capacities of GONC with other low cost adsorbent:

The adsorption capacity of GONC is comparable with the other low cost adsorbents in terms of Congo red (CR), Metanil yellow (MY) and Crystal violet (CV) and for aromatic hydrocarbons Phenol (PH) and Naphthalene is investigated through the literature. Table no 6.1 represent the list of various adsorbents' adsorption capacity for the removal of dyes (CR, MY and CV) and aromatic hydrocarbons (PH and NAP).

Table no 6.1. List of adsorption capacity (mg/g) of various adsorbents with GONC:

Adsorbents	Adsorbate	Adsorption Capacity (mg/g)	References
Cattail root	Congo red	38.79	Hu. et al 2010
Crassipes root	Congo red	15.32	Chuah et al 2014
Ground nut shells	Congo red	56.8	Rani et al 2014
Graphene oxide	Congo red	145.6	Ansari et al 2017
Coinage nanoparticle	Congo red	36.4	Ozacar et al., 2005
GONC	Congo red	142.32	
Blast furnace sludge	Metanil Yellow	1.4	Jain et al 2003

Pine saw dust	Metanil yellow	39.8	Ozacar et al 2005
Saw dust carbon	Metanil yellow	183.8	Malik et al 2003
Rice husk carbon	Metanil yellow	86.9	Malik et al 2003
PVA with TiO ₂	Metanil yellow	23.4	Hassan et al 2012
Graphene oxide	Metanil yellow	112.4	Chen et al 2008
Amino Graphene	Metanil yellow	71.62	Xiaoyao et al 2013
Succinamic acid	Metanil yellow	34.5	Aneesh et al 2016
GONC	Metanil yellow	133.2	
Brazil nut shell	Crystal Violet	26.5	Brito et al 2010
Chitosan beads	Crystal Violet	76.9	Anjali et al 2013
Nano porous carbon	Crystal Violet	68.4	Fuat et al 2014
Chitin nano whisker	Crystal Violet	39.7	Sreerag et al 2016
Ramie biomass	Crystal Violet	16.4	Xiao et al 2016
Magnetic particle	Crystal Violet	0.25	Chandrakesh et al 2016
Graphene oxide chitosan	Crystal Violet	96.4	Zhou et al 2018
GONC	Crystal Violet	121.5	
Activated carbon	Phenol	33.5	Grabowska et al., 2013
Mill waste	Phenol	16.4	Abdelkreem 2013
Activated carbon	Phenol	20.4	Grilaldo et al., 2014
Graphene oxide	Phenol	13.4	Wang et al., 2013

Graphene oxide	Phenol	30.4	Yang et al., 2014
Graphene oxide saw dust	Phenol	135.5	Wu et al., 2014
Titania graphene oxide	Phenol	23.7	Fu et al., 2016
Graphene oxide flakes	Phenol	25.4	Catheri et al., 2018
Graphene oxide electrode	Phenol	45.8	Wang et al., 2018
GONC	Phenol	132.6	
Activated carbon (Bean pods)	Naphthalene	85.5	Cabal et al., 2009
Heptanes	Naphthalene	26.4	Ania et al., 2006
Sonicated Talc	Naphthalene	267.2	Sener et al., 2010
Graphene oxide	Naphthalene	64.5	Pei et al., 2012
Magnetic graphene	Naphthalene	84.3	Yang et al., 2013
Graphene	Naphthalene	72.3	Xu et al., 2014
GONC	Naphthalene	115.6	

6.3 Summery:

Humans become fascinated about the color or dye; it is used as an identifier. Dyes are highly stable in nature and cannot be degradable naturally. Huge amounts of non-biodegradable, toxic and inhibitory nature of spent dyes being lost directly into water channels constitutes an accumulative, persistent, carcinogenic, mutagenic and detrimental impact towards the survival of aquatic compartments, flora, fauna and environmental matrix. Excessive exposure to colored effluents is vulnerable to create some seriously acute problems such as immune-suppression, respiratory, circulatory, central nervous disorders, leukemia, cyanosis and affects other functions.

Various technologies are available to remove dye and PAH from aqueous phase but most of them are either expensive or less efficient in nature among them adsorption is the easiest and

effect full technologies. Adsorbent cost in the main concern in this technology, voluminous number of adsorbents are available, they are mainly categorized in two form based on cost. Those are expensive, require environmentally disruptive manufacture or are capable of removing dye and PAH effectively when operating medium of the pH is maintained within a narrow range. Low-cost adsorbents require high treatment time and possess less treatment efficiency. There have been several recent attempts to treat dye and PAH by different biosorbents. Although removal capacities of such biosorbents are fine but most of them processed environmentally disruptive processes or commence with some undesirable characteristics to the water.

Recent have studies shown that GONC remove dye and PAH from aqueous medium effectively than R-GO, GO. From the batch experiments it was conclude that GONC have remove dye in all categories such as acidic (MY), basic (CV), azo (CR) along with naphthalene and phenol. For instance only 0.1 g remove around 92% of MY, around 95 % of CV and around 88 % of CR. PAH around 85 % of NAP and around 58 % of PH effectively. Different characterizations result i.e., XRD, FTIR, SEM, AFM, Raman shows that more number of active sites presents in GONC surface. Interaction between adsorbate and adsorbent was depicted by different isotherms models, Langmuir model was best represent the experimental data with high regrational coefficient along with low linear error (χ^2), established monolayer adsorption take place in all cases. Pseudo-second order kinetic model was established with the high regrational coefficient value and low linear error (χ^2) value during process rate kinetics analysis. Thermodynamic study conclude that the adsorption process is spontaneous, endothermic with high randomness exist between solid solute interface. The value of gibbs free energy indicate that physisorption take place between adsorbate and adsorbent molecules. RSM study conclude that the process exist with high F-value and low p-value, better co-relate the experimental data with statistical model for all

experiment. Column adsorption study revealed that breakthrough time increased with increasing bed height and decreased with increasing flow rate and influent adsorbate concentration. Comparative analysis of toxic effect of untreated and treated solution of dye and PAH was determined with *Cicer arietinum* seeds, results shows that root-shoot length was increased for treated solution. Experimental data conclude that the harmful elements presents in the untreated solution were minimized by GONC. Regeneration study shows that GONC remove dye and PAH molecules form solution second and third times are up to fifty percent. Wastewater experimental analysis shows that GONC have potential to remove contaminants during batch and column mode and degradation was analyzed by COD removal.

Mechanism for dye and PAH removal from aqueous solution shows that the mainly hydrogen bonds and other physical bonds such as Vander Wall, London separation force were acted between adsorbate and adsorbent molecules.

6.4 Cost analysis of GONC and comparable with GO (Commercially):

Cost analysis of GONC (material cost) (without GST) was calculated and comparable with R-GO (Reduced Graphene Oxide) and GO (Graphene oxide) commercially was listed in table no 6.2 and 6.3. All the instrumental cost, electricity cost and establishment cost and water being nullified during this experiment.

Table no 6.2 List of material cost for the preparation of GO (calculated) and comparable with GO (Commercially):

SL No.	Material	Unit cost, INR	Amount used	Net price INR
1.	Graphite Powder	800.00 kg ⁻¹	0.667 kg	533.34
2.	Sulphuric acid	380.00 L ⁻¹	6 L	2280.00
3.	Potassium per magnate	140 kg ⁻¹	0.533 kg	74.62
4.	Hydrogen per oxide	240 L ⁻¹	4.5 L	1080.00
5.	Cost of filter paper	1 per sheet	20 pc	20.00
6.	Cost of shaking (in Incubator Shaker)	2.50 kWh ⁻¹	4kWh (2 h)	10.00
7.	Cost of drying	2.50 kWh ⁻¹	4.8 kWh (5 h)	12.00
	Net cost			4009.96
	Other overhead cost (10% of the net cost)			400.996
	Total cost			4410.95
Cost of GO (Graphene oxide) commercially in India = 6000 to 9000 kg ⁻¹				

Total no 6.3 Cost of preparing 1 kg of R-GO (Reduce Graphene oxide)

SL No.	Material	Unit cost, INR	Amount used	Net price INR
1.	Graphene oxide (synthesized)	4410.95 kg ⁻¹	1.07 kg	4719.700
2.	Hydrazine hydrate	300.00 L ⁻¹	1.034 L	310.000
3.	Cost of filter paper	1 per sheet	20 pc	20.000
6.	Cost of shaking (Magnetic starrer)	0.1 kWh ⁻¹	0.05kWh (0.5 h)	0.005
7.	Cost of drying	2.50 kWh ⁻¹	2 kWh (2 h)	5.000
	Net cost			5054.705
	Other overhead cost (10% of the net cost)			505.47
	Total cost			5560.17
Cost of GO (Graphene oxide) commercially in India = 10000- 150000 kg ⁻¹				

From the table 6.2 it was observed that the GO prepared from graphite powder possesses low manufacturing cost than purchased one. From the table 6.3 it was observed that GONC prepared from GO (prepared) also posses low manufacturing cost than GO (purchased). So it can be concluded that GONC is a highly efficient and cost effective adsorbent.

6.5 Limitations:

Although in laboratory investigation showed that GONC have potential to remove dye and PAH compounds successfully, but its usefulness in a pilot scale application was not studied.

6.6 Scope of Future work:

A pilot scale investigation could, therefore, be undertaken for assessing the suitability of the GONC in full scale applications. Potential of using GONC in removing undesirable constituents from gasses could also be investigated. This research indicated that GONC with showed higher removal efficiency for NAP and PH molecules further investigation will be done for other PAH constituents.

6.7 Conclusion:

Newly synthesized GONC is inexpensive, environmentally safe and efficiently remove dyes, poly aromatic hydrocarbons and wastewater (textile and petrochemical) has been followed in this research with full scale application. The major conclusions are:

1. GONC efficiently remove CR, MY and CV from their aqueous solution with varying operational parameters.
2. Poly aromatic hydrocarbons such as PH and NAP were effectively removed from their aqueous mode by GONC at different operational parameters.
3. The material cost of GONC was comparable or lower than available alternatives.
4. GONC have efficiency to remove the contaminants from wastewater ie, textile as well as petrochemical industry.
5. GONC posses higher removal efficiency than R-GO and GO. It was noticed that for CR more than 90 %, for MY more than 95% and for CV more than 98% removal were observed at optimum condition.
6. For poly aromatic hydrocarbons more than 65% for PH and 80% for NAP were noticed for GONC.
7. Batch study data fitted reasonably well isotherms model which reflects the surface adsorption takes place for both dye and PAH.

8. Adsorption rate kinetics data conclude that adsorption process led by GONC was more significant and continuous mode.
9. Research surface methodology (RSM) shows that the adsorption process led by the GONC for dye and PAH was better correlate the mathematical and statistical data.
10. GONC was efficiently remove dye and PAH not only in batch mode but also in column mode and the data obtained from the experiment well fitted the models.
11. GONC have potential to remove contaminants from wastewater and hence reduce the TDS, TSS, BOD, COD, salinity and conductivity of wastewater.
12. It could be deposited in proper land filling purpose.

References:

Agata Rosinska and Lidia Da Browska, 2018, Selection of Coagulants for the Removal of Chosen PAH from Drinking Water, *Water*, 65, 42-56.

Ahmad, A.A., Hameed, B.H., 2009. Reduction of COD and color of dyeing effluent from a cotton textile mill by adsorption onto bamboo-based activated carbon. *J. Hazard. Mater.* 172, 1538–1543.

Ahmad, A.A., Hameed, B.H., 2009. Reduction of COD and color of dyeing effluent from a cotton textile mill by adsorption onto bamboo-based activated carbon. *J. Hazard. Mater.* 172, 1538–1543.

Alok Mittal , V.K. Gupta ,Arti Malviya , Jyoti Mittal, 2008, Process development for the batch and bulk removal and recovery of a hazardous, water-soluble azo dye (Metanil Yellow) by adsorption over waste materials (Bottom Ash and De-Oiled Soya, *Journal of Hazardous Materials* 151 821–832.

Anderson, M.J., Whitcomb, P.J., 2005. RSM simplified: optimizing processes using
Aneesh Mathew, Surendran Parambadath, Mary Jenisha Barnabas, Hyun Jin Song, Jae-Sung Kim, Sung Soo Park, Chang-Sik Ha, 2016, Rhodamine 6G assisted adsorption of metanil yellow over succinamic acid functionalized MCM-4, *Dyes and Pigments* 131 (2016) 177e185.

Anirudhan, T.S., Radhakrishnan, P.G., 2008. Thermodynamics and kinetics of adsorption of Cu(II) from aqueous solutions onto a new cation exchanger derived from tamarind fruit shell. *J. Chem. Thermodynamics* 40, 702–709.

Anjali Pal , Satyajit Pan, Sandip Saha, 2013, Synergistically improved adsorption of anionic surfactant and crystal violet on chitosan hydrogel beads, *Chemical Engineering Journal* 217 426–434.

Annadurai, G.R, L. Jung, D. J. Lee, 2002, Use of cellulose based wastes for adsorption of dye from aqueous solution, *Journal of Hazardous material*, 269-274.

Anouzla, A., Abrouki, Y., Souabi, S., Safi, M., Rhabal, H., 2009. Color and COD removal of disperse dye solution by a novel coagulant: Application of statistical design for the optimization and regression analysis. *J. Hazard. Mater.* 166,1302–1306.

Anupam, K., Dutta, S., Bhattacharjee, C., Datta, S., 2011. Adsorptive removal of chromium (VI) from aqueous solution over powdered activated carbon: Optimisation through response surface methodology. *Chem. Eng. J.* 173, 135– 143, Australia.

Banerjee, P., Sau, S., Das, P., Mukhopadhyay, A., 2015. Optimization and modelling of synthetic azo dye wastewater treatment using graphene oxide nanoplatelets: characterization toxicity evaluation and optimization using artificial neural network. *Ecotoxicol. Environ. Saf.* 119, 47–57.

Belen Cabab, Temenuzhka Budinova, Conchi O. Aniab, Boyko Tsyntsarski, Jose´ B. Parrab, Bilyana Petrova, 2009, Adsorption of naphthalene from aqueous solution on activated carbons obtained from bean pods, *Journal of Hazardous Materials* 161, 1150–1156.

Bhattacharyya, K.G., Sharma, A., 2004. Azadirachta indica leaf powder as an effective biosorbent for dyes: a case study with aqueous Congo Red solutions. *Journal of Environmental Management* 71, 217–229.

Bingol, D., Tekin, N., Alkan, M., 2010. Brilliant Yellow dye adsorption onto sepiolite using a full factorial design. *Appl. Clay Sci.* 50, 315–321.

Blanchard, G., M. Maunaye, G. Martin, Removals of heavy metals from waters by means of natural zeolites, *Water Research*, 18 (1984) 1501-1507.

Brito. S.M.D, H.M.C Andrade, L.F. Soares, 2010, Brazil nut shells as anew bio adsorbents to remove methelene blue and gentian violet from aqueous solution, *Journal of Hazardous Material*, 84-92.

C. H. Weng, Y. T. Linb, T. W. Tzeng *J. Hazard mater* , 2009, Removal of methylene blue from aqueoussolution by adsorption onto pineapple leaf powder. *J. Hazard. Mater.* 170, 417–424.

C.O. Ania, T.J. Badosz, 2006, Metal-loaded polystyrene-based activated carbons as dibenzothiophene removal media via reactive adsorption, *Carbon* 44 , 2404–2412.

Chandrasekaran Muthukumaran ,Vaiyazhipalayam Murugaiyan Sivakumar , Marimuthu Thirumarimurugan, 2016, Adsorption isotherms and kinetic studies of crystal violet dye removal from aqueous solution using surfactant modified magnetic nanoadsorbent, *Journal of the Taiwan Institute of Chemical Engineers* 63 (2016) 354–362.

Chao Long, Aimin Li, Haisuo Wu, Fuqiang Liu , Quanxing Zhang, 2008, Polanyi-based models for the adsorption of naphthalene from aqueous solutions onto nonpolar polymeric adsorbents, *Journal of Colloid and Interface Science* 319 , 12–18.

Chatterjee, S., Chatterjee, S., Chatterjee, B.P., Guha, A.K., 2007. Adsorptive removal of congo red, a carcinogenic textile dye by chitosan hydrobeads: Binding mechanism, equilibrium and kinetics. *Colloids Surf. A: Physicochem. Eng. Aspects* 299, 146–152.

Chen. B.N, C.W. Hui, G. Mackay, 2008, Flim pore diffusion modeling and contact time optimization for the adsorption of dye stuffs on pith, *chemical engineering Journal*, 84, 77-94.

Chenhao Gong, Haiou Huang, Yu Qian, Zhongguo Zhang and HongbinWu , 2017 , Integrated electrocoagulation and membrane filtration for PAH removal from realistic industrial wastewater: effectiveness and mechanisms, *RSC*, 7, 52366.

Chuah T.G, Jumashish A., I, Anzi, Thomas Choong, 2014, Rice husk as a potential of bio-adsorbent for the removal of dye, *Desalination* , 175, 305-3016.

Chun-Chieh Fu , Ruey-Shin Juang , Mohammad Mahmudul Huq , Chien-Te Hsieh, 2016, Chutima Jarusiripot, 2015, Removal of Reactive Dye by Adsorption over Chemical Pretreatment Coal Based Bottom Ash, *Procedia Chemistry* 9 121 – 130.

Crini G., H.N. Peindy, F. Gimbert, C. Robert, 2007, removal of C.I basic green 4 from aqueous solution by adsorption using cyclodextrin based Kinetics equilibrium studies, separation and purification technology, 53, 97-110.

D. Robati, B. Mirza, M. Rajabi, O.Moradi, I. Tyagi, S. Agarwal, V. K. Gupta, 2016, Removal of hazardous Dyes-BR 12 and methyl orange using graphene 1 oxide as and 2 adsorbent from aqueous phase, S1385-8947-01214.

Dawood S., Sen T.K., 2012. Removal of anionic dye Congo red from aqueous solution by raw pine and acid-treated pine cone powder as adsorbent: Equilibrium, thermodynamic, kinetics, mechanism and process design. *Water res.* 46, 1933-1946.

Debajyoti Ghosal, Arindam Dutta, Joydeep Chakraborty, Soumik Basu, Tapan K. Dutta, 2013, Characterization of the metabolic pathway involved in assimilation of acenaphthene in *Acinetobacter* sp. strain AGAT-W, *Research in Microbiology* 164 (2013) 155e163.

Dimitrios Konios, Minas M. Stylianakis, Emmanuel Stratakis and Emmanuel Kymakis, 2014, Dispersion behaviour of graphene oxide and reduced graphene oxide, *journal of Collid and Interface science*.

E. Lorenc-Grabowska , G. Gryglewicz , M.A. Diez, 2013, Kinetics and equilibrium study of phenol adsorption on nitrogen-enriched activated carbons, *Fuel* 114 (2013) 235–243.

Edilson do Vale-Júnior , Djalma, R. da Silva , Ana S. Fajardo , Carlos A. Martínez-Huitle graphene oxide, *Colloids and Surfaces B: Biointerfaces* 89, 79– 85.

El-Gohary, F., Tawfik, A., 2009. Decolorization and COD reduction of disperse and reactive dyes wastewater using chemical-coagulation followed by sequential batch reactor (SBR) process. *Desalination* 249, 1159–1164.

Enhanced adsorption and photodegradation of phenol in aqueous suspensions of titania/graphene oxide composite catalysts, *Journal of the Taiwan Institute of Chemical Engineers* 67, 338–345.

F. Haghseresh, G. Lu Adsorption characteristic of phenolic compounds onto coal-reject-revised adsorbents, *Energy Fuels* 12 (1998) 1100-1107.

F.Haghseresht , G.Lu., Adsorption Characteristic of Phenolic compounds onto coal rejected derived adsorbents, *Energy Fuels* 12(1998)1100-1107.

Febrianto, J., A.N. Kosasiha, J. Sunarso, Y.H. Ju, N.Indraswati, S.Ismadji, Equilibrium and kinetics studies in adsorption of heavy metals using bio-adsorbents: A summary of recent studies , *Journal of Hazardous materials*, 162(2009) 616-645.

Fernando de Juan, Alberto Cortijo, María A. H. Vozmediano, and Andrés Cano , 2011, Aharonov–Bohm interferences from local deformations in graphene, *Nature Physics*10.1038/NPHYS2034.

Foo, K.Y., B.H. Hameed Insights into the modeling of adsorption isotherm systems, *chemical engineering journal* , 156 (2010)2-10.

Freundlich, H.M.F Over the adsorption in the solution, *Journal of Physical Chemistry* 57 (1906) 385-471

Fuat Gu zel , Hasan Sayg, Gu Ibarah, Akkaya Sayg , Filiz Koyuncu , 2014, Decolorisation of aqueous crystal violet solution by a new nanoporous carbon: Equilibrium and kinetic approach,

G. Zhou , K.P. Wang, H.W. Liu, L.Wang, X.F. Xiao , D.D. Dou, Y.B. Fan, 2018, Three-dimensional polylactic acid@graphene oxide/chitosan sponge bionic filter: Highly efficient adsorption of crystal violet dye, *International Journal of Biological Macromolecules* 113 (2018). 792–803.

G.Limousin, J-P Gaudet Sorption isotherms : a review on physical bases modeling and measurement, *Applied Geochemistry* 22 (2) 249-275, 2007.

Ganesh K. Parshetti, Shamik Chowdhury and Rajasekhar Balasubramanian, 2014, Plant derived porous graphene nanosheets for efficient CO₂ capture, *RSC Adv.*, 2014, 4, 44634.

Geetha S.J., Sanket J. Joshia, Shailesh Kathrotiyab, 2013, Isolation and characterization of hydrocarbon degrading bacterial isolate from oil contaminated sites, *APCBEE Procedia* 5, 237 – 241.

Gizem Karaca ,Hüseyin S. Baskaya, Yücel Tasdemir., 2017 Removal of polycyclic aromatic hydrocarbons (PAHs) by graphene oxide chitosan nano composite: Bentonite *Environ Sci Pollut Res* 23:242–252.

Gizem Karaca, Hüseyin S. Baskaya and Yücel Tasdemir, 2016, Removal of polycyclic aromatic hydrocarbons (PAHs) from inorganic clay mineral: Bentonite, *Environ Sci Pollut Res* (2016) 23:242–252 DOI 10.1007/s11356-015-5676-z.

Goswami MR, Banerjee P, Swarnakar S, Mukhopadhyay A 2013, Carbaryl mediated biochemical alterations in Eggplant (*Solanum melongena* L.). *Int J Res Environ Sci Technol* 3(2):51.

Greluk, M., Hubicki, Z., 2009. Sorption of SPADNS azo dye on polystyrene anion exchangers: Equilibrium and kinetic studies. *J. Hazard. Mater.* 172, 289–297.

Greluk, M., Hubicki, Z., 2011. Efficient removal of Acid Orange 7 dye from water using the strongly basic anion exchange resin Amberlite IRA-958. *Desalination* 278, 219–226.

Guangzhou, China, *International Journal of Environmental research and Public Health*.

Guo-Liang Shi, Gui-Rong Liu, Ying-Ze Tian, Xiao-Yu Zhou, Xing Peng, Yin-Chang Feng, 2014, Chemical characteristic and toxicity assessment of particle associated PAHs for the short-term anthropogenic activity event: During the Chinese New Year's Festival in 2013, *Science of the Total Environment* 482–483 (2014) 8–14.

Gupta, V.K., Suhas, 2009. Application of low-cost adsorbents for dye removal – A review. *J. equilibrium and kinetics. Colloids Surf. A: Physicochem. Eng. Aspects* 299, 146–152.

Environ. Manag. 90, 2313–2342

Gurgel, L.V.A., Gil, L.F., 2009a. Adsorption of Cu(II), Cd(II) and Pb(II) from aqueous

Han, R., Wang, Y., Zhao, X., Wang, Y., Xie, F., Cheng, J., Tang, M., 2009. Adsorption of methylene blue by phoenix tree leaf powder in a fixed-bed column: experiments and prediction of breakthrough curves. *Desalination* 245, 284–297.

Han, R., Wang, Y., Zhao, X., Wang, Y., Xie, F., Cheng, J., Tang, M., 2009. Adsorption of methylene blue by phoenix tree leaf powder in a fixed-bed column: experiments and prediction of breakthrough curves. *Desalination* 245, 284–297.

Hassan A. Abd El-Rehim , El-Sayed A. Hegazy, Doaa A. Diaa, 2012, Photo-catalytic degradation of Metanil Yellow dye using TiO₂ immobilized In to polyvinyl alcohol/acrylic acid microgels prepared by ionizing radiation, *Reactive & Functional Polymers* 72 (2012) 823–831.

Hepsiba Niruba Catherine , Ming-Han Ou , Basavaraju Manu , Yang-hsin Shih, 2018,

Adsorption mechanism of emerging and conventional phenolic compounds on graphene oxide nanoflakes in water, *Science of the Total Environment* 635 , 629–638.

Ho, Y.S., Review of second-order models for adsorption systems, *Journal of Hazardous Materials*, B136 (2006) 681-689.

Hongmei Sun, Linyuan Cao, and Lehui Lu, 2018, Magnetite/Reduced Graphene Oxide Nanocomposites: One Step Solvothermal Synthesis and Use as a Novel Platform for Removal of Dye Pollutants, *Journal of Hazardous Materials*, 4(6): 550-562.

Hu, Z., Chen, H., Ji, F., Yuan, S., 2010. Removal of Congo Red from aqueous solution by cattail root. *J. Hazard. Mater.* 173, 292-297.

Hummers, W., Offeman, R., 1958. Preparation of graphitic oxide. *J. Am. Chem. Soc.* 80, 1339-1339.

Imran Ali, V K Gupta, 2007, *Advances in water treatment by adsorption technology*, Nature, 10.1038/nprot.2006.370.

Jain, M., V. K. Garg, K. Kadriavelu, 2003, Investigation of Metanil Yellow dye adsorption onto Blast furnace activated sludge, *Bioresource Technology* 120, 704-711.

Jiasheng Xu, Dinh Khoi Dang, Van Tam Tran, Xiaoyang Liu, Jin Suk Chung, Seung Hyun Hur,

Jing Xu, Li Wang and Yongfa Zhu, 2012, Decontamination of bisphenol A from aqueous solution by graphene adsorption, *ACS*, 2-22.

Kettunen R, Keskitalo P (2000). Combination of membrane technology and limestone filtration to control drinking water quality. *Desalination*, 131, 271-283.

Khan, T.A., Nazir, M., Khan, E.A., 2013. Adsorptive removal of rhodamine B from textile wastewater using water chestnut (*Trapa natans* L.) peel: adsorption dynamics and kinetic studies. *Toxicol. Environ. Chem.* 95, 919-931.

Khayet, M., Zahrimb, A.Y., Hilal, N., 2011. Modelling and optimization of coagulation of highly concentrated industrial grade leather dye by response surface methodology. *Chem. Eng. J.* 167, 77–83.

Kim S.G, Park O-K, Lee JH, Ku B-C, 2013, Layer-by-layer assembled graphene oxide films and barrier properties of thermally reduced graphene oxide membranes. *Carbon Lett*, 14 (4), 247-250.

Lagergren, S., About the Theory of so-called adsorption of soluble substances, *Kungliga Svenska Vetenskapsakademiens Handlingar*, 24 (1898) 1-39.

Langmuir, I., The constitution and fundamental properties of solids and liquids, *Journal of American Chemical Society*, 38 (1916) 2221-2295.

Liliana Giraldo, Juan Carlos Moreno-Piraján, 2014, Study of adsorption of phenol on activated carbons obtained from egg shells, *Journal of Analytical and Applied Pyrolysis* 106 ,41–47.

Liuyun Chen , Yanhong Tang , Ke Wang , Chengbin Liu , Shenglian Luo, 2011, Direct electrodeposition of reduced graphene oxide on glassy carbon electrode and its electrochemical application, *Electrochemistry Communications* 13 , 133–137.

LÜ Guocheng, HAO Jiao , LIU Liu , MA Hongwen , FANG Qinfang , WU Limei , WEI Mingquan and ZHANG Yihe , 2011, The Adsorption of Phenol by Lignite Activated Carbon, *Chinese Journal of Chemical Engineering*, 380 to 385.

M. Abdelkreem, 2013, Adsorption of Phenol from Industrial Wastewater Using Olive Mill Waste, *APCBEE Procedia* 5 , 349 – 357.

M. Ozacar, I.A. Sengil, A kinetic study of metal complex dye sorption onto pine sawdust, *Process Biochem.* 40 (2005) 565–572.

M. S. Ivanov, V. A. Khomchenk, M. Salimian, T. Nikitin, S. Kopyl, A. M. Buryakov, E. D. Journal of Industrial and Engineering Chemistry 20 3375–3386. functionalized with triethylenetetramine. Water Res. 43, 4479–4488.

Mishina, F. Salehli, P. A. A. P. Marques, G. Goncalves, R. Fausto, J. A. Paixão and A. L. methylene blue from aqueous solution by jackfruit (*Artocarpus heteropyllus*) leaf

Kholkin, 2018, Self-assembled diphenylalanine peptide microtubes covered by reduced graphene oxide/spiky nickel nanocomposite: an integrated nanobiomaterial for multifunctional applications, S0264-127530025.

Malgorzata Wojtoniszak , Xuecheng Chen , Ryszard J. Kalenczuk , Anna Wajda , Joanna Łapczuk, Mateusz Kurzewski, Marek Drozdziak, Pual K. Chu, Ewa Borowiak-Palen, Synthesis, dispersion, and cytocompatibility of graphene oxide and reduced.

Malik P.K., 2003, use of activated carbons prepared from saw dust and rice husk removal of acid yellow dye, Dyes and Pigments 239-249.

Mall, I.D., Srivastava, V.C., Agarwal, N.K., Mishra, I.M., 2005. Removal of congo red from aqueous solution by bagasse fly ash and activated carbon: Kinetic study and equilibrium isotherm analyses. Chemosphere 61, 492–501.

Marzena Smol, Maria Włodarczyk-Makula, 2012, Effectiveness in the removal of Polycyclic aromatic hydrocarbons from industrial wastewater by ultrafiltration technique. 10.2478/v10265-012-0040-6.

N. Nausha, B.H. Hameed, Chem, Eng.J. 166(2011) 783.methylene blue from aqueous solution by jackfruit (*Artocarpus heteropyllus*) leaf. Hazardous materials, 254-259.

Mijia Zhu, Jun Yao, Lifu Dong, Jing jing Sun, 2016, Adsorption of naphthalene from aqueous solution onto fatty acid modified walnut shells, Chemosphere 144 (2016) 1639–1645.

Mijia Zhu, Jun Yao, Lifu Dong, Jingjing Sun, 2016, Adsorption of naphthalene from aqueous solution onto fatty acid modified walnut shells, *Chemosphere* 144 ,1639–1645.

Ming-Kuang Wang,2016, Comparison and characterization of chemical surfactants and bio-surfactants intercalated with layered double hydroxides (LDHs) for removing naphthalene from contaminated aqueous solutions, *Colloids and Surfaces A: Physicochem. Eng. Aspects* 366 , 170–177.

Mohammad Omaish Ansari , Rajeev Kumar , Sajid Ali Ansari , Shahid Pervez Ansari , M.A. Barakat Ahmed Alshahrie , Moo Hwan Cho, 2017, Anion selective pTSA doped polyaniline@graphene oxide-multiwalled carbon nanotube composite for Cr(VI) and Congo red adsorption, *Journal of Colloid and Interface Science* 496 (2017) 407–415.

Nicoll H (2001). Nanofiltration makes surface water drinkable. *Filtration and Separation*, 38, 22–23.

O. Abdelwahab,, N.K. Amin, E-S.Z. El-Ashtoukhy, 2009, Electrochemical removal of phenol from oil refinery wastewater, *Journal of Hazardous Materials* 163 (2009) 711–716.

Oladoja, N.A., Akinlabi, A.K., 2009. Congo Red Biosorption on Palm Kernel Seed Coat. *Industr. Eng. Chem. Res.* 48 (13), 6188–6196.

Onal, Y., 2006, Lineyics of adsorption of dyes from aqueous solution using activated carbon prepared from waste apricot, *Journal of Hazardous Materials*, B137, 1719-1728.

Ozacar M, F. Rozada, L.F. Calvo, Elimination of organic water pollurtants using adsorbents obtained, from sewage sludge, dyes and Pigments 2003, 55-65.

P. Gregory 1990, Classification dyes by chemical structure, chapter no 2 fine chemical research centre Manchester ME9 3DA , England.

Panda, G.C., Das, S.K., Guha, A.K., 2009. Jute stick powder as a potential biomass for the removal of congo red and rhodamine B from their aqueous solution. *J. Hazard. Mater.* 164, 374–379.

Park OK, Hahm MG, Lee S, Joh HI, Na SI, Vajtai R, Lee JH, Ku BC, Ajayan PM, 2012, In situ synthesis of thermochemically reduced graphene oxide conducting nanocomposites. *Nano Lett.* 12, 1789.

Price, M.L., Butler, L.G., 2011. Rapid visual estimation and spectrophotometric determination of tannin content of sorghum grain. *J. Agric. Food Chem.* 25, 1268–1273.

Purkait, M.K., Maiti, A., DasGupta, S., De, S., 2007. Removal of congo red using activated carbon and its regeneration. *J. Hazard. Mat.* 145, 287–295.

R Mulyanti and H Susanto, Wastewater treatment by nanofiltration membranes, 2018, *Earth and Environmental Science* 142 012017.

Ramachandra, T.V., Kiran, R., Ahalya, N., 2002., response surface methods for design of experiments. Productivity Press, New York, review. *J. Environ. Manag.* 90, 2313–2342.

Rijsberman, F.R., 2006. powder: A fixed-bed column study. *J. Environ. Manag* Water scarcity: Fact or friction. *Agri. Water Manag.* 80, 5-22.

Rosa, M.F., Chiou, B., Medeiros, E.S., Wood, D.F., Williams, T.G., Mattoso, L.H.C., Orts, W.J., Imama, S.H., 2009. Effect of fibre treatment on tensile and thermal properties of starch/ethylene vinyl copolymers/coir biocomposites. *Bioresour. Technol.* 100, 5196–5202.

S. Sadri Moghaddam, M.R. Alavi Moghaddam , M. Arami, 2010, Coagulation/flocculation process for dye removal using sludge from water treatment plant: Optimization through response surface methodology, *Journal of Hazardous Materials* 175 (2010) 651–657.

S, ahika Sena Bayazit , Mahmut Yildiz , Yavuz Selim As, ç i , Musa S, ahin , Mustafa Bener , Songül E_glence , Mohamed Abdel Salam, 2017, Rapid adsorptive removal of naphthalene from water using graphene nanoplatelet/MIL-101 (Cr) nanocomposite, *Journal of Alloys and Compounds* 701 (2017) 740-749.

Saeed, A., Sharif, M., Iqbal, M., 2010. Application potential of grapefruit peel as dye sorbent: Kinetics, equilibrium and mechanism of crystal violet adsorption. *J. Hazard. Mater.* 179, 564–572.

Sajab, M.S., Chia, C.H., Zakaria, S., Jani, S.M., Ayob, M.K., Chee, K.L., Khiew, P.S., Chiu, W.S., 2011. Citric acid modified kenaf core fibres for removal of methylene blue from aqueous solution. *Bioresour. Technol.* 102, 7237–7243.

Seema Rani, Kaur Sumanjit ,R.K. Mahajan, 2014, Synthesis of mesoporous material SBA-3 for adsorption of dye congo red, *Desalination and Water Treatment*, 1-12.

Sekhar, C.P, S. Kalidarshan, V. rajesh, N. Rajesh, 2009, Bio-polymer adsorbents for the removal of malachite green from aqueous solution, *Chemosphere*, 77, 842-847.

Senthilkumaar, S., Kalaamani, P., Subburaam, C.V., 2006. Liquidphase adsorption of crystal violet onto activated carbons derived from male flowers of coconut tree. *J. Hazard. Mater.* 136, 800–808.

Shanti Lamichhane , K.C. Bal Krishna , Ranjan Sarukkalige, 2016, Polycyclic aromatic hydrocarbons (PAHs) removal by sorption: A review, *Chemosphere* 148 (2016) 336e353.

Shaoxia Yang,, Yuhong Cui, Yu Sun, Hongwei Yang, 2014, Graphene oxide as an effective catalyst for wet air oxidation of phenol, *Journal of Hazardous Materials* 280 ,55–62.

Shenai, V. A, Azo dye Ban- facts and figures, 1997, single metal solutions by succinylated twice-mercerized sugarcane bagasse *Chemical Weekly*, july 15, 137-156.

Singh, K.P., Gupta, S., Singh, A.K., Sinha, S., 2011. Optimizing adsorption of crystal violet dye from water by magnetic nanocomposite using response surface modeling approach, *J. Hazard. Mater.* 186, 1462–1473.

Somayeh Golbaz , Ahmad Jonidi Jafari , Mohammad Rafiee, Roshanak Rezaei Kalantary, 2014, Separate and simultaneous removal of phenol, chromium, and cyanide from aqueous solution by coagulation/precipitation: Mechanisms and theory *Chemical Engineering Journal* 253 (2014) 251–257.

Sperczyn ska, E.; Da browska, L.; Wisniowska, E. , 2016, Removal of turbidity, colour and organic matter from surface water by coagulation with polyaluminium chlorides and with activated carbon as coagulant aid. *Desalin. Water Treat.*, 57, 1139–1144.

Sreerag Gopi, Anitha Pius, Sabu Thomas, 2016, Enhanced adsorption of crystal violet by synthesized and characterized chitin nano whiskers from shrimp shell, *Journal of Water Process Engineering* 14 1–8.

Suman Thakur and Niranjana Karak, 2015, Alternative methods and nature-based reagents for the reduction of graphene oxide - a review, *CARBON* 10032.

Sureshkumar, M.V., Namasivayam, C., 2008. Adsorption behavior of Direct Red 12B and Rhodamine B from water onto surfactant-modified coconut coir pith. *Colloids and Surfaces A: Physicochem. Eng. Aspects* 317, 277–283.

T. Rajeswaria, B. Elayarajahb, B. Venkatrajahc, S. Rajakumard, S. Meenatchisundarame and R. Vijayaraghavane, (2011) Biodegradation of Petroleum Hydrocarbon Using *Pseudomonas* and Its Antifungal Activity Against Phytopathogens, *Bangladesh J. Sci. Ind. Res.* 46(3), 297-302.

T. Takagi, Y. Ohyama, T. Goto, H. Matsuharn, S. Oyabu, T. Wada, C. P. Pearson, H. M. Lee, M. Im, M. G. Lee, H. Shim, H. Hanami, T. Ishigaki, K. Imai, G. J. White , S. Serjeant, and M.

Malkan, 2010, Polycyclic aromatic hydrocarbon (PAH) luminous galaxies at $z \sim 1$, DOI: 10.1051/0004-6361/200913466.

Thomas Wenzl, Rupert Simon, Juliane Kleiner, Elke Anklam, 2006, Analytical methods for polycyclic aromatic hydrocarbons (PAHs) in food and the environment needed for new food legislation in the European Union, Trends in Analytical Chemistry, Vol. 25, No. 7.

Tonghao Liu, Yanhui Li, Qiuju Du, Jiankun Sun, Yuqin Jiao, Guangming Yang, Zonghua Wang, Yanzhi Xia, Wei Zhang, Kunlin Wang, Hongwei Zhu, Dehai Wu, 2012, Adsorption of methylene blue from aqueous solution by graphene, Colloids and Surfaces B: Biointerfaces 90,197–203.

Toor, M.K., 2010. Enhancing adsorption capacity of Bentonite for dye removal: Treatment of an azo dye effluent by peroxi-coagulation and its comparison to traditional electrochemical advanced processes Chemosphere 204 (2018) 548-555.

trichlorophenol, 2-naphthol and naphthalene on graphene and graphene oxide, C A R B O N 5 1 , 1 5 6 – 1 6 3 .

Uddin, M.T., Rukanuzzaman, M., Khan, M.M.R., Islam, M.A., 2009. Adsorption of methylene blue from aqueous solution by jackfruit (*Artocarpus heterophyllus*) leaf powder: A fixed-bed column study. J. Environ. Manag. 90, 3443–3450.

UNESCO, 2003. Water for People Water for Life, The United Nations World Water Development Report. USA.

Verma, A.K., Dash, R.R., Bhunia, P., 2012. A review on chemical coagulation/flocculation technologies for removal of color from textile wastewaters. J. Environ. Manag. 93, 154–168.

Vimonses, V., Lei, S., Jin, B., Chow, C.W.K., Saint, C., 2009. Kinetic study and equilibrium isotherm analysis of Congo Red adsorption by clay materials, Chem. Eng. J. 148, 354–364.

Wang X.S, Zhou Y, C. Sun, 2008, The removal of basic dye from aqueous solution using agricultural by products, *Journal of Hazardous Materials*, 157, 374-385.

Wasay SA, MJ Haron, S Tokunaga, 1996, Adsorption of fluoride, phosphate, and arsenate ions on lanthanum-impregnated silica gel. *Water Environment Research*, 68, 295–300.

Wawrzkiwicz, M., 2011. Comparison of gel anion exchangers of various basicity in direct dye removal from aqueous solutions and wastewaters. *Chem. Eng. J.* 173, 773–781.

Weber , W.J., J.C.Morris, Kinetics of adsorption of carbon from solution, *Journal of Sanitary Engineering Division, ASCE*, 89 (1963) 31-39.

Won Mook Choi, Eui Jung Kim, Paul A. Kohl, 2014, Liquid-phase exfoliation of graphene in organic solvents with addition of naphthalene, *Journal of Colloid and Interface Science* 418 , 37–42.

Xiaoxi Cai , Xin-jiang Hu , Hui Wang , Si-mian Liu , Lu-hua Jiang, 2016, Biochar pyrolyzed from MgAl-layered double hydroxides pre-coated ramie biomass (*Boehmeria nivea* (L.) Gaud.): Characterization and application for crystal violet removal, *Journal of Environmental Management* 184 (2016) 85e93.

Xiaoyao Guo, Qin Wei, Bin Du, Yakun Zhang, Xiaodong Xin, Lianguo Yan, Haiqin Yu, 2013, Removal of Metanil Yellow from water environment by amino functionalized graphenes (NH₂-G) – Influence of surface chemistry of NH₂-G, *Applied Surface Science* 284 (2013) 862– 869.

Yan Wu, Hanjin Luo, Hou Wang, Li Zhang, Peipei Liu, Linqiang Feng, 2014, Fast adsorption of nickel ions by porous graphene oxide/sawdust composite and reuse for phenol degradation from aqueous solutions, *Journal of Colloid and Interface Science* 436 (2014) 90–98.

Yang, C., Gao, P., Xu, B., 2009. Investigations of a controllable nanoscale coating on natural fiber system: effects of charge and bonding on the mechanical properties of textiles. *J Mater. Sci.* 44, 469–476.

Yang, H., Reichert, P., Abbaspour, K., Zehnder, A.J.B., 2003. A water resources threshold and its implications for food security. *Environ. Sci. Technol.* 37, 3048–3054.

Yu Wu, Feng Yang, Xiaoxia Liu, Guangqun Tan, Dan Xiao, 2018, Fabrication of N, P-codoped reduced graphene oxide and its application for organic dye removal, *Applied Surface Science* 435 (2018) 281–289.

Yue Wang, Fengge Zhai, Yasushi Hasebe, Hongmin Jia, Zhiqiang Zhang, 2018, A highly sensitive electrochemical biosensor for phenol derivatives using a graphene oxide-modified tyrosinase electrode, *Bioelectrochemistry* 122 (2018) 174–182.

Zambrano, J.B., Szygula, A., Ruiz, M., Sastre, A.M., Guibal, E., 2010. Biosorption of Reactive Black 5 from aqueous solutions by chitosan: Column studies. *J. Environ. Manage.* 91, 2669–2675.

Zhiguo Pei, Lingyun Li, Lixiang Sun, Shuzhen Zhang, Xiao-quan Shan, Shuang Yang, Bei Wen, 2012, Adsorption characteristics of 1,2,4-trichlorobenzene, 2,4,6.

Zhihong Tang, Shuling Shen, Jing Zhuang, and Xun Wang, 2010, Noble-Metal-Promoted Three-Dimensional Macroassembly of Single-Layered Graphene Oxide, *ange.*201000270.

Zhineng Liu, Qing Li, Qihang Wu, Dave T. F. Kuo, Shejun Chen, Xiaodong Hu, Mingjun Deng, Haozhi Zhang and Min Luo, 2015, Removal Efficiency and Risk Assessment of Polycyclic Aromatic Hydrocarbons in a Typical Municipal Wastewater Treatment Facility in